EXPERIMENTAL STUDY OF FISH RESPONSE TO TURBULENT FLOW FIELDS GENERATED BY IN-STREAM STRUCTURES

BY

JIEYU QIN

THESIS

Submitted in partial fulfillment of the requirements
for the degree of Master of Science in Civil Engineering
in the Graduate College of the
University of Illinois at Urbana-Champaign, 2018

Urbana, Illinois

Adviser:

Assistant Professor Rafael O. Tinoco

ABSTRACT

The influence of hydrodynamics on habitat choice and migration path of fish is of great interest for biologists and engineers, especially when considering the impact of in-stream structures like dams or fish passages during stream restoration projects. Research is needed in both laboratory and field environments to better understand how fish respond to different hydrodynamic conditions resulting from various aquatic environments, to better predict fish behavior in altered streams. While work has been done to observe fish response, including locomotion and tail beat behavior under increasingly complex flow conditions, models often rely on bulk or simplified flow parameters to correlate with fish behavior. The present study, uses a novel system to obtain high spatial and temporal resolution data that allows for correlation of mean and turbulent flow statistics with swimming behavior. Mean velocities, turbulent intensity, Reynolds stresses, and vorticity are investigated to explore both intensity and orientation of turbulent flow structures and their impact on swimming speed, acceleration, as well as tail beat frequency and amplitude in response to modified flows.

A volumetric three-component velocimetry (V3V) system was used to investigate the 3D velocity field generated by various obstructions: horizontal cylinder, vertical cylinder, gravel bed, and splitter plate, in addition to a flat bed case for reference as control group. Videos of fish swimming behavior (Micropterus salmoides) for each scenario were analyzed to determine fish position, swimming speed, and fish tail beat behavior. Multiple comparisons were made between hydraulic parameters and fish swimming response, as well as among different scenarios to reveal the relationship between intensity and orientation of turbulent flow structures and fish swimming preferences. Based on this project, it is found that bulk mean velocity didn't show any consistent correlation with fish swimming preferences. However, our investigated species showed a clear preference for regions with low turbulent inten-

sity, turbulent kinetic energy and vorticity, even with high levels of Reynolds stress. Studies on both vertical and horizontal obstructions also highlighted the relevance of coherent flow structure orientation, with horizontal eddies, generated by the vertical obstruction, being more easily utilized than those in a vertical plane. While this study provides valuable information on flow-fish interactions, further studies are required with a broader variable space and larger-scale facilities to find general correlations under more realistic scenarios.

To my parents, for their love and support.

ACKNOWLEDGMENTS

This work won't be finished smoothly without support of many people. I would like to first thank my advisor, Professor Rafael O. Tinoco, for his patient instruction on experiment and thesis writing. He is always there when I countered any difficulties and spends time discussing with me. I also appreciate the help on maintaining tested fish and oxygen consumption examination provided by Professor Cory Suski and his student Eric VC Schneider. Group members in our research team are all very nice to be helping hands. Jorge San Juan and Andrew S. Leman help a lot, especially in the beginning experimental set up parts. Pallav Ranjan, Andrés Prada and Chien-Yung Tseng are great friends to work with too. Finally, I'm grateful for my parents' support for the last 2 years' living abroad.

TABLE OF CONTENTS

CHAPTER 1

INTRODUCTION

Fish swimming mechanics, such as preferred locomotion mechanisms, fish propulsion, and energy consumption under varying turbulent flow fields are still open research areas that require an increasingly multidisciplinary approach. Hydrodynamics and fish body kinematics are often the two main parts considered when developing fish swimming models, since flow forces, and turbulent properties, have a dominant influence on fish swimming behavior [1]. Kondolf (2003) [2] pointed out the need to understand how fish employed the hydraulic conditions based on a review of different computational models used to predict hydraulic environments in real streams. Many other researches have looked at the influence of bulk flow characteristics, most commonly mean flow velocity, on fish swimming behavior in both numerical and experimental methods. However, there are still gaps to link detailed hydraulic conditions, especially turbulent characteristics, with fish behavior.

In this project, turbulent flow fields were generated by setting different obstacles in a laboratory flume, including a horizontal cylinder, a vertical cylinder, a splitting plate, and a gravel bed, to investigate the effect of both intensity and orientation of the turbulent flow structures on fish response. Mean and turbulent flow statistics were captured and analyzed thoroughly in 3 dimensions, employing a volumetric three-component velocimetry (V3V) system. Correspondingly, fish swimming behaviors under each condition were recorded by high-speed cameras (GoPro Hero4-Black) from top and side views for further analysis of their body kinematics, focusing on swimming speeds, orientation, and tail beat mechanics. Hydrodynamics and fish-swimming studies were conducted separately, analyzed and compared using the same experimental setup and flow conditions to correlate fish response to different mean and turbulent flow structures.

1.1 Fish Swimming Behavior

Early studies on fish swimming kinematics analyzed the morphological or muscle adaptation for high swim efficiency among fish species comparing their body kinematics [3]. Simple laboratory experiments under free or steady flow conditions were conducted to investigate swimming behavior and factors influencing them. For example, Webb (1988) [4] studied the swimming kinematics of trout and tiger musky under increasing flow velocity, concluding that tail beat frequency as well as amplitude increased with swimming speed based on experimental data.

Researchers have investigated more complex flows, closer to fish natural environments. Among these, setting obstructions with simplified geometries, such as cylinders in a flume, are of interest to many researchers due to the opportunity to investigate intensity, position and orientation of vortex shedding near the obstructions, and thus investigate specific swimming preferences of fish in response to the altered flows [5]. Research has showed that trout can reduce their swimming cost by using only axial muscles with the help of the vortices generated by a vertical D-shaped cylinder [6]. Other experiments have shown that swimming costs increase significantly in high-amplitude turbulence [7, 8].

Tail beat mechanics, in particular, is a significant parameter for biologists. Tail beat frequency (TBF) of free swimming rainbow trout in steady flow was found related to swim speed (U) and body length (BL), which were expressed by Equation (1.1) [9]

$$U = 0.4 \times BL \times TBF + 6.1, \tag{1.1}$$

where swimming speed also showed a linear relationship to tail beat amplitude, while the amplitude over body length remained a relative constant value to the TBF [9, 10]. With the understanding of tail beat behavior in steady swimming, more efforts were paid on investigate this activity in undulatory swimming and how flow conditions influence it. Liao et al. (2003) [6] reported that trout tail beat frequency tended to match the vortex shedding frequency generated by a D-shape cylinder when Kárman gaiting. Tail beat frequency showed an obvious decrease compared to free-swimming trout, but tail beat amplitude showed an increase [6]. Research with rainbow trout

swimming behind a D-shaped cylinder confirmed the above findings, and gave statistical relationships between tail beat behavior and flow velocity, with tail beat frequency and amplitude both increasing with flow velocity following Equation (1.2) [11]

$$TBF = 0.005u;\ TBA = 8.59u/(4.63 + u) \tag{1.2}$$

Laboratory observation of fish behavior in predictable turbulence generated by simplified obstructions reveals that fish could either actively employ vortex energy for locomotion or seek favorable regions for refuge to lower their swimming costs [5]. Silva et. al. (2016) found that both European eels and Iberian barbel can pass more easily through modified spillways which created lower turbulent and more steady flows because they tend to avoid turbulence [12]. They also summarized that different fish species responded differently to the perceived flow changes, either avoiding them, being attracted to flow structures, or remaining stationary [12].

The "refuging behavior" shown in past studies is known as Kárman gaiting. Kárman gaiting is a specific swimming behavior in which fish find refuge behind cylinders, employing the energy generated by Kárman vortices to keep stable with smaller swimming costs [13]. Liao (2003) [13] found that trout could tune their swimming kinematics to the vortices based on the observation of corresponding body wave frequencies and decreasing tail-beat amplitude in certain regions near the D-shape cylinders fixed in the flume. For example, Stewart et al. (2016) conducted an experiment observing trout swimming behavior behind two D-shaped cylinders positioned in tandem, changing space between these cylinders for comparison, and reported that trout Kárman gait more frequently when the D-shaped cylinders were closer, which was largely because of the stronger vortex shedding region generated by cylinders in that case [14]. Bergendahl et al. (2017) compared the avoiding behavior of rainbow trout that were pre-exposed to the complex aquatic environment to those that were kept in a flat tank, finding that the agility was obviously increased among pre-exposed trout, which meant that trout could control their body much better if they were trained in environments with obstacles, resulting in more efficient foraging and predator avoidance [15].

The mechanisms of fish sensing the flow, in order to detect prey and preda-

tors, have been studied since the 1950s, assuming that lateral line fish could function as a detector with the absence of visual assistance for holding positions with lower energy cost [16, 17]. It was shown that the lateral line along the fish body helped navigating and perceiving obstacles, sensing the information of velocity and pressure gradient based on the flow speed response along the lateral line, which decided weather to keep original swim direction or to turn around [18]. Akanyveti et. al. (2016) found that head movements, instead of recoils of tail beating, could actually reduce swimming cost and improve the function of lateral line navigating system [19].

Based on previous findings of swimming mechanisms, the scale and orientation of flow structures are highlighted when analyzing the swimming performance, since the length scale of vortices compared to the body length, and the direction of the vortex would influence the way that fish adapt to those flow conditions [1, 20]. Experiments found that smaller trout has larger body wavelength when Kárman gaiting compared to larger fish, which contrasted with their behavior in free stream [11]. Lupandin (2005) also pointed out that the influence of turbulence intensity on flow rate depended on the size of fish body: those with longer body length needed higher intensity to decrease their swimming speed, which demonstrated the importance of the turbulence length scale compared to fish size [21]. Thus, in the present study, horizontal and vertical cylinders were set to study the effect of orientation.

Most existing fish swimming experiments focused on measuring the lateral locomotion, tail beat behavior, oxygen consumption, muscle activity of fish or vortex speed along fish under different unsteady flow. Such studies aimed to correlate fish body kinematics parameters with bulk hydraulic conditions. Other studies focused on the area around the fish to reveal how fish behavior altered the flow structures. Lauder and Ducker (2004) focused on investigating the flow structure around the fish body, especially fins of different fish species to summarize how they drove the fish response [22]. Tytell and Lauder (2008) investigated hydrodynamics of the region where sunfish experienced escape response to figure out power transformation from biota to fluid [23]. Smith (2005) studied the hydraulic conditions in a laboratory flume with the presence of fish, to investigate how trout respond to turbulence altered by various geometries [24]. In this project, quantitative analysis of turbulent characteristics including Reynolds stress, turbulent intensity, vorticity and turbulent kinetic energy were obtained separately from the fish swim-

ming studies, and correlated to the swimming parameters obtained under the same experimental conditions.

1.2 Hydraulic Environments

Turbulent flows are expected for flows with Reynolds numbers ($Re = uL/\nu$, where u is the flow velocity, L is the hydraulic diameter, ν is kinematic viscosity of the fluid) larger than 500 [25]. Turbulence can be viewed as a composition of eddies in various scales (e.g., visualized by researchers as [26, 27]. Turbulence flows are highly three-dimensional, and this study is uniquely positioned to obtain such volumetric, 3D flow variations.

The choice of flow obstructions for our study: vertical and horizontal cylinder, splitting plate and gravel bed, require analysis of perturbed boundary layer, mixing layers, and coherent flow structures (CFS). Turbulent flow structures in boundary layers can be identified by fluctuating large eddies, breaking down into smaller eddies until dissipating because of viscosity [28]. Velocity profile under these flows can be described by a universal function: the law of the wall (Equation(1.3))[29].

$$\frac{u}{u_\tau} = ln(\frac{y}{y_0(x)}) + constant \tag{1.3}$$

CFS are another characteristic of turbulence caused by shear and mixing layers, as well as vortex shedding generated by flow passing through and around rough surfaces [30], as noticed in the gravel bed case in the near-wall region. Ejections, sweeps and wakes are both common large-scale coherent structures expected in these flows [31].

The study of vortex generation has a long history, with early research enabling the statistical analysis of turbulence on both time and frequency domains [32]. Kárman vortex street described the periodic double-row vortices formed when free stream passes around rough obstructions, which has been studied theoretically and experimentally since the 1900s because of its importance to many technical issues [33]. The asymmetric, discrete, counter-rotating vortices can form behind a fixed cylinder within a certain region of Reynolds number: 300-150,000 [34]. Vortices caused by physical objects like cylinders have been extensively analyzed through both laboratory ex-

periments and numerical simulations. Vortex wake characteristics largely depend on Reynolds number (Re), spacing between obstructions, and flow velocity [32].

For a proper statistical analysis of turbulence, we follow a Reynolds decomposition, to obtain the instantaneous fluctuations in the flow field, as:

$$u = \overline{u} + u' \tag{1.4}$$

$$v = \overline{v} + v' \tag{1.5}$$

$$w = \overline{w} + w' \tag{1.6}$$

where $\overline{u}$, $\overline{v}$, and $\overline{w}$ are time-averaged lateral, longitudinal, and vertical velocity, respectively, and u', v', and w' are the instantaneous fluctuations.

Reynolds stresses $\overline{u'v'}$, $\overline{u'w'}$, $\overline{v'w'}$, are derived from the Reynolds averaged Navier-Stokes Equation for incompressible fluids, and allow us to characterize the flow turbulence as:

$$\frac{\partial \overline{u_i}}{\partial t} + \overline{u_j}\frac{\partial \overline{u_i}}{\partial x_j} = -\frac{1}{p}\frac{\partial \overline{p}}{\partial x_i} + \nu\frac{\partial^2 \overline{u_i}}{\partial x_j^2} - \frac{\partial \overline{u_i' u_j'}}{\partial x_j} \tag{1.7}$$

Turbulence intensities are calculated via the root-mean-square of velocity fluctuations: $u_{rms}, v_{rms}, w_{rms}$, representing turbulence intensity in lateral, longitudinal, and vertical directions, respectively, and obtained as:

$$u_{rms} = \sqrt{\overline{u'^2}} \tag{1.8}$$

$$v_{rms} = \sqrt{\overline{v'^2}} \tag{1.9}$$

$$w_{rms} = \sqrt{\overline{w'^2}} \tag{1.10}$$

Turbulent kinetic energy (TKE) is calculated as:

$$TKE = 0.5 \times (\overline{u'^2} + \overline{v'^2} + \overline{w'^2}) \tag{1.11}$$

Vorticity, a pseudovector field that describes the rotating tendency of a

continuum, is mathematically defined as the curl of velocity:

$$\begin{aligned}\vec{\omega} =& \nabla \times \vec{v} = (\frac{\partial}{\partial x}, \frac{\partial}{\partial y}, \frac{\partial}{\partial z}) \times (v_x, v_y, v_z) \\ &= (\underbrace{\frac{\partial v_z}{\partial y} - \frac{\partial v_y}{\partial z}}_{\text{Y-Z plane}}, \underbrace{\frac{\partial v_x}{\partial z} - \frac{\partial v_z}{\partial x}}_{\text{X-Z plane}}, \underbrace{\frac{\partial v_y}{\partial x} - \frac{\partial v_x}{\partial y}}_{\text{X-Y plane}})\end{aligned} \tag{1.12}$$

Equation (1.12), as a whole, shows all components of vorticity in all planes, Y-Z, X-Z, and X-Y. This derivative quantity $\vec{\omega}$ is of great importance since it shows fluid rotation, allowing for identification and characterization of coherent flow structures.

Power spectral density (PSD) is usually employed to evaluate time series power distribution over frequency for continuous and discrete signals. The PSD can be calculated as:

$$S_{uu} = \lim_{T \to \infty} E(|\widehat{u_T}(\omega)|)^2 \tag{1.13}$$

Where $\widehat{u_T}(\omega)$ is a truncated Fourier transform, integrating the signal over a time region [0, T]:

$$\widehat{u_T}(\omega) = \frac{1}{\sqrt{T}} \int_0^T v(t) e^{-i\omega t} dt, \tag{1.14}$$

and E is the expected value of the random variable:

$$E[v] = v_1 p_1 + v_2 p_2 + ... + v_k p_k \tag{1.15}$$

The power spectral density of our experimental data, S_{uu}, was calculated using Equation (1.16), where e is the reshaped velocity by number of group for ensemble average, N_p is the number of groups, fs is the sample frequency, FFT is the fast Fourier transform, and conj returns the complex conjugate of the elements of FFT(e).

$$S_{uu} = \frac{FFT(e) \cdot conj[FFT(e)]}{fs \times N_p} \tag{1.16}$$

Using the obstructions studied for this work, fully turbulent flow is expected, with vorticity patterns fluctuating randomly in all three dimensions. Therefore, velocities in three dimensions need to be detected for analysis of turbulent characteristics. Measurements of turbulent characteristics have

progressed with the development of novel technologies, starting with single point measurements, using devices like electromagnetic (EM) current meter, laser Doppler velocimeter (LDV), and acoustic Doppler velocimetry (ADV) [35]—[37]. Yusoff et al. (2016) summarized achievements by research on unsteady flows employing advanced 2 or 3-dimensional visualization techniques to obtain more comprehensive data-sets [38]. Particle image velocimetry (PIV) and digital PIV (DPIV) were employed in laboratory tests, which can detect velocities of a surface or even a whole volume, which largely increase the size of data available to describe turbulence characteristics. Despite the much more extensive data-sets available by PIV, ADV is still popular in field experiments because of the strict requirements and difficulty of field PIV settings. For small scale turbulence studies, however, PIV, and volumetric 3D PIV in particular, are optimal tools for further understanding of turbulent characteristics since it records data with high-spatial and temporal resolution.

1.3 Thesis Structure

The thesis is organized as follows. Chapter 1 introduces the background of this project with respect to both fish swimming mechanisms and hydrodynamics. Chapter 2 details the experiment set up and methodology including 3D velocity measurements, recording and analysis of fish swimming response. Chapter 3 presents the results of mean and turbulent velocity statistics, as well as fish locomotion, and fish tail beat behavior. Chapter 4 discusses correlation between fish response and hydraulic environment, focusing on specific hydraulic parameters that seem to drive changes in fish response.

CHAPTER 2

METHODOLOGY

2.1 Materials

Tests were conducted in a 30 L swim-tunnel respirometer (Loligo Systems, Denmark). Flow is driven by a frequency controlled propeller, allowing for mean flows between 0.05 - 1.75 m/s. Tests reported herein were set at 110 Hz, for a mean velocity of approximately 0.10 m/s for all scenarios. The rectangular test section is 0.55 m long, with a 0.14 m x 0.14 m cross section, as shown in Figure 2.1.

Five scenarios were investigated (Table 2.1): 1) a flat-bed case set for reference, 2) a rigid cylinder, with diameter d=1.27 cm (1/2 inch) placed vertically at the center of the tunnel, 3) same rigid cylinder placed horizontally at mid height, 4) a splitter plate with a length of 18.27 cm and maximum width upstream of 2 cm, set symmetrically along the centerline, and 5) a gravel-bed with a single layer of d=1.2 cm glass marbles.

Several specimens of Micropterus salmoides were transported to the Aquatic Research Facility in Champaign, Illinois several days before the experiment to recover from the transportation and acclimate to the holding tanks. The smallest fish were selected to guarantee enough space within the tunnel to swim behind and around the obstructions.

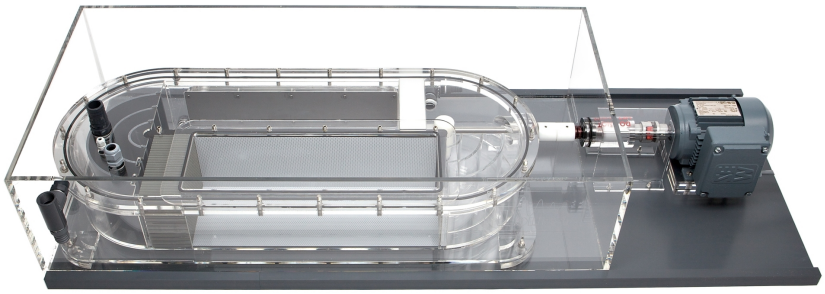

Figure 2.1: Swim tunnel respirometer

Table 2.1: Basic information for studied case

Case	Obstruction	Capture Frequency	Pump Frequency
Hori.Cyl	Horizontal Cylinder	25	119
Vert.Cyl	Vertical Cylinder	25	119
Splitter	Splitter Plate	25	119
Gravel Bed	Gravels	25	119
Flat Bed	No obstruction	25	119

2.2 Hydraulic Analysis

2.2.1 Volumetric 3-Component Velocimetry (V3V) System

Velocity fields were characterized using a volumetric three-component velocimetry (V3V) system. The V3V system was developed based on the principles of defocusing digital particle image velocimetry (DDPIV) [39], which is a new technique measuring instantaneous velocities within a $14 \times 14 \times 10 cm^3$ volume in three dimensions. Pereira and Gharib (2002) discuss the concept of DDPIV, which detects the distance between particles and camera, adding a third dimension, based on the images on a focal plane and reference plane, extending 2D PIV techniques into 3D [39]. The V3V system used in this project consists of three cameras, a laser system for illumination (Litron 100Hz Yag Laser), a 610036 LaserPulse Synchronizer, and an image acquisition computer system with TSI-V3V software. The 3D setup uses three cameras (POWERVIEW 4M-180), calibrated for a coplanar triangle pattern. The 3-camera array captures the same particles in three different planes, forming coplanar triangles, which are used to determine the particle distance to the camera and thus its displacements [39]. In other words, algorithms can be established based on the triangle pattern, which extract particle positions in three dimensions. The raw images of particles are saved and analyzed by the V3V software for further processing.

The V3V software contains a pre-processing and processing steps to analyze the images. The pre-processing consists of input, image generator (generator type: minimum intensity), image calculator (operation: subtraction, Operand: Passed in generator image), image calculator (operation: multiplication, Operand: Constant 1.7) , and output. The processing part includes

4 sections: particle identification, particle matching, velocity calculating and velocity interpolation. The report level of the 4 sections was set as 1.

For particle identification, the size of recognizable particles was set between 1-5 pixels, and only particles which overlapped less than 50% are identified. Parameters for particle matching were as follows: coarse search tolerance was 300 microns; fine search tolerance was 270 microns; WPR threshold and neighbor tracking reconstruction were 0; neighbor tracking window size was 16 pixels; search strategy was set as option 2; near-side plane distance was 350 mm, and far-side plane distance was 800 mm. Once the identified particles were matched between 2 contiguous frames, the velocity of each particle could be calculated based on their displacement and Δt. The chosen tracking algorithm (option 3), used a universal median threshold as a filter (option 6). Settings for post processing included: node volume dimensions (8,8,8 mm), node volume overlap (75%), minimum number of particles (1), smoothing factor (1), girded hole filling neighborhood size (1), and grid coordinates (default). All other parameter are set to zero by default.

2.2.2 Hydraulic Parameters

The 3-camera array captures images at a frequency of 25 Hz for 5 minutes. Analysis of only the first minute is presented hereafter. The output velocity fields from the V3V software were arranged in a specific 6-column format: it went through the direction of X (longitudinal), then Z (vertical) direction and Y (lateral) direction in order; with each (X, Y, Z) coordinate corresponding to velocities (u, v, w). Instantaneous velocities can be called from output data files, to calculate mean and turbulent statistics, Reynolds stress, turbulence intensity, TKE, vorticity, and PSD using custom algorithms using MATLAB (Mathworks Inc.) as described in Chapter 1. For the power spectra, two filters were used to remove the noise: a despiking routine and median filter. The despiking filter removed the spatial averaged velocity value that fell far away from the region of interest, and replaced those with interpolation values [40], while the median filter chose the spatial median value of velocity for PSD calculation.

The velocity fields were analyzed from two perspectives: time-averaged information and instantaneous information. The time averaged variables

(Reynolds stress, turbulence intensity, TKE) showed the main characteristics of flow structure behind different in-stream structures, while the instantaneous fluctuations showed vortex frequency as well as small scale turbulent characters, such as vorticity, propagating with time.

2.3 Fish swimming behavior observation

2.3.1 Video records of fish behavior

Two high-speed cameras (GoPro Hero4 Black) were positioned to record (1080p, 30fps) fish swimming for 5 minutes for each scenario, synchronous from both top and side-views. Each fish was guaranteed at least 48 hours of rest before testing. A graded ruler was included in the videos' field of view for spatial calibration. Samples of top- and side-view frames are shown in Figure 2.2.

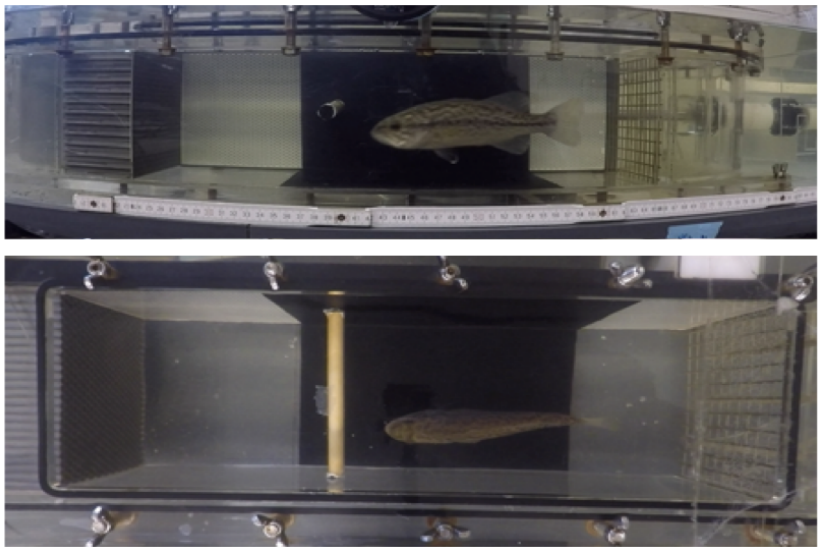

Figure 2.2: One frame of side view and top view of fish videos respectively (Horizontal Cylinder case)

2.3.2 Analysis of fish body kinematics

The useful segments of each video, when fish was actively swimming and not resting against the downstream grid, were identified before extracting

frames in MATLAB. For each side view case, coordinates of points 1-8 (Figure 2.3) were identified to set a consistent reference frame for hydraulic analysis, and to determine the spatial calibration. Similarly, for top view videos, coordinates of 4 points shown in the sketch were identified to set the Y coordinates for the hydraulic analysis. For each frame studied, the location of fish eye, and edges of fish tail (1', 2', 3' shown in Fig. 2.5) were collected by manually clicking within a MATLAB program to determine the fish locomotion (location, swim speed and swim acceleration) and tail beat frequency. For top view frames, point 1',2' 3' represent the position of fish head, starting point of tail and end of tail respectively for calculation of fish swim speed, acceleration, and tail beat amplitude in an X-Y plane.

The displacement speed of fish were determined by the absolute location change (change of point 1') between frames, while the fish swimming speed were calculated by adding the flow speed. Both speed mentioned above were considered to be negative value when fish was swimming against the mean flow direction. To calculate the tail beat amplitude and frequency, a local, moving coordinate system was set upon the fish tail (See Figure 2.3).

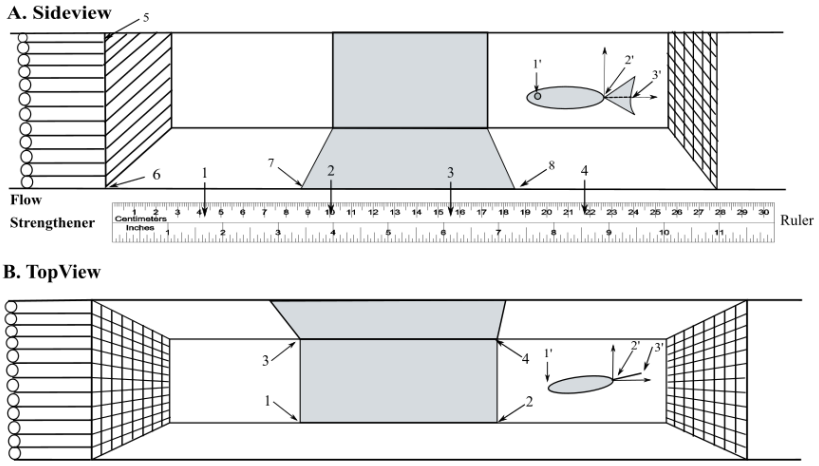

Figure 2.3: Sketch for detecting points in each frame of fish video

Oxygen consumption rate can reflect the energetics swimming cost for fish, which were also tested by Prof. Cory Suski's group, a collaborator of this project. MINI-DO, an oxygen probe developed by Loligo Systems, were used to examine the oxygen change in the flume for each scenario, to correlate oxygen consumption, and thus fish energetics, to the turbulence characteristics associated to each in-stream structure.

CHAPTER 3

RESULTS

3.1 Hydraulic Characteristic

3.1.1 3D Flow Visualization

The mean lateral, longitudinal, and vertical velocity, as well as Reynolds stress, turbulent intensity, and turbulent kinetic energy, are presented below in a three-dimensional way, to identify spatial variations within the whole investigated volume, together with the 3D sketch of each case (See Figure 3.1–3.5).

Compared with case without obstruction (Figure 3.1), the longitudinal velocities were altered in the gravel bed case (Figure 3.2, with an apparent decrease in the near bed area) and horizontal cylinder case (Figure 3.3, wake past the cylinder), while vertical cylinder (Figure 3.4) and splitter plate cases (Figure 3.5) hardly show differences apart from the areas very close to obstruction. The lateral velocity distributions were almost the same for all cases: transiting from negative to positive values as flow moves through the sampling volume, likely due to the elliptical flume shape, generating large scale vortices from the bends. The vertical cylinder enhanced this trend slightly, which is opposite to the horizontal cylinder and gravel case. The gravel bed enhanced the positive vertical velocity distribution of the sampling volume, while the vertical cylinder enhanced the negative vertical velocity distribution. Also, vertical rotation was generated as flow passed the horizontal cylinder, showing as negative w above and positive w beneath the cylinder. The vertical velocity showed a more uniform trend behind a large splitter plate. For turbulent intensity, gravel enhanced turbulence intensity in the near-bed region as expected, while the upper region shows small variance compared to flat bed case. Turbulent intensity in all directions behind

the horizontal cylinder (the waking area) showed a clear increase. However, vertical cylinder only increased the lateral turbulent intensity (v_{rms}), and caused a slightly increase of u_{rms} and w_{rms} in a small region right behind the cylinder. The splitter plate increased the longitudinal and lateral turbulent intensity (u_{rms}, v_{rms}) of the sampling volume, while it decreased the vertical turbulent intensity. As these 3D figures shown, gravel increased TKE in the whole region, decreasing progressively from bottom to top. Horizontal cylinder mainly increased TKE in its wake. TKE of the sampling volume behind the vertical cylinder was increased as well, but to a lower degree than that caused by the horizontal cylinder. The splitter plate, instead, increased turbulent kinetic energy of the whole region the most compared to other 3 cases.

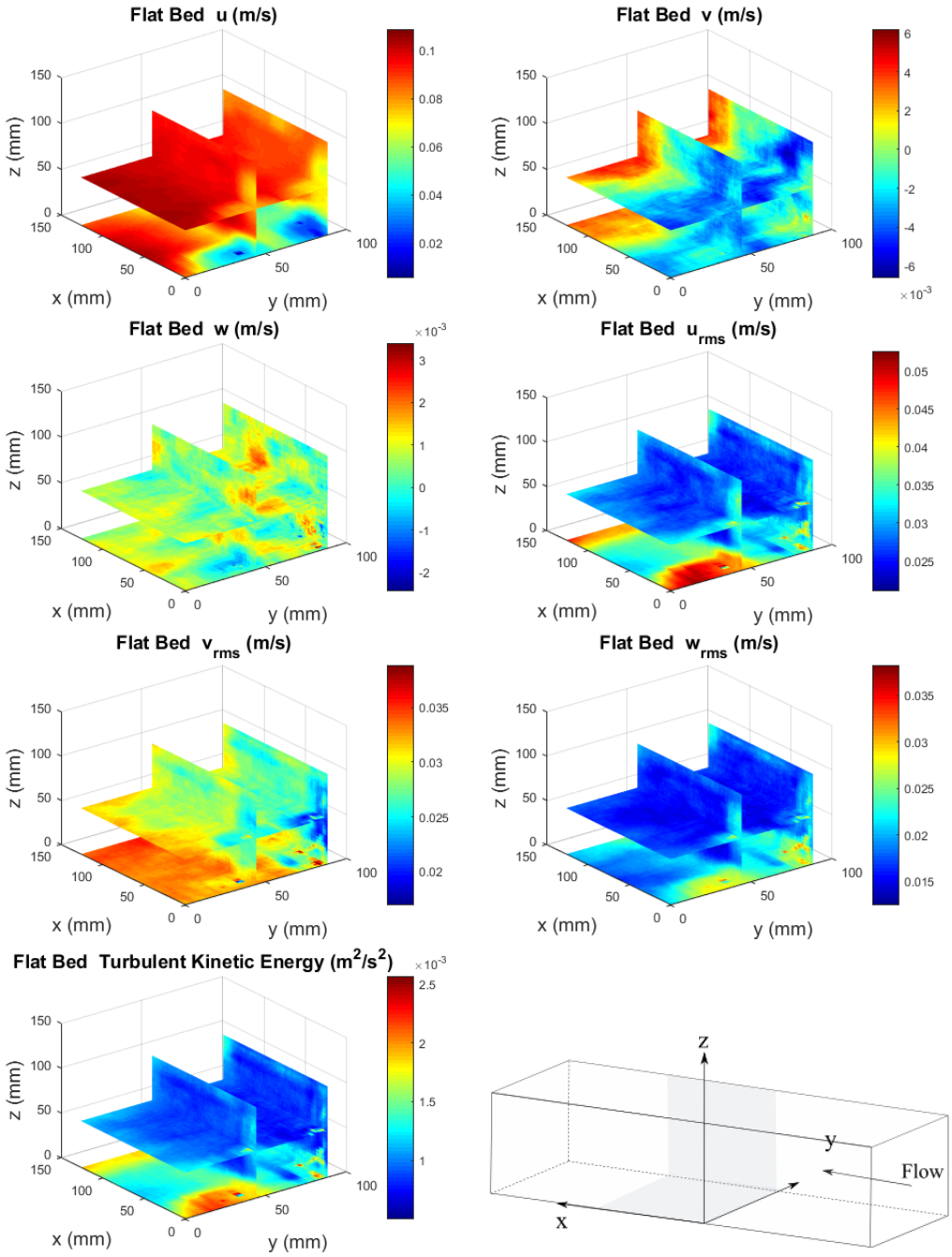

Figure 3.1: FB Case: Bulk velocities (u, v, w), time-averaged turbulent intensity (u_{rms}, v_{rms}, v_{rms}), time-averaged turbulent kinetic energy, and a sketch of the set flume, organized in 3D form. Flow went along the positive x direction.

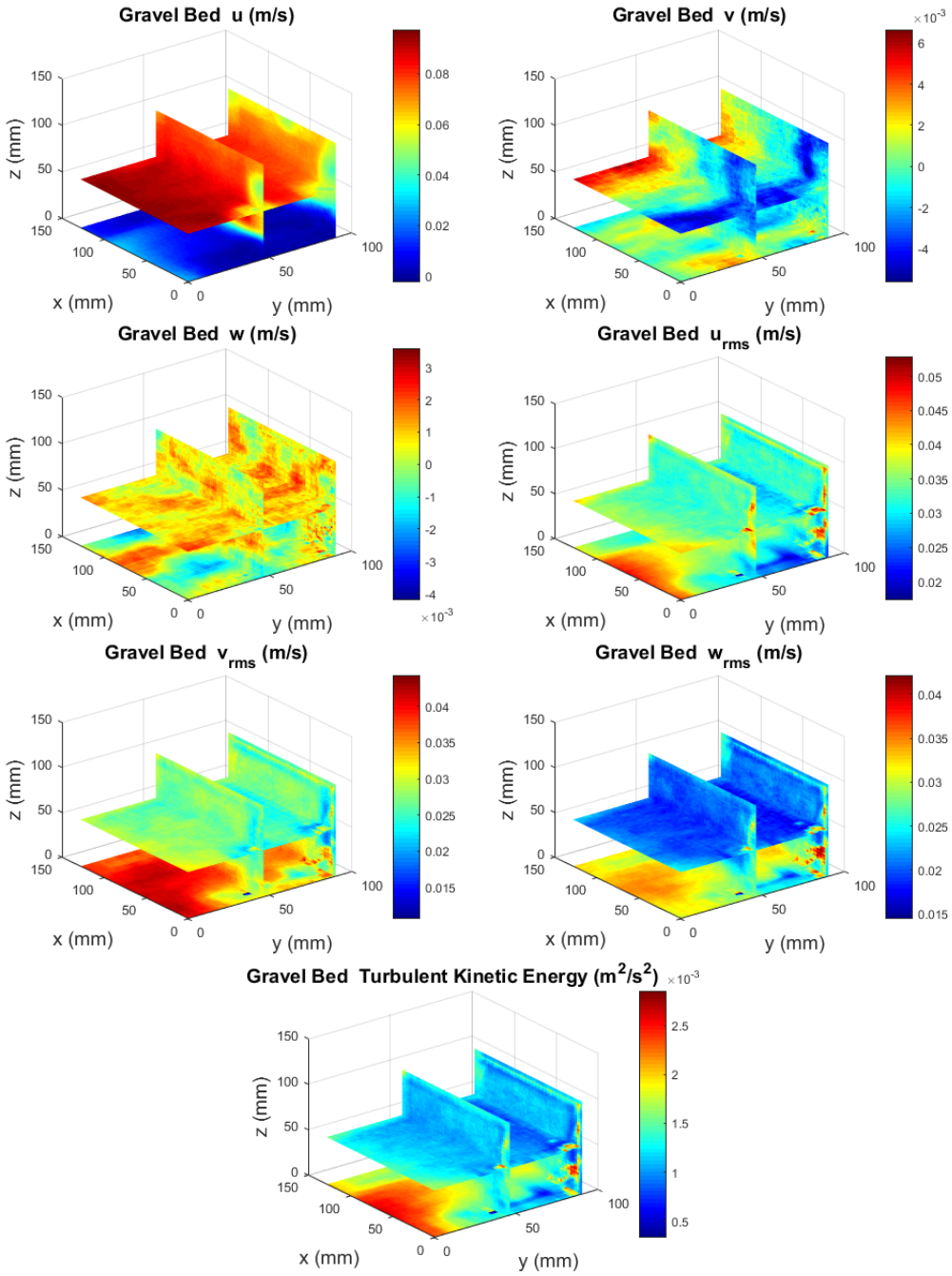

Figure 3.2: GB Case: Bulk velocities (u, v, w), time-averaged turbulent intensity (u_{rms}, v_{rms}, v_{rms}), and time-averaged turbulent kinetic energy, organized in 3D form. Flow went along the positive x direction.

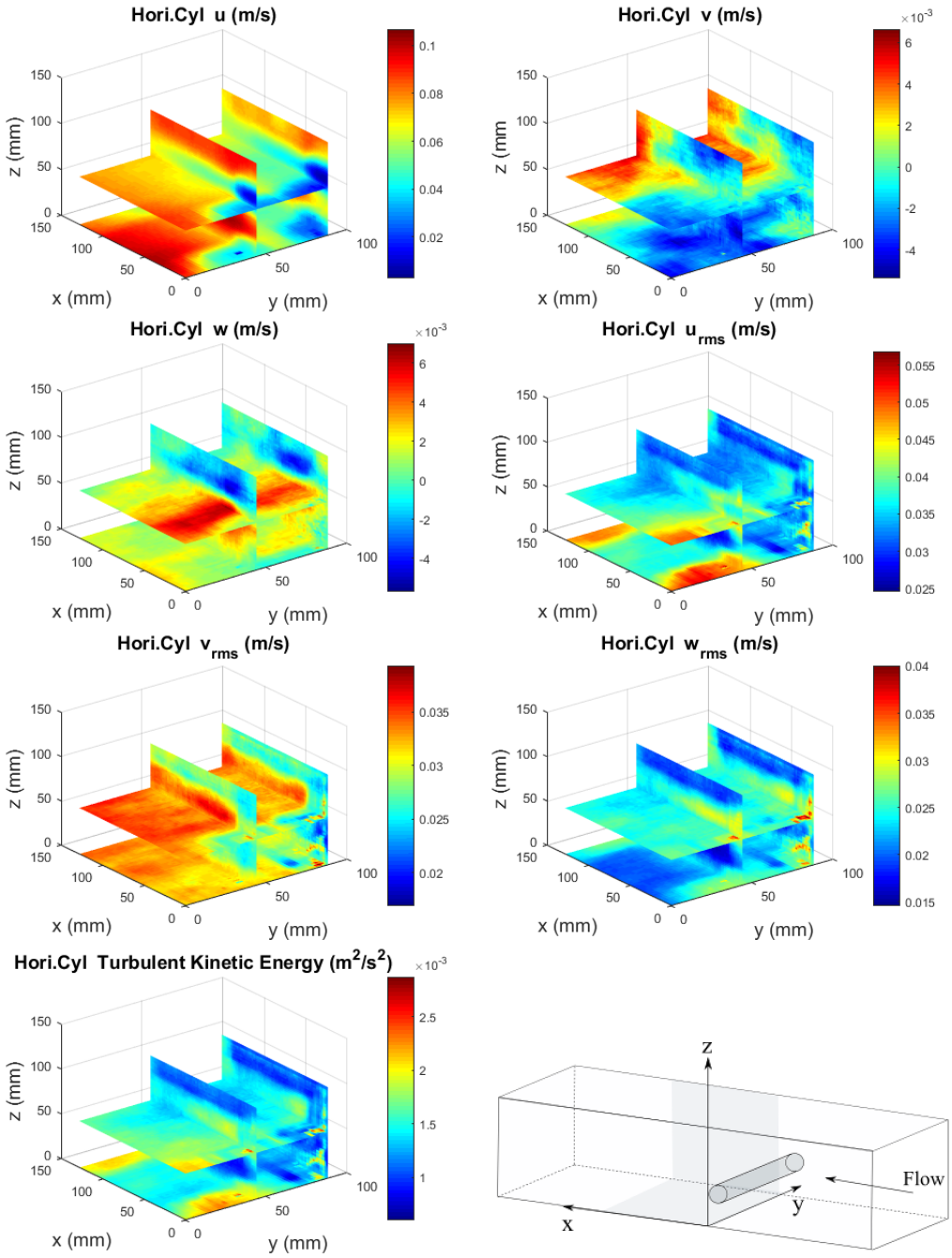

Figure 3.3: Horizontal Cylinder Case: Bulk velocities (u, v, w), time-averaged turbulent intensity (u_{rms}, v_{rms}, v_{rms}), time-averaged turbulent kinetic energy, and a sketch of the set flume, organized in 3D form. Flow went along the positive x direction.

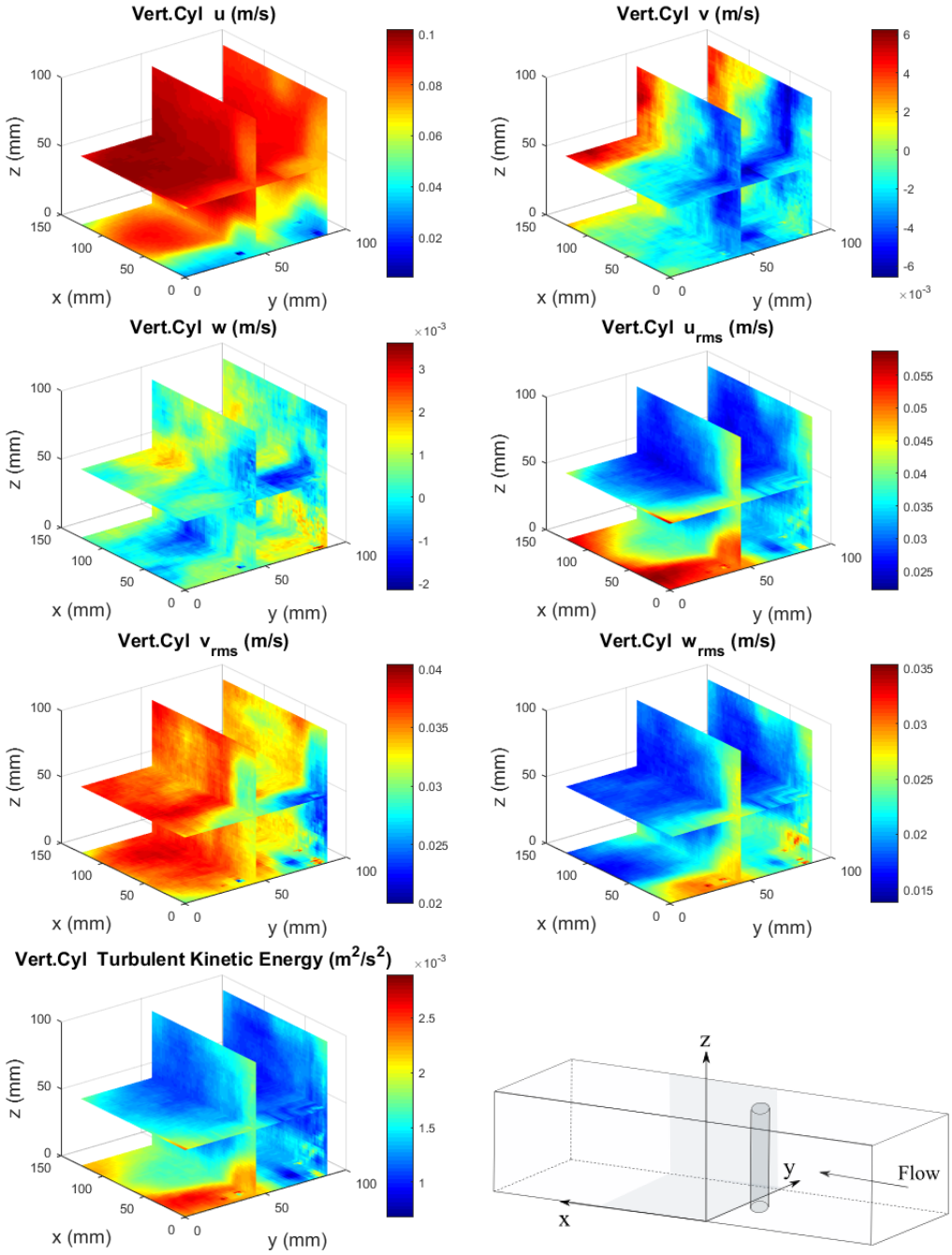

Figure 3.4: Vertical Cylinder Case: Bulk velocities (u, v, w), time-averaged turbulent intensity (u_{rms}, v_{rms}, v_{rms}), time-averaged turbulent kinetic energy, and a sketch of the set flume, organized in 3D form. Flow went along the positive x direction.

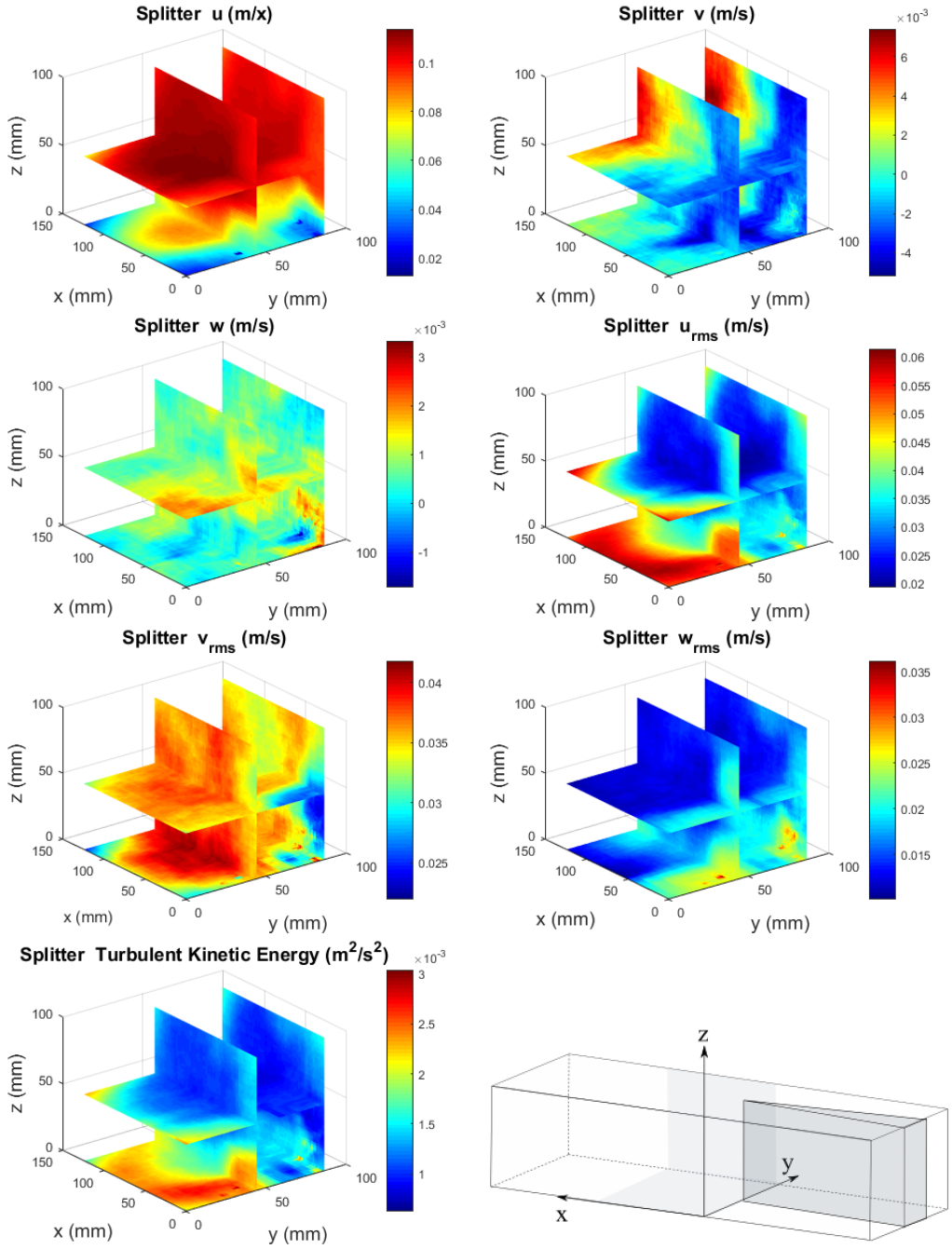

Figure 3.5: Splitter Case: Bulk velocities (u, v, w), time-averaged turbulent intensity (u_{rms}, v_{rms}, v_{rms}), time-averaged turbulent kinetic energy, and a sketch of the set flume, organized in 3D form. Flow went along the positive x direction.

3.1.2 2D Plane Analysis (Time-averaged and Instantaneous Parameters)

To facilitate interpretation of the data, the volumetric velocity fields were processed to present flow characteristics in the form of 2D XY and XZ planes. The mean velocities, as well as instantaneous velocity, velocity fluctuations, vorticity, and the time-series power spectra density (PSD) were calculated to have a more detailed understanding of flow structures.

(1) Horizontal XY plane

The chosen XY plane is at Z=50 mm (50mm above the bed) of the detected volume. The mean velocity fields (Figure 3.6–3.10) are consistent with those presented in 3D format. Gravel bed, as reported above, strengthens the vertical velocity w (Figure 3.7), but still shares the same distribution pattern as the flat bed case. Horizontal cylinder (Figure 3.8), however, changes w distribution to be more uniform. Vertical cylinder (Figure 3.9) and splitter plate (Figure 3.10) similarly altered the lateral velocity, v, compared to the no obstruction case.

The instantaneous velocity and velocity fluctuation values on Figure 3.11–3.15 of XY planes were scaled for visual comparison purposes ([-0.1, 0.1] and [-0.5, 0.5], respectively). The instantaneous velocity pattern of gravel bed case (Figure 3.12) is similar to that of flat bed case (Figure 3.11), while the velocity fluctuation value of gravel bed are more intense and random over the whole plane. More obvious differences of velocity and velocity fluctuation were present between horizontal and vertical cylinder cases, especially that of u', v', w' (Figure 3.13 and Figure 3.14). The presence of the splitter plate smoothed the variation of theses values over the plane (Figure 3.15).

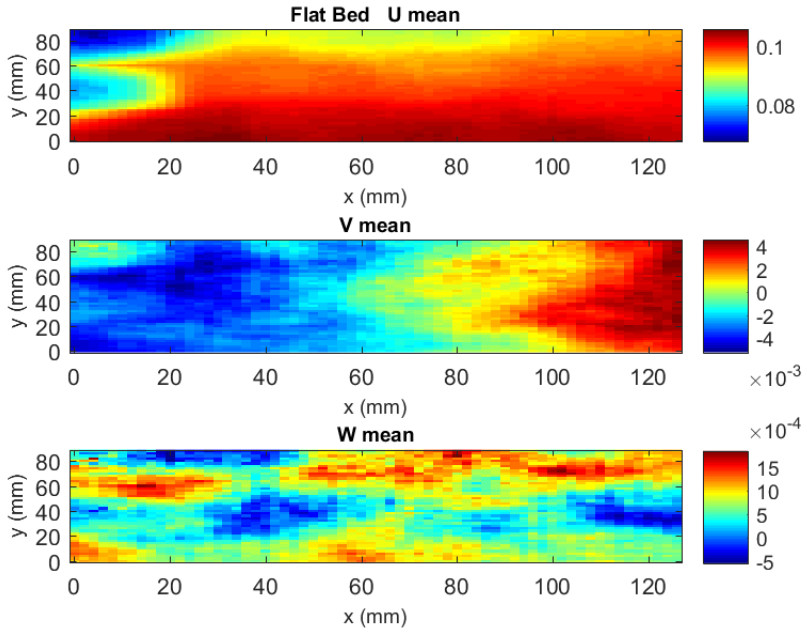

Figure 3.6: FB Case: Mean velocity on XY plane (Z=50 mm)

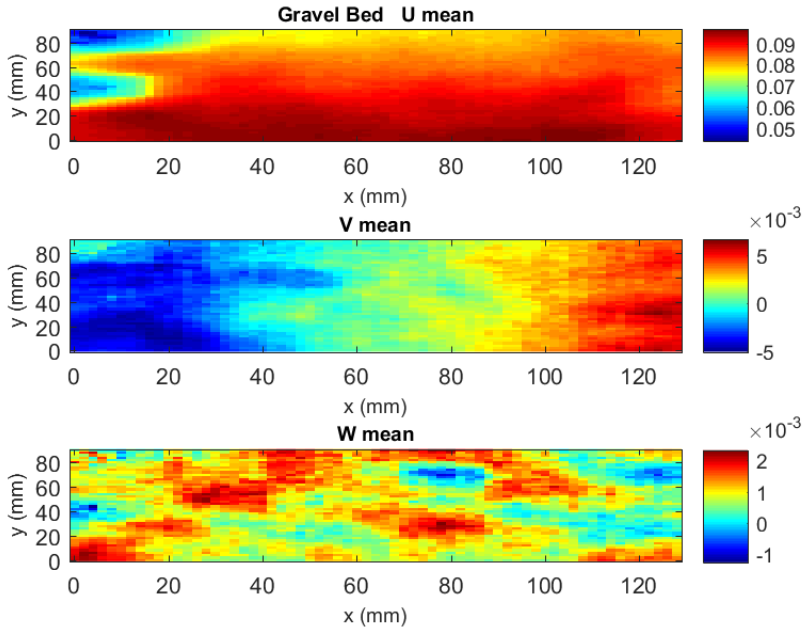

Figure 3.7: GB Case: Mean velocity on XY plane (Z=50 mm)

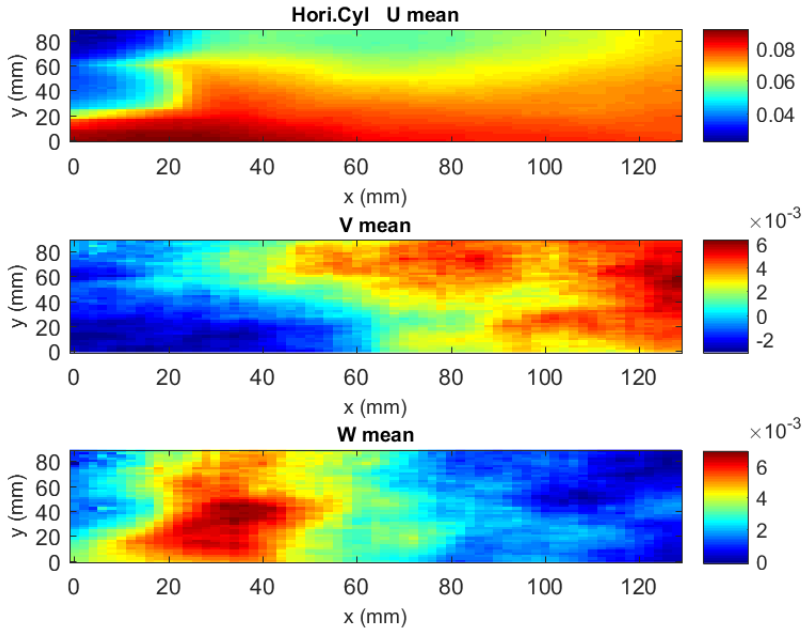

Figure 3.8: Horizontal Cylinder Case: Mean velocity on XY plane (Z=50 mm)

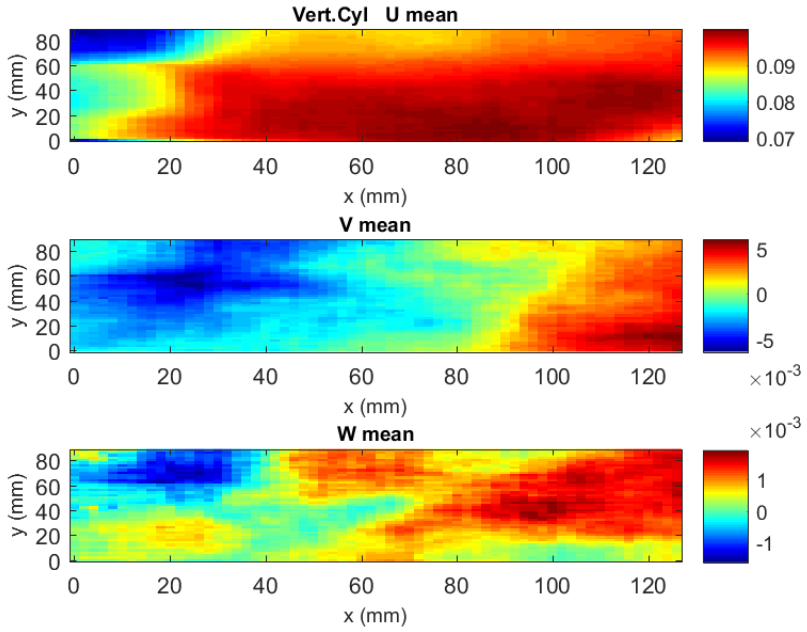

Figure 3.9: Vertical Cylinder Case: Mean velocity on XY plane (Z=50 mm)

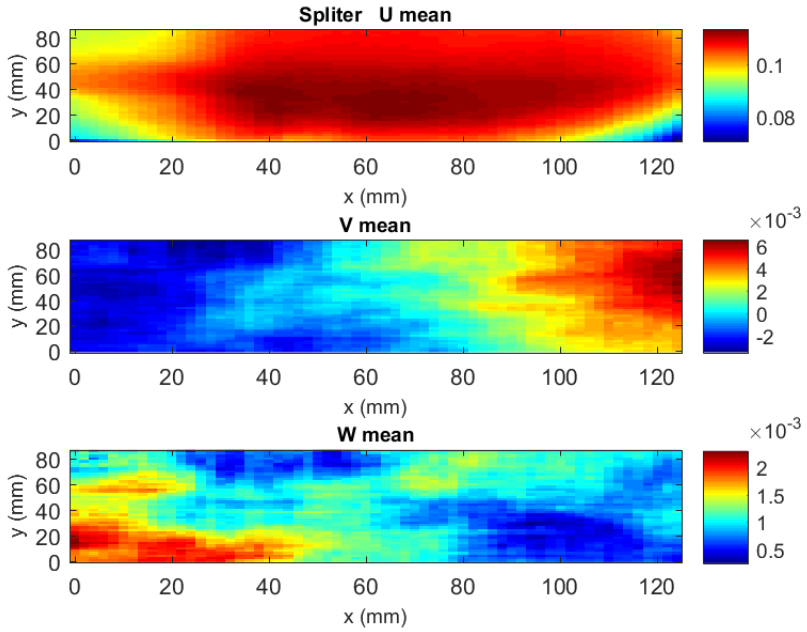

Figure 3.10: Splitter Case: Mean velocity on XY plane (Z=50 mm)

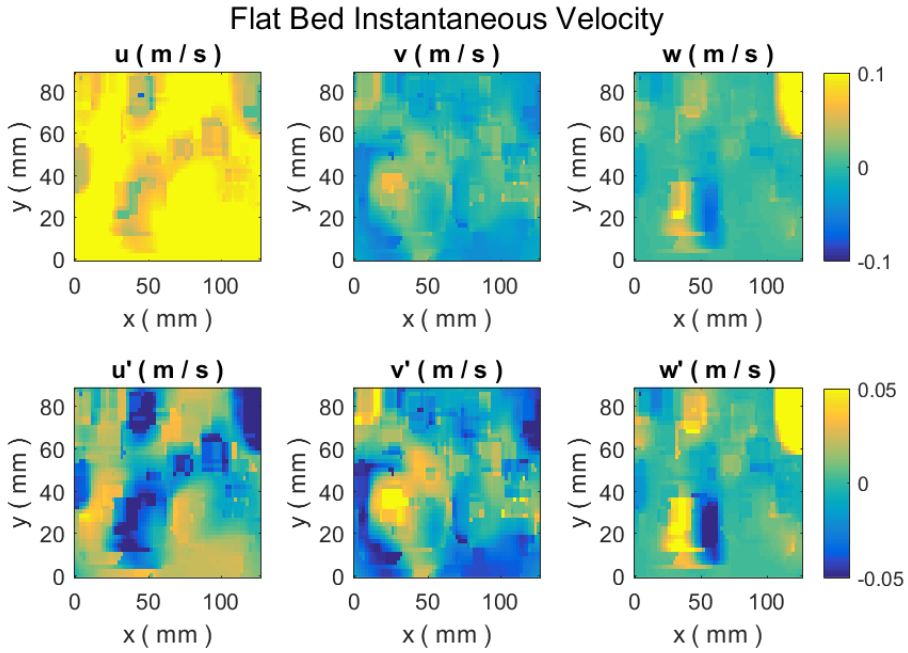

Figure 3.11: FB Case: Instantaneous velocity (u, v, w) and velocity fluctuation (u', v', w') on XY plane (Z=50 mm)

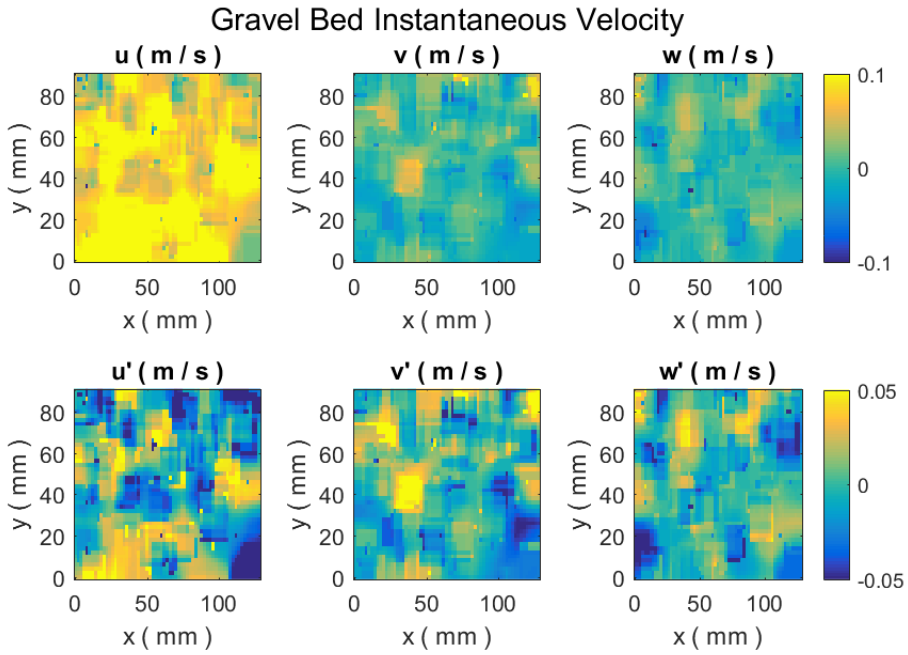

Figure 3.12: GB Case: Instantaneous velocity (u, v, w) and velocity fluctuation (u', v', w') on XY plane (Z=50 mm)

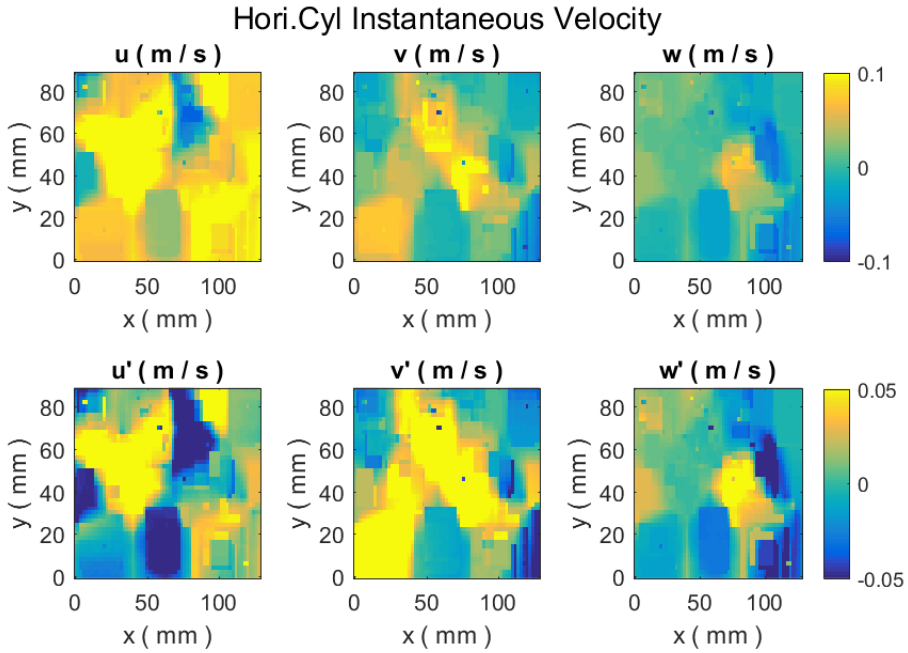

Figure 3.13: Horizontal Cylinder Case: Instantaneous velocity (u, v, w) and velocity fluctuation (u', v', w') on XY plane (Z=50 mm)

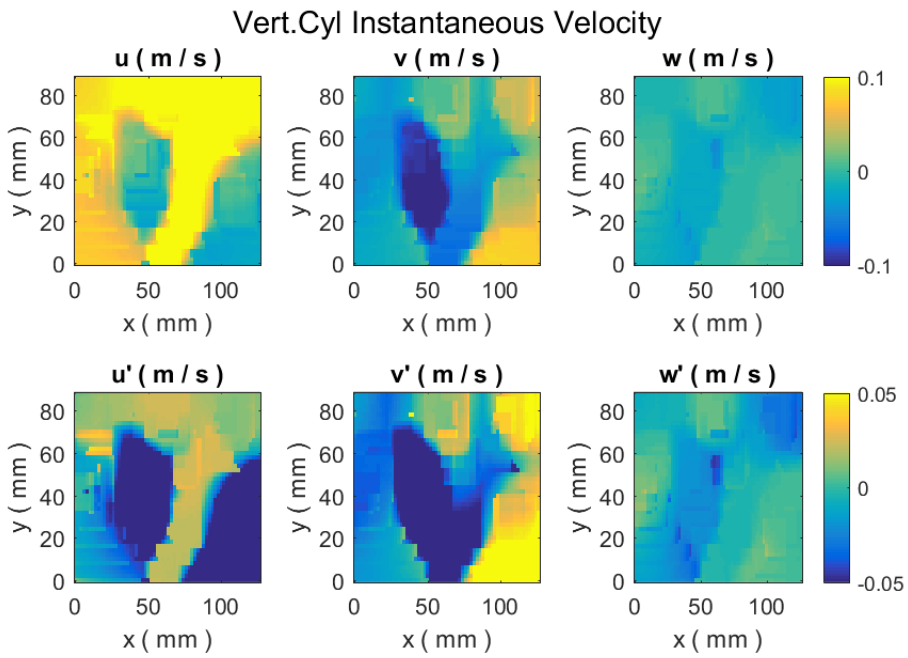

Figure 3.14: Vertical Cylinder Case: Instantaneous velocity (u, v, w) and velocity fluctuation (u', v', w') on XY plane (Z=50 mm)

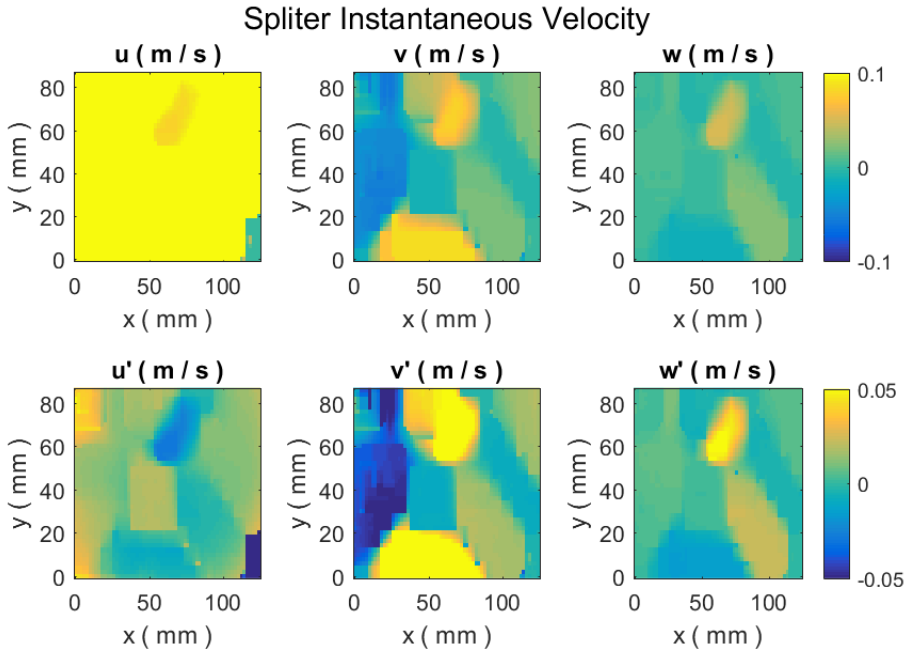

Figure 3.15: Splitter Case: Instantaneous velocity (u, v, w) and velocity fluctuation (u', v', w') on XY plane (Z=50 mm)

Figure 3.16–3.20 present the instantaneous turbulent intensity u_{rms}, v_{rms} and w_{rms} of the chosen XY plane under different obstruction types. Both gravel (Figure 3.17) and horizontal cylinder (Figure 3.18) cases enhanced the instantaneous turbulent intensity compared with no obstruction case, showing a consistent gradient pattern, while the splitter case reduced it slightly (Figure 3.20). Vertical cylinder, apart from enhancing the turbulent intensity, changed the distribution pattern (Figure 3.19). The influence of different obstructions on turbulent kinetic energy (Figure 3.21) shows a clear impact due to the geometry and orientation of the in-stream structure. One result to be noticed is that turbulent kinetic energy was seemingly weaker with the splitter plate, which yields a smoother flow transition, compared to the otter obstructions.

Figure 3.22 illustrates the rotating tendency on the XY plane. Gravel bed strengthened the intensity of rotation in the vertical direction through mainly small eddies. The negative and positive vorticity values were symmetric along the y-direction with relative larger scale eddies for the vertical cylinder case. The rotating tendency against z-direction was largely reduced by the splitter plate as shown in the figure. Vorticity is present on the XY plane in flume with no obstructions; but is clearly showing regular trends behind the vertical cylinder: negative values in x belonged to the range [20mm, 40mm], positive in the range [40mm, 60mm], and reduced near the end.

From the instantaneous information (velocity and vorticity), more clear differences were shown between vertical cylinder and flat bed case compared to the time averaged information, giving a better organization of vertical cylinder influence on flow structures.

In addition, Figure 3.23-3.27 presents the time-series information of velocity and PSD at a specific point (X=6 mm, Y=50 mm). These profile included three types of velocity information, which were raw velocity data and filtered velocity data with 2 different filters. PSD of filtered data, which employed a median filter, are used later for calculation of vortex frequency.

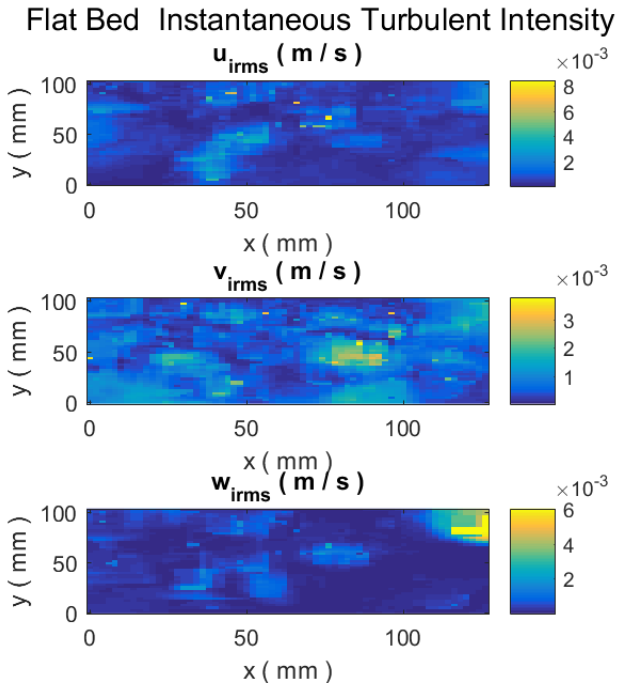

Figure 3.16: FB Case: Instantaneous turbulent intensity (u_{rms}, v_{rms}, w_{rms}) on XY plane (Z=50 mm)

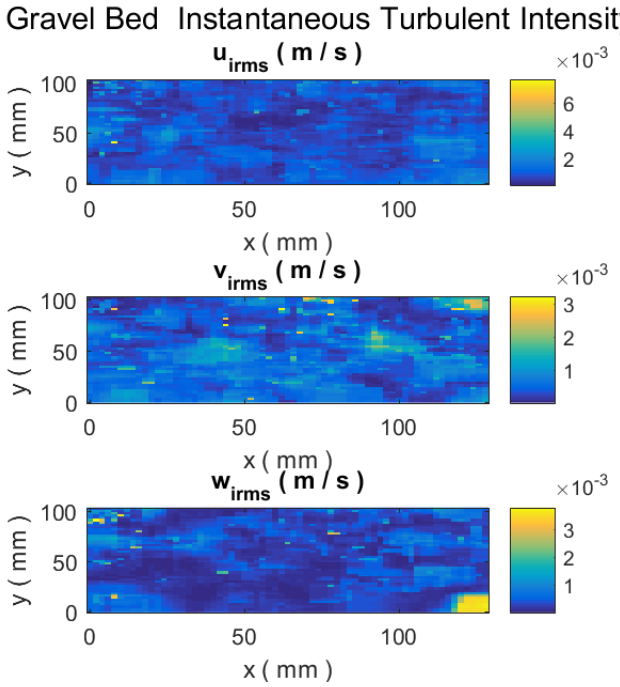

Figure 3.17: GB Case: Instantaneous turbulent intensity (u_{rms}, v_{rms}, w_{rms}) on XY plane (Z=50 mm)

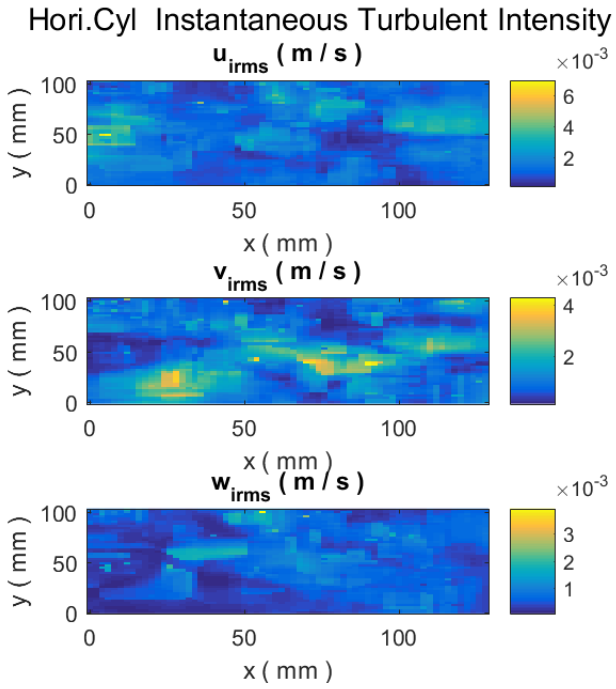

Figure 3.18: Horizontal Cylinder Case: Instantaneous turbulent intensity (u_{rms}, v_{rms}, w_{rms}) on XY plane (Z=50 mm)

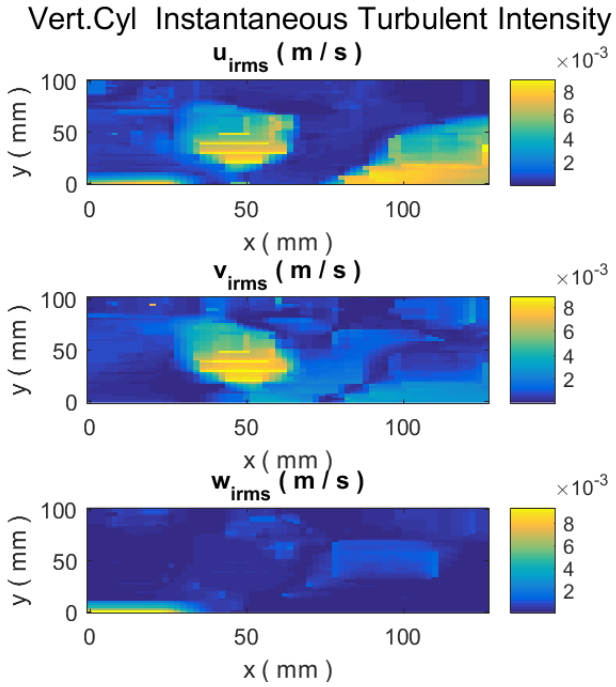

Figure 3.19: Vertical Cylinder Case: Instantaneous turbulent intensity (u_{rms}, v_{rms}, w_{rms}) on XY plane (Z=50 mm)

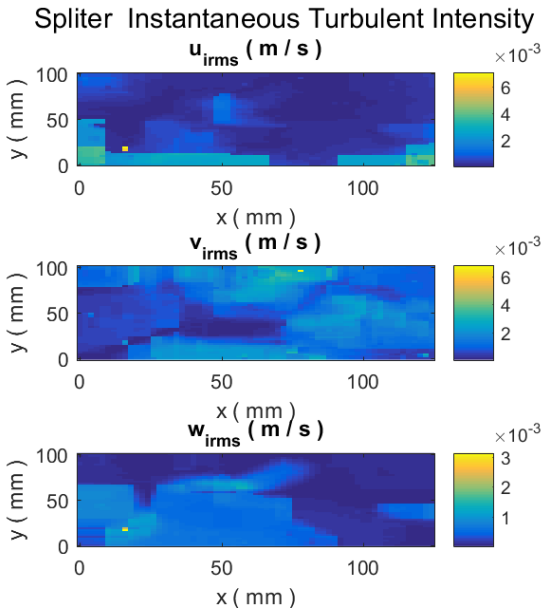

Figure 3.20: Splitter Case: Instantaneous turbulent intensity (u_{rms}, v_{rms}, w_{rms}) on XY plane (Z=50 mm)

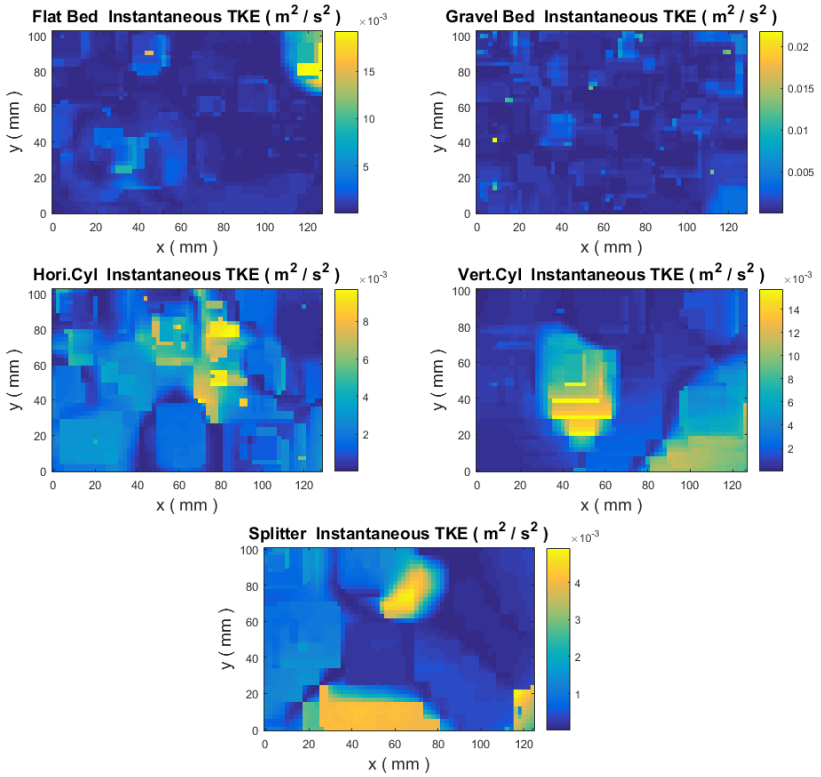

Figure 3.21: Turbulent kinetic energy on XY plane (Z=50 mm) for FB, GB, Horizontal Cylinder, Vertical Cylinder, and Splitter cases respectively

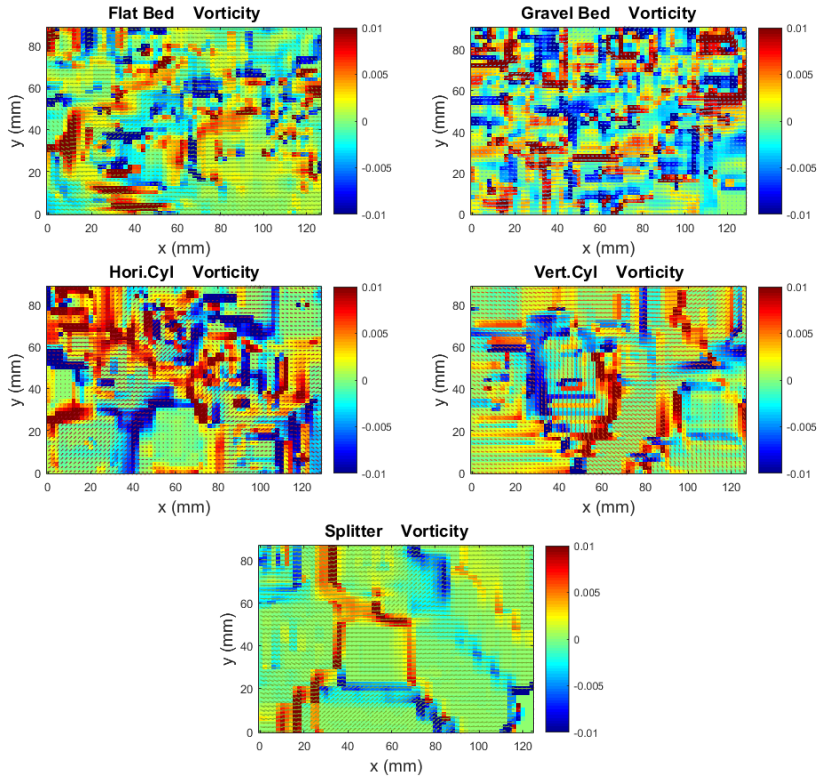

Figure 3.22: Vorticity on XY plane (Z=50 mm) for FB, GB, Horizontal Cylinder, Vertical Cylinder, and Splitter cases respectively

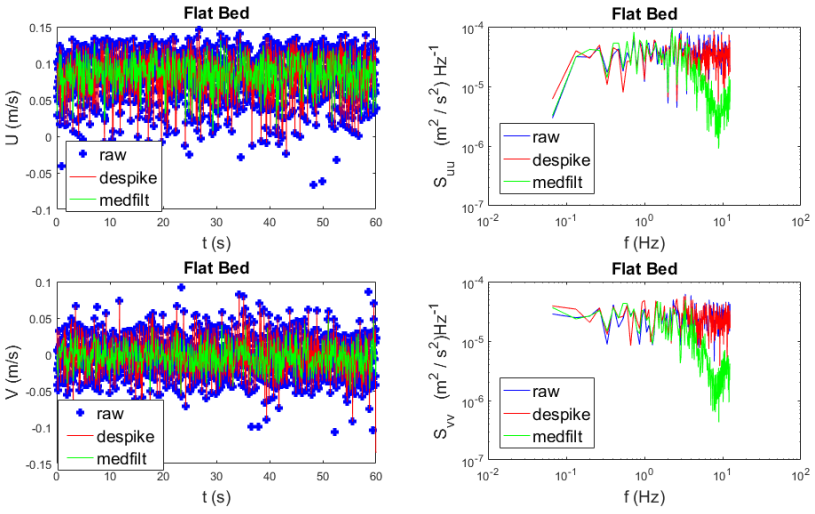

Figure 3.23: FB Case: Two left figures showed the raw and filtered velocity u and v respectively; two right figures showed the corresponding power spectra density S_{uu}, S_{vv}

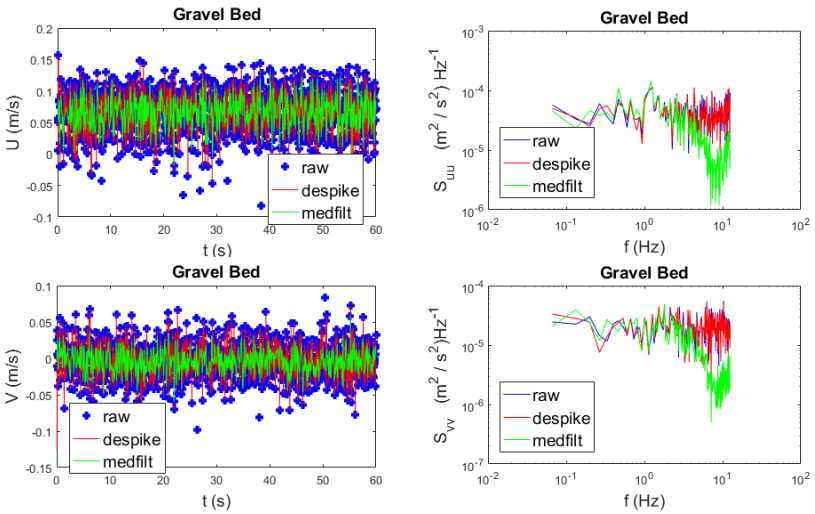

Figure 3.24: GB Case: Two left figures showed the raw and filtered velocity u and v respectively; two right figures showed the corresponding power spectra density S_{uu}, S_{vv}

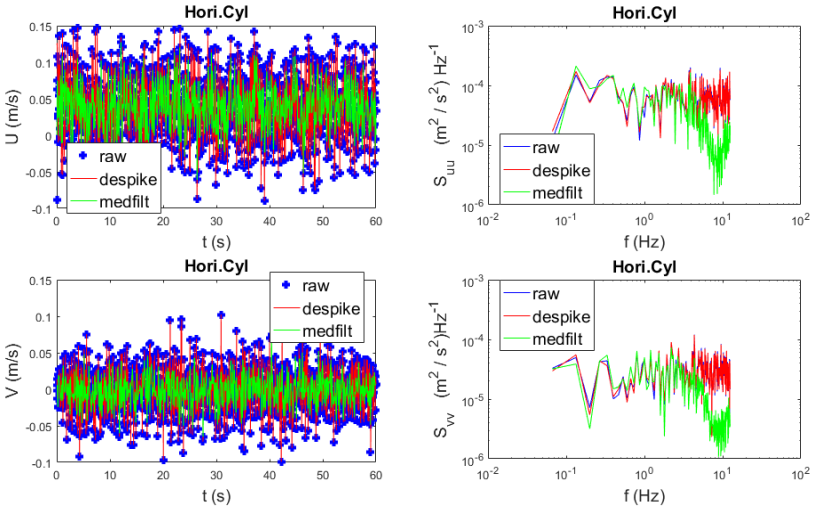

Figure 3.25: Horizontal Cylinder Case: Two left figures showed the raw and filtered velocity u and v respectively; two right figures showed the corresponding power spectra density S_{uu}, S_{vv}

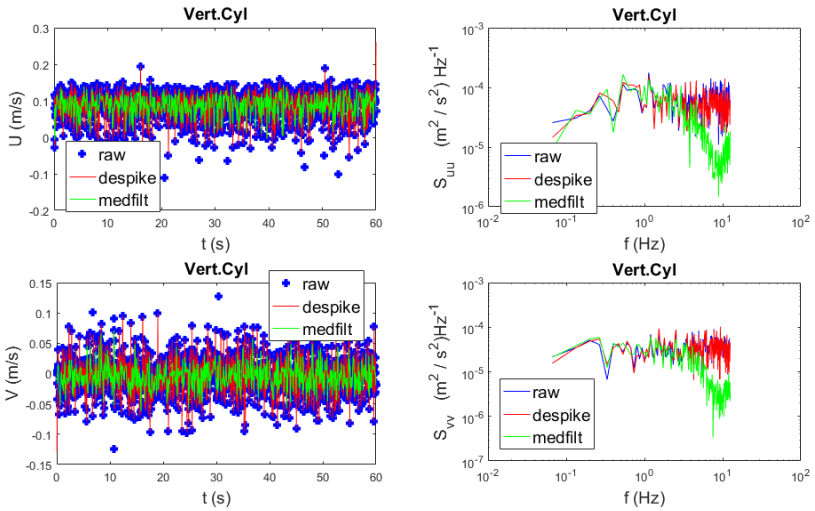

Figure 3.26: Vertical Cylinder Case: Two left figures showed the raw and filtered velocity u and v respectively; two right figures showed the corresponding power spectra density S_{uu}, S_{vv}

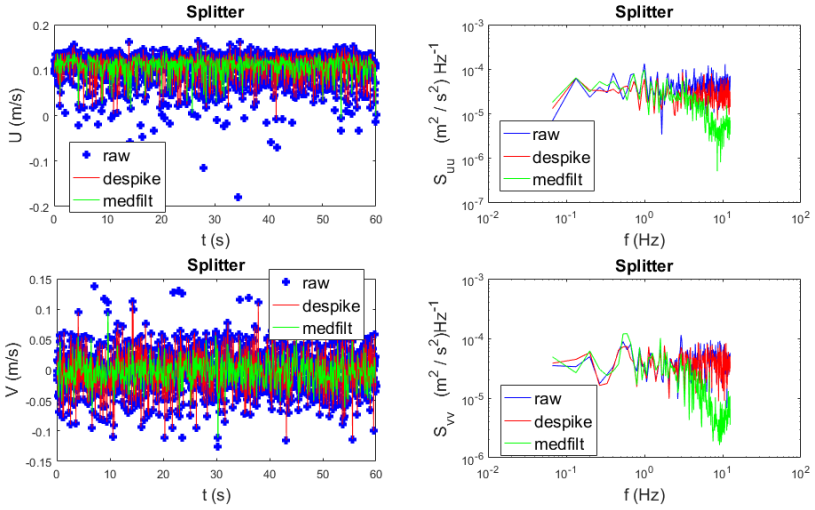

Figure 3.27: Splitter Case: Two left figures showed the raw and filtered velocity u and v respectively; two right figures showed the corresponding power spectra density S_{uu}, S_{vv}

(2) Vertical XZ plane

The same variables are calculated for a vertical XZ plane. Comparing with flat bed case (Figure 3.28), the mean u values present larger spatial gradients in the gravel bed case as Figure 3.29 shows. The horizontal cylinder showed a stronger effect than the vertical cylinder case, which shows similar characteristics as the flat bed case: a uniform u value and opposite v velocity region in front and at the end of the sampling volume, with little differences in w

values (Figure 3.30 and Figure 3.31). In Figure 3.30, the mean lateral velocity shows an obvious wake behind the horizontal cylinder (Z=50-60 mm), and the vertical velocity shows two opposite value regions (positive and negative) above (Z>50mm) and below (Z<50 mm) the horizontal cylinder. The existence of vertical cylinder and splitter plate hardly affected bulk u and v distribution on the chosen XZ plane, while the vertical mean velocities were altered more significantly (Figure 3.31 and Figure 3.32).

The instantaneous velocity and velocity fluctuation values on Figure 3.33–3.37 of XZ planes were also scaled for visual comparison purposes ([-0.1, 0.1] and [-0.5, 0.5], respectively), which showed the same changing patterns among cases as those in XY plane.

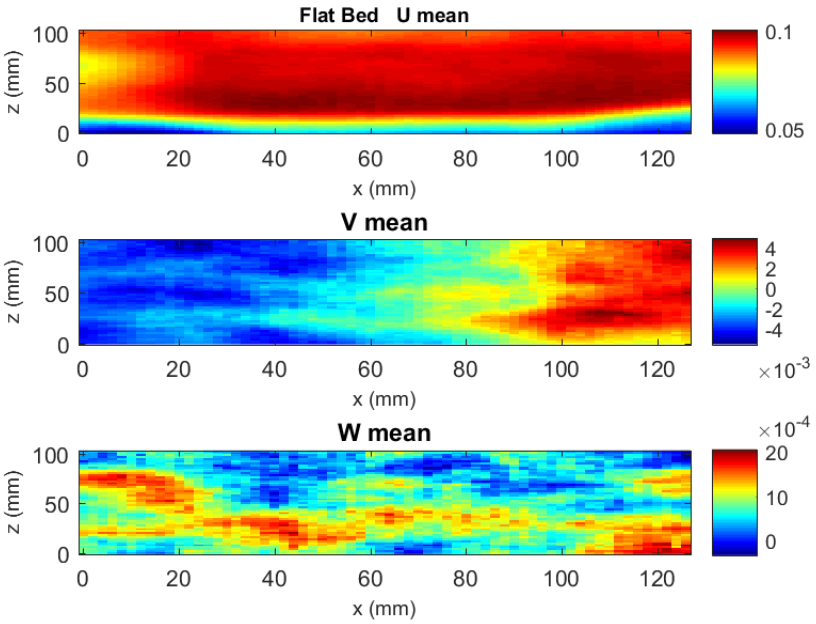

Figure 3.28: FB Case: Mean velocity on XZ plane (Y=54 mm)

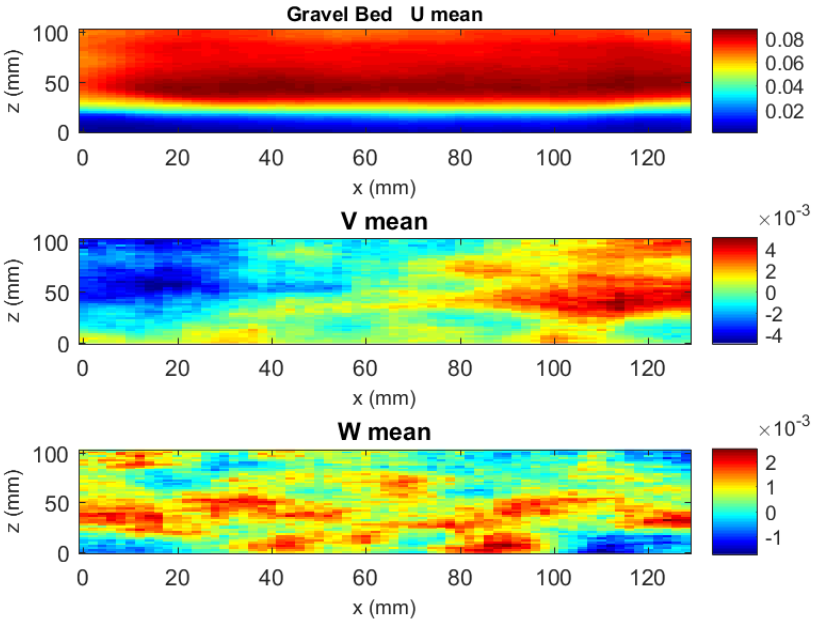

Figure 3.29: GB Case: Mean velocity on XZ plane (Y=54 mm)

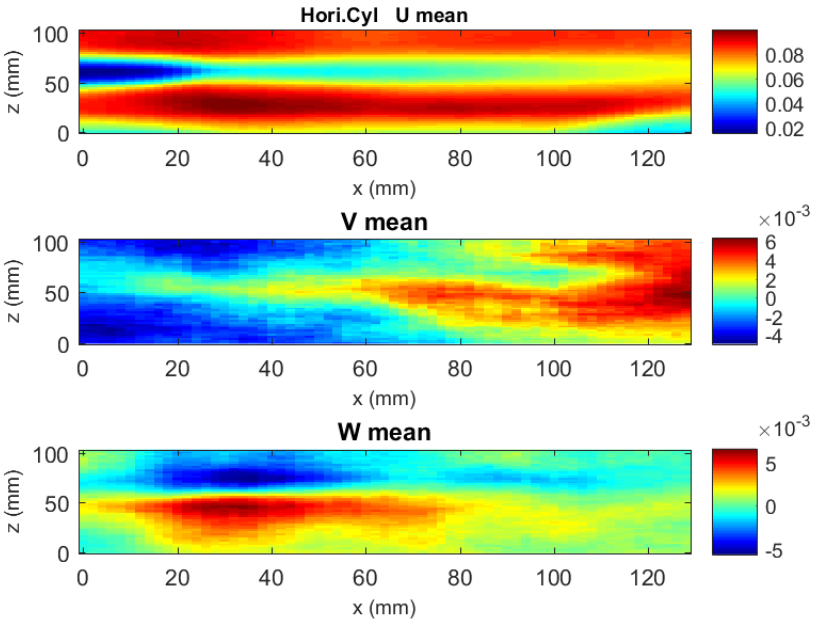

Figure 3.30: Horizontal Cylinder Case: Mean velocity on XZ plane (Y=54 mm)

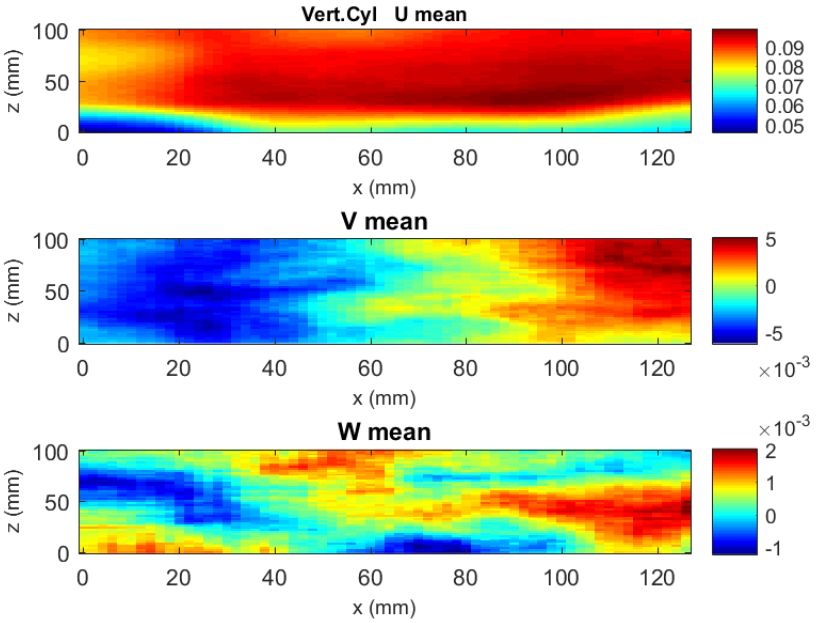

Figure 3.31: Vertical Cylinder Case: Mean velocity on XZ plane (Y=54 mm)

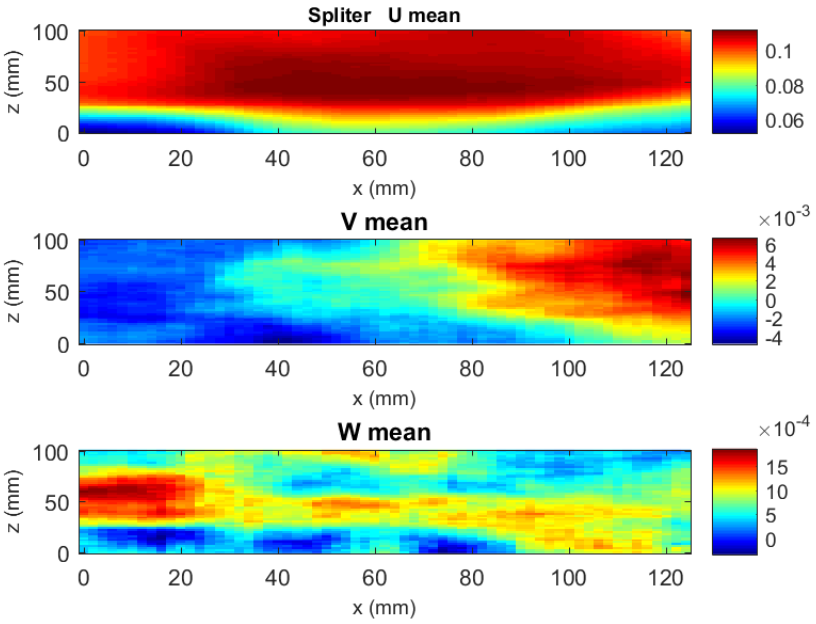

Figure 3.32: Splitter Case: Mean velocity on XZ plane (Y=54)

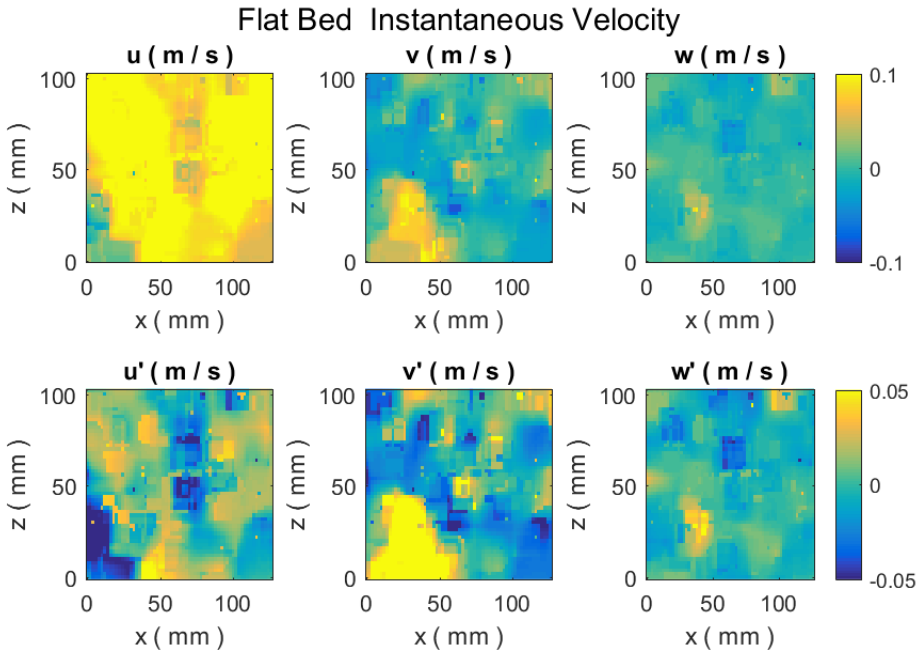

Figure 3.33: Flat Bed Case: Instantaneous velocity (u, v, w) and velocity fluctuation (u', v', w') on XZ plane (Y=54 mm)

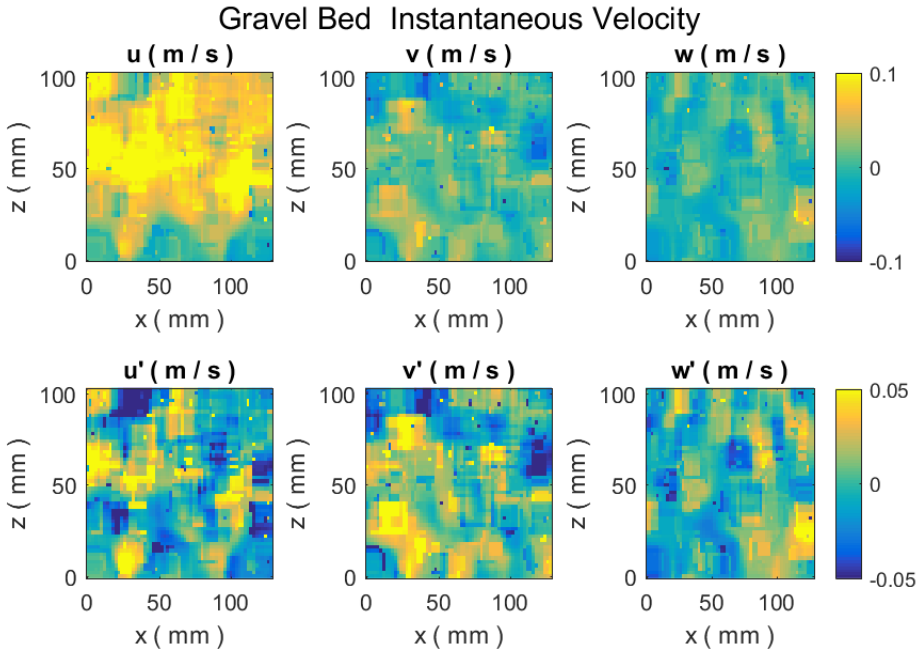

Figure 3.34: Gravel Bed Case: Instantaneous velocity (u, v, w) and velocity fluctuation (u', v', w') on XZ plane (Y=54 mm)

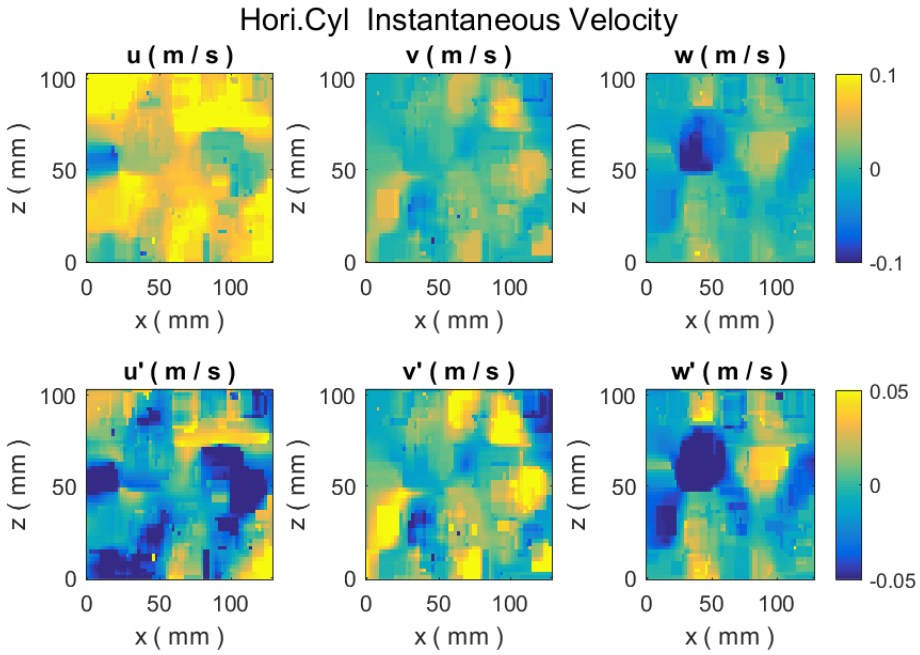

Figure 3.35: Horizontal Cylinder Case: Instantaneous velocity (u, v, w) and velocity fluctuation (u', v', w') on XZ plane (Y=54 mm)

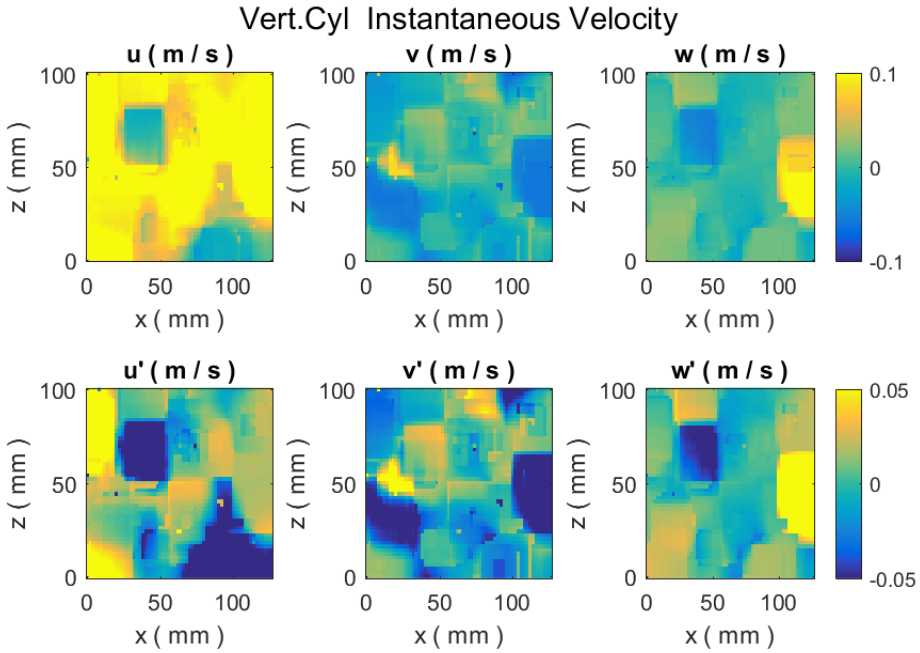

Figure 3.36: Vertical Cylinder Case: Instantaneous velocity (u, v, w) and velocity fluctuation (u', v', w') on XZ plane (Y=54 mm)

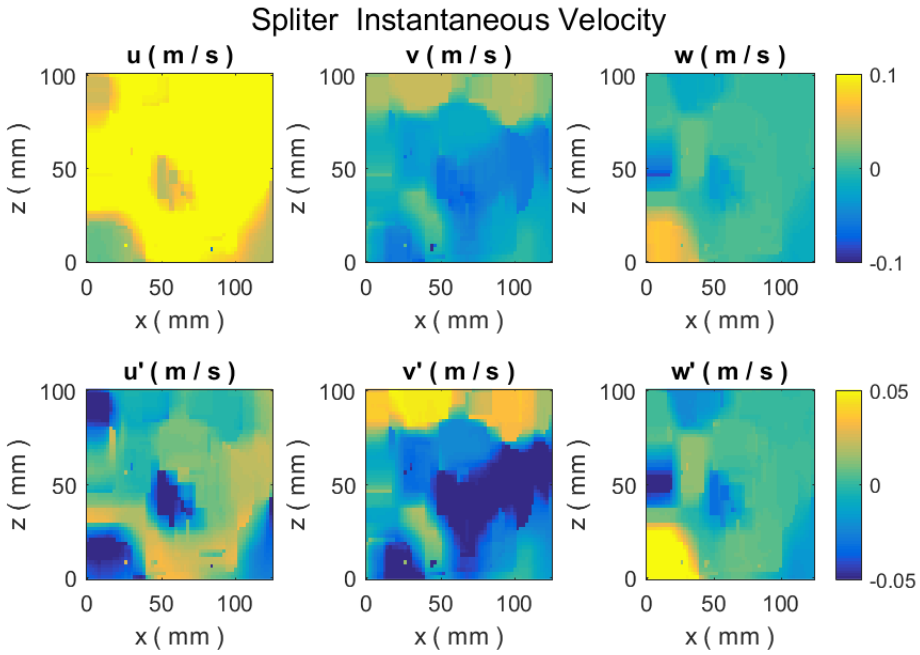

Figure 3.37: Splitter Case: Instantaneous velocity (u, v, w) and velocity fluctuation (u', v', w') on XZ plane (Y=54 mm)

Figure 3.38–3.42 and Figure 3.43 show the instantaneous turbulent intensity u_{rms}, v_{rms} and w_{rms} and TKE of the chosen XZ plane for all 5 scenarios, which exhibited similar variation among cases as described above for the XY plane. Basically, gravel bed and horizontal cylinder both intensified turbulence intensity and TKE evenly over the XZ plane when compared with no obstruction case, and horizontal cylinder increased the parameters much higher than gravel bed. The most obvious increase of turbulence intensity is in the vertical direction (w_{rms}), which was the same for gravel bed and horizontal cylinder cases. Vertical cylinder and splitter plate slightly reduced u_{rms}, but in contrast with the time averaged 3D turbulence intensity information, the instantaneous w_{rms} slightly increased with the splitter plate.

Figure 3.44 collects the vorticity information on the vertical XZ plane. Vorticity on XZ plane of the flume with no obstructions is seemingly uniform. The rotating tendency against y-direction of the control case was less than that against the z-direction. The influence of gravel bed was much more remarkable on the rotation against the y-direction. When flow passed around the horizontal cylinder, it showed opposite vorticity values above (negative, Z>60mm) and below (positive, Z<50mm) the cylinder right be-

hind it ($X < 20mm$), decreasing as flow moves downstream. For the vertical cylinder case, more coherent rotation (larger eddies) were detected through the vorticity field. Opposite values of vorticity on XZ plane with splitter plate were symmetric with respect to the x-direction.

The PSD of a specific point ($X = 6mm, Z = 10mm$), Suu, S_{ww} and S_{vv} were calculated for time series of the velocity at specific representative locations for each scenario (Figure 3.45–3.49) following the description in Chapter 1.

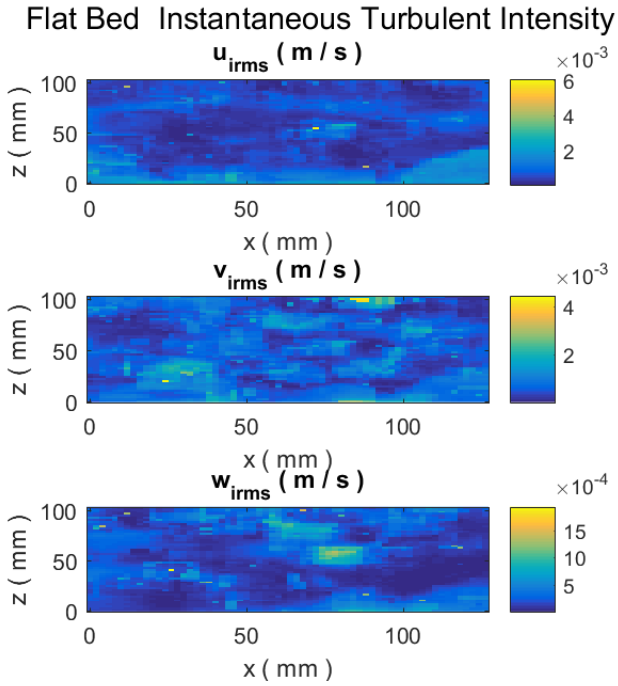

Figure 3.38: FB Case: Instantaneous turbulent intensity (u_{rms}, v_{rms}, w_{rms}) on XZ plane (Y=54 mm)

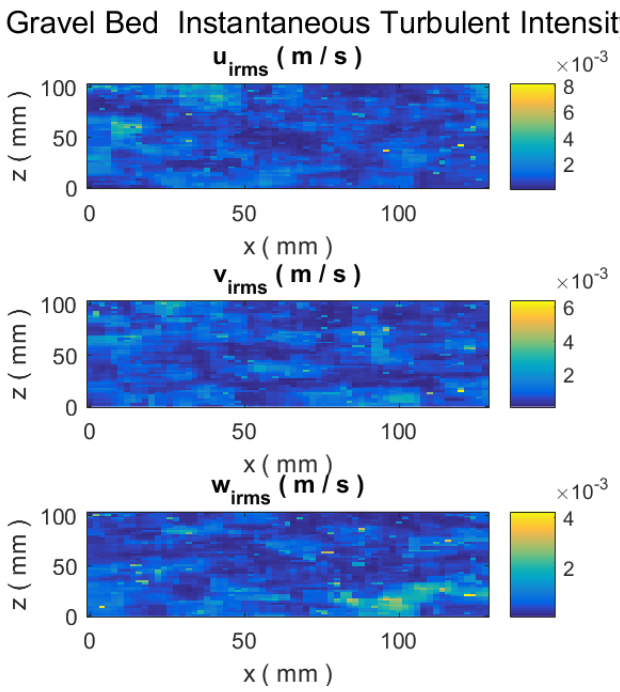

Figure 3.39: GB Case: Instantaneous turbulent intensity (u_{rms}, v_{rms}, w_{rms}) on XZ plane (Y=54 mm)

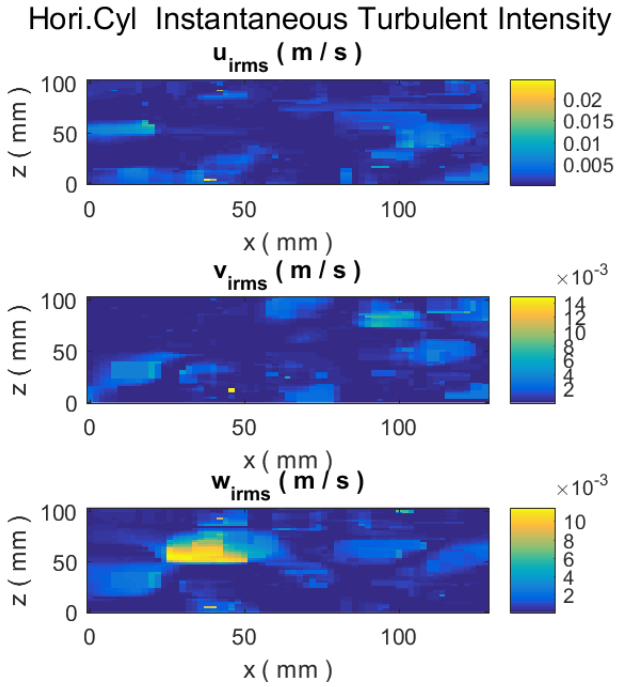

Figure 3.40: Horizontal Cylinder Case: Instantaneous turbulent intensity (u_{rms}, v_{rms}, w_{rms}) on XZ plane (Y=54 mm)

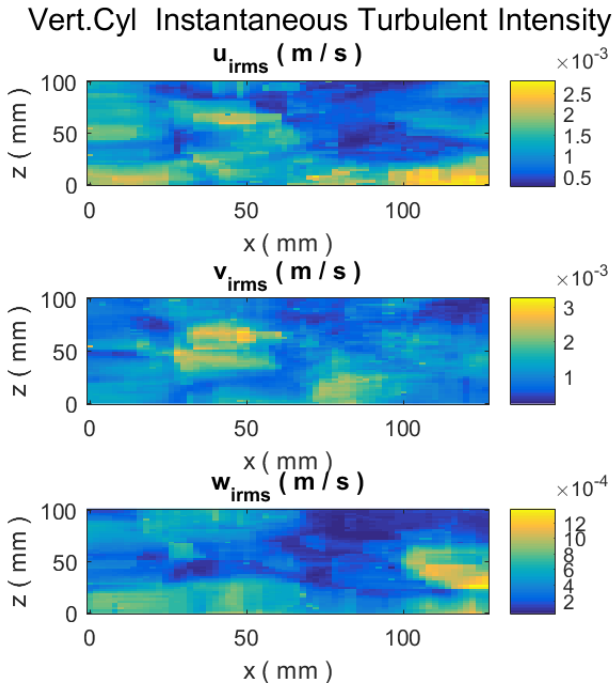

Figure 3.41: Vertical Cylinder Case: Instantaneous turbulent intensity (u_{rms}, v_{rms}, w_{rms}) on XZ plane (Y=54 mm)

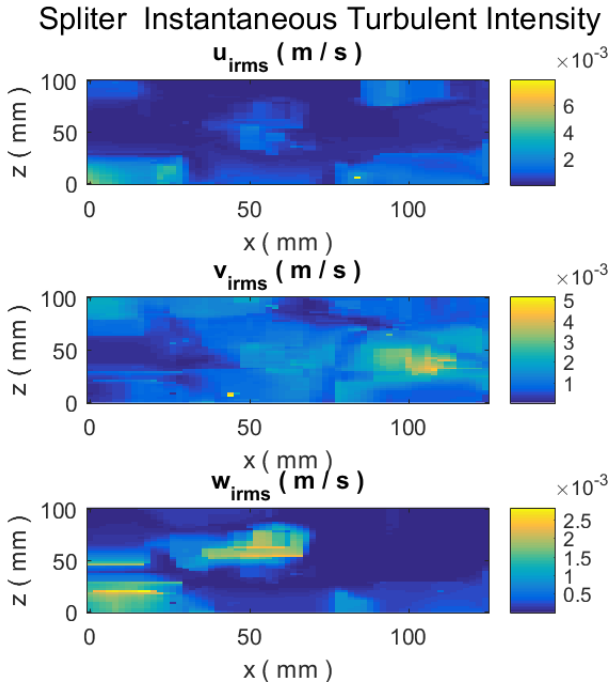

Figure 3.42: Splitter Case: Instantaneous turbulent intensity (u_{rms}, v_{rms}, w_{rms}) on XZ plane (Y=54 mm)

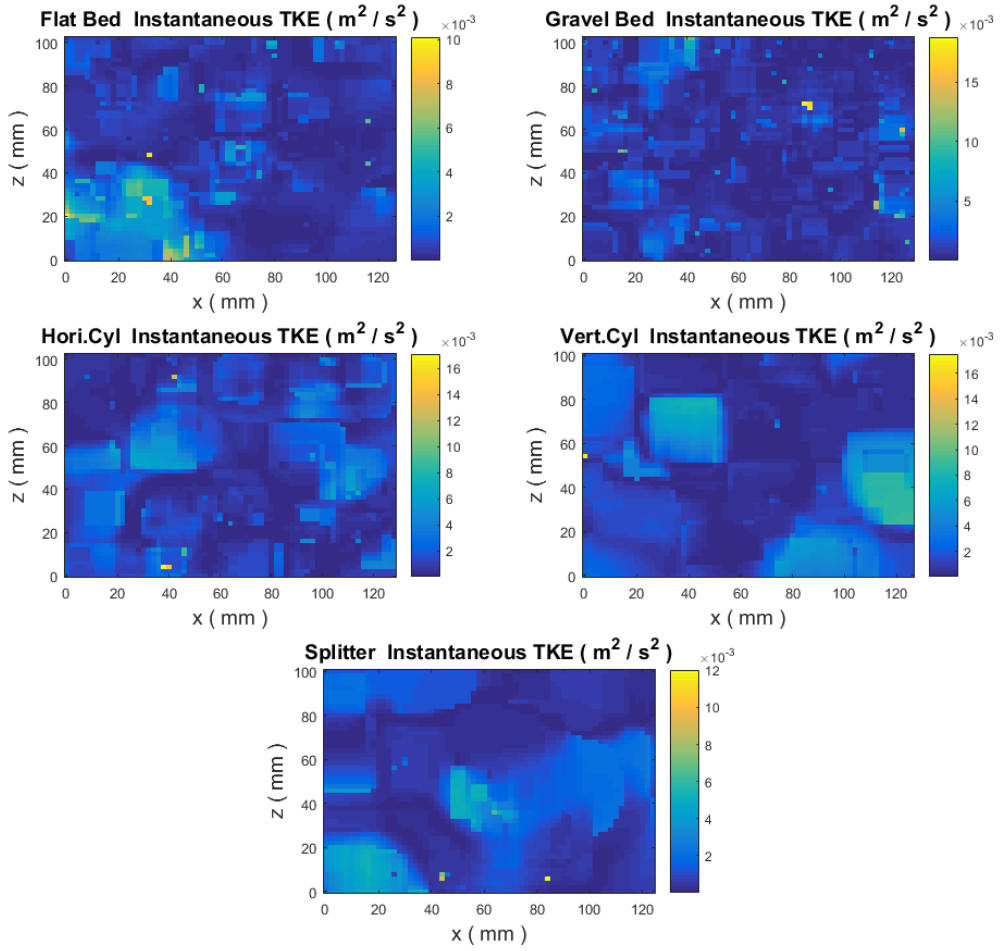

Figure 3.43: Turbulent kinetic energy on XZ plane (Y=54 mm) for FB, GB, Horizontal Cylinder, Vertical Cylinder, and Splitter cases respectively

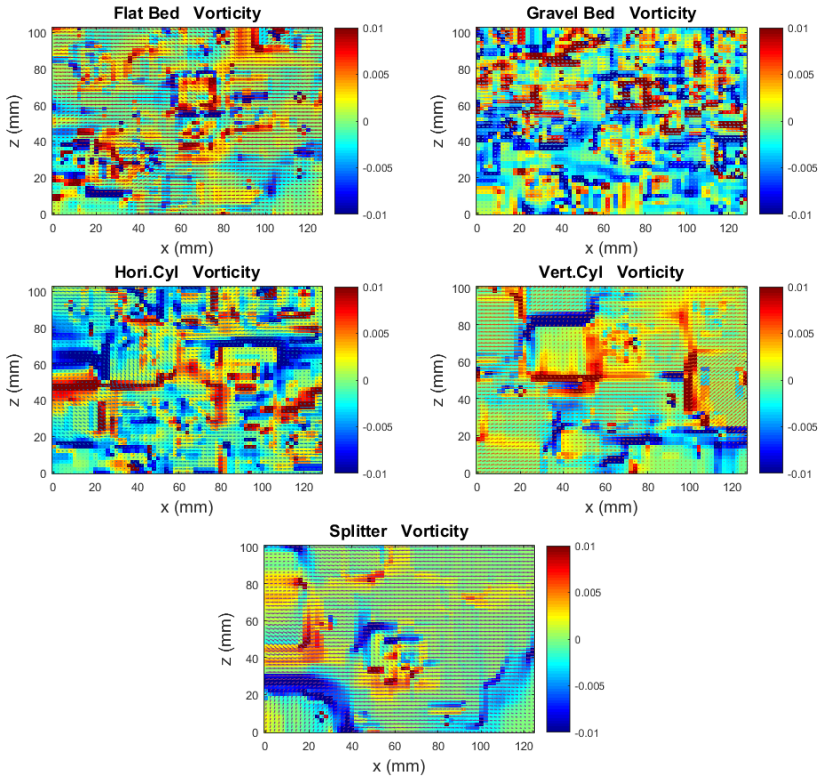

Figure 3.44: Vorticity on XZ plane (Y=54 mm) for FB, GB, Horizontal Cylinder, Vertical Cylinder, and Splitter cases respectively

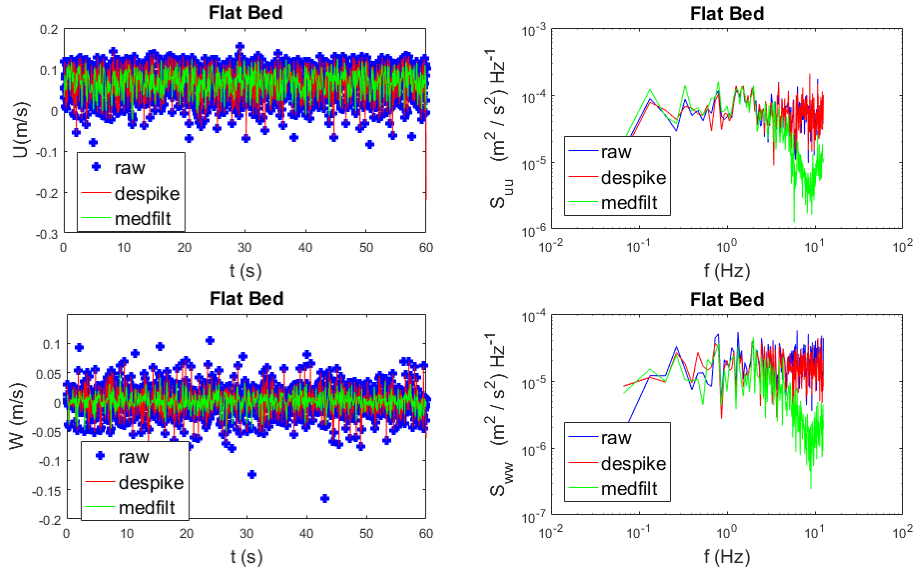

Figure 3.45: FB Case: Two left figures showed the raw and filtered velocity u and w respectively; two right figures showed the corresponding power spectra density S_{uu}, S_{ww}

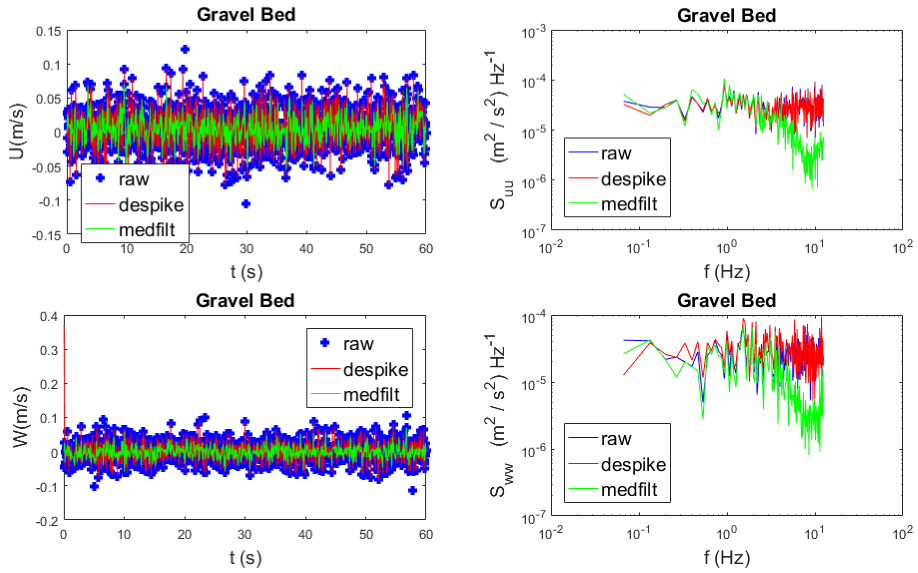

Figure 3.46: GB Case: Two left figures showed the raw and filtered velocity u and w respectively; two right figures showed the corresponding power spectra density S_{uu}, S_{ww}

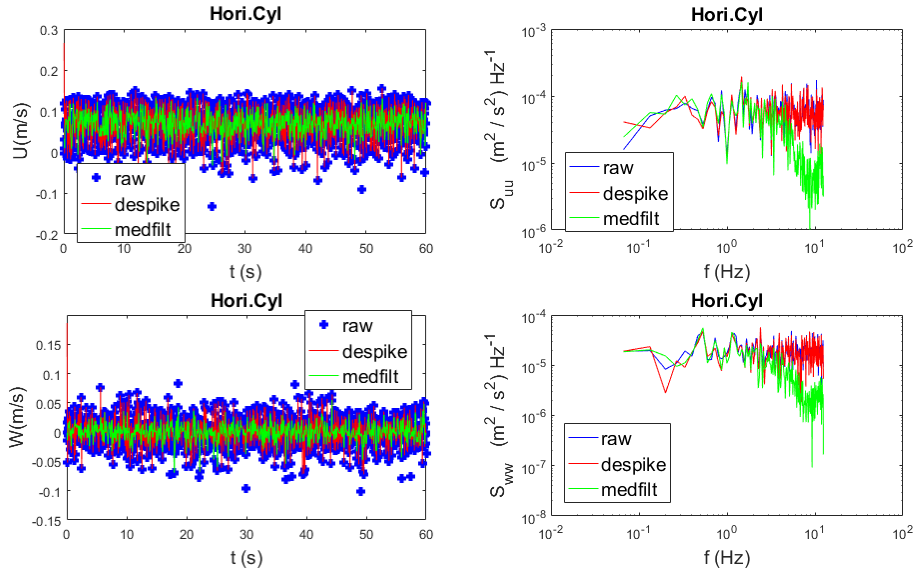

Figure 3.47: Horizontal Cylinder Case: Two left figures showed the raw and filtered velocity u and w respectively; two right figures showed the corresponding power spectra density S_{uu}, S_{ww}

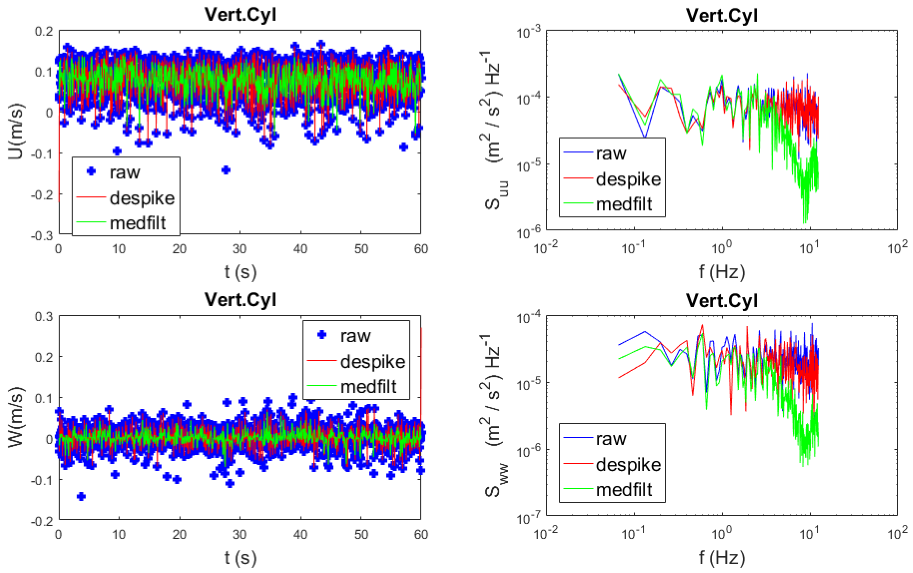

Figure 3.48: Vertical Cylinder Case: Two left figures showed the raw and filtered velocity u and w respectively; two right figures showed the corresponding power spectra density S_{uu}, S_{ww}

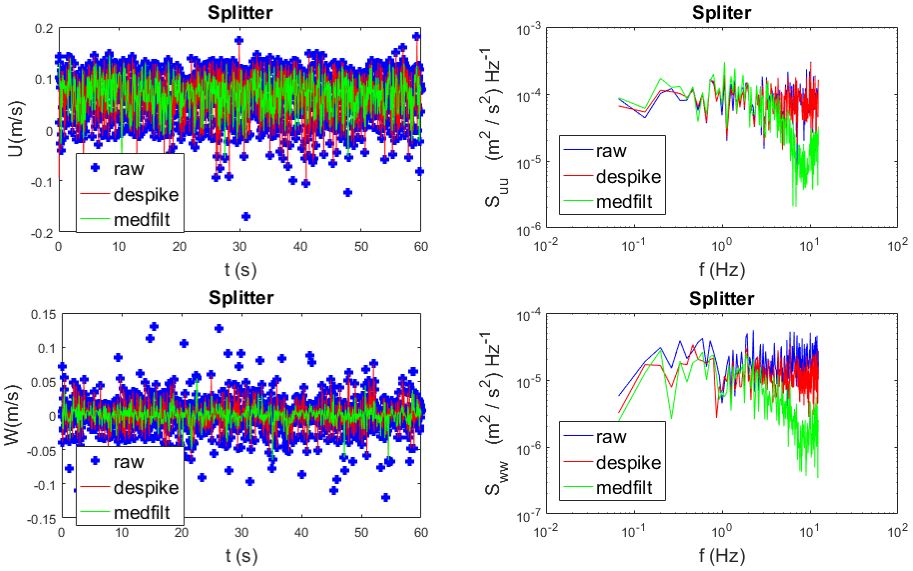

Figure 3.49: Splitter Case: Two left figures showed the raw and filtered velocity u and w respectively; two right figures showed the corresponding power spectra density S_{uu}, S_{ww}

3.2 Fish Swimming Kinematics

3D Position of fish was obtained after analyzing videos of fish swimming from top- and side-view (in XY and XZ planes respectively) in MATLAB. With the position information of fish eye (side view) and snout (top view) arranged as time series, swim speed and acceleration were straightforward calculated. The location of tail starting- and end-points were also identified at each time-step, and used to calculate tail beat amplitude and frequency for each scenario.

3.2.1 Fish Position

Figure 3.50 shows the (X, Z) position of fish eye and fish locomotion through time extracted from side view videos for each of the 5 cases. Similarly, the (X, Y) position and locomotion of fish snout are shown in Figure 3.50–3.51.

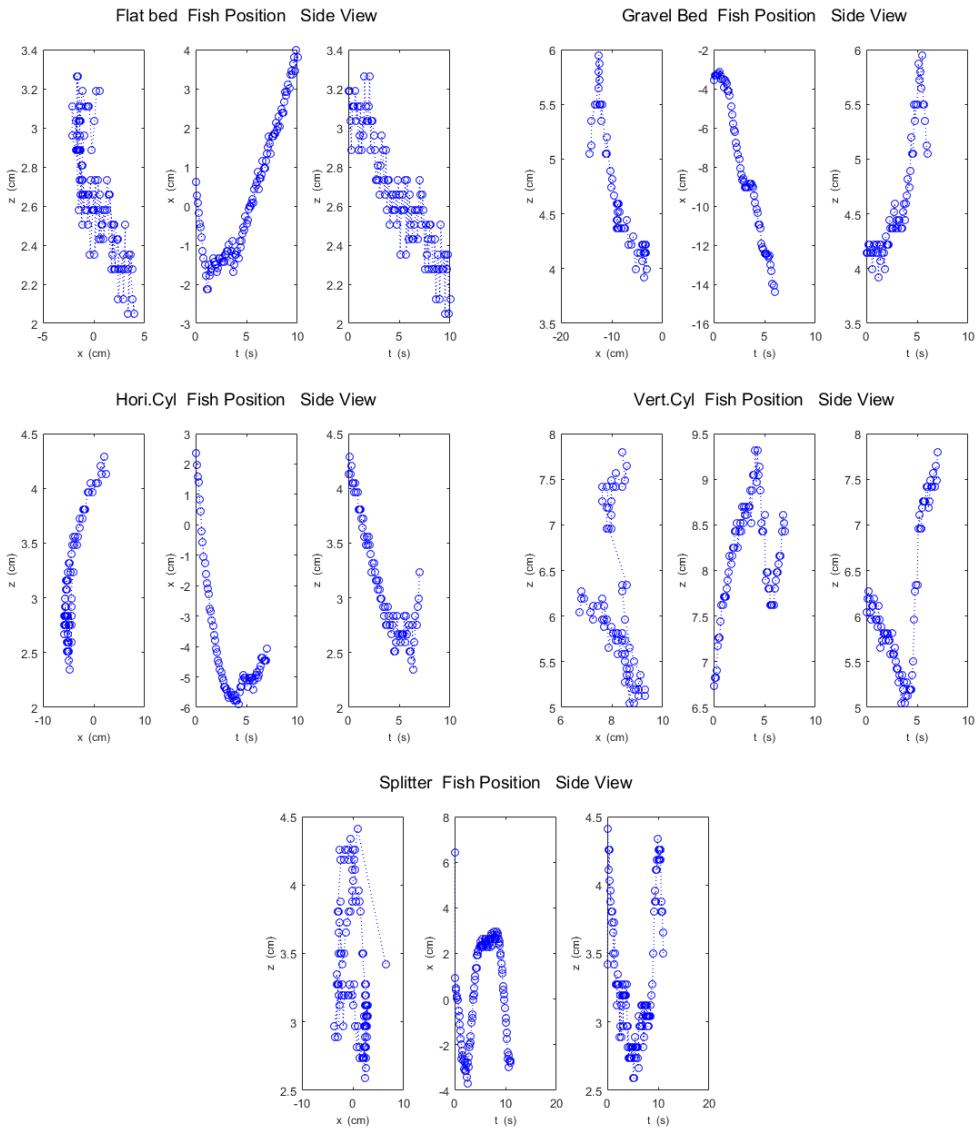

Figure 3.50: Fish position shown in side plane and in time series under 5 cases

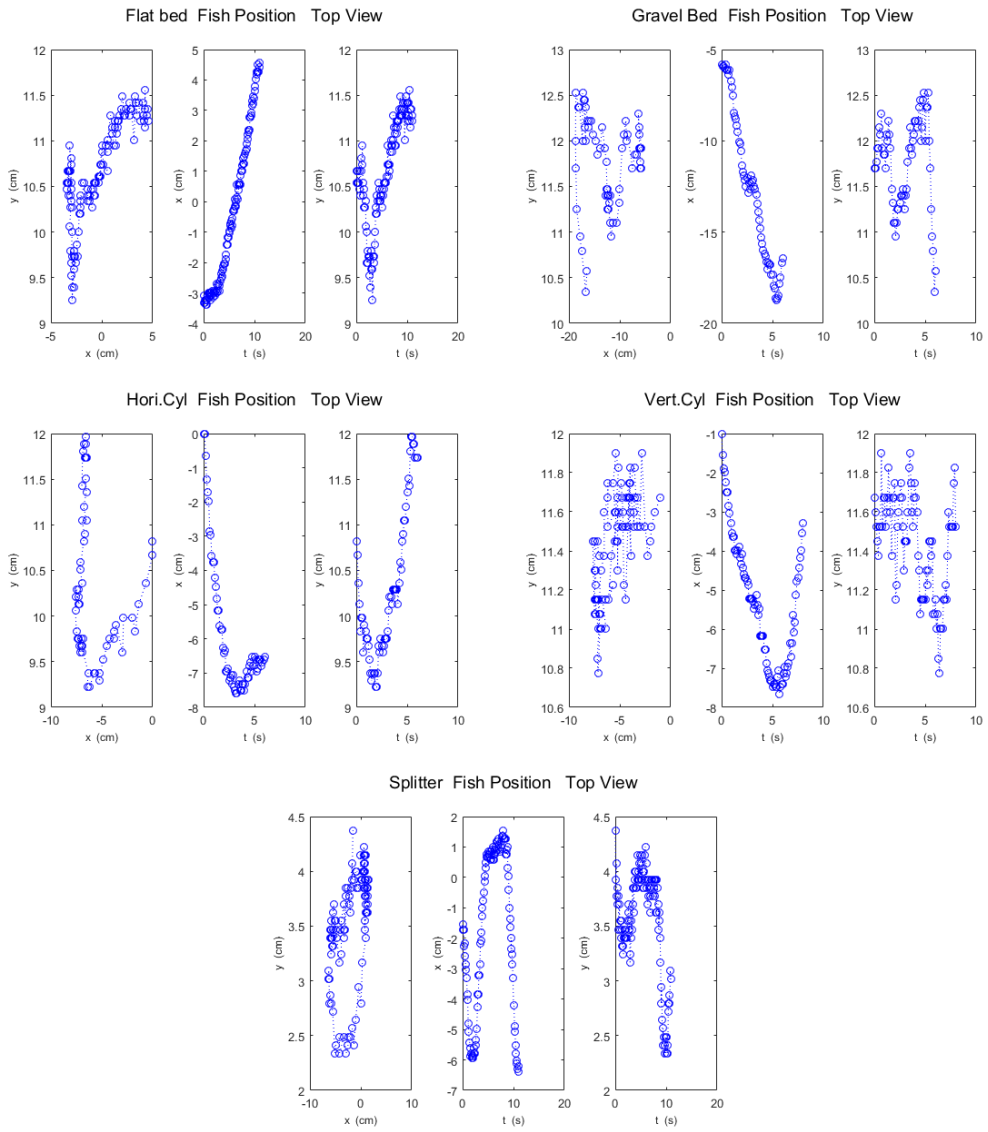

Figure 3.51: Fish position shown in top plane and in time series under 5 cases

3.2.2 Fish Swimming speed and Acceleration

Figure 3.52 shows a 6-second segment of displacement and swimming speed of fish. Figure 3.53 shows speed acceleration in X, Y, Z direction.

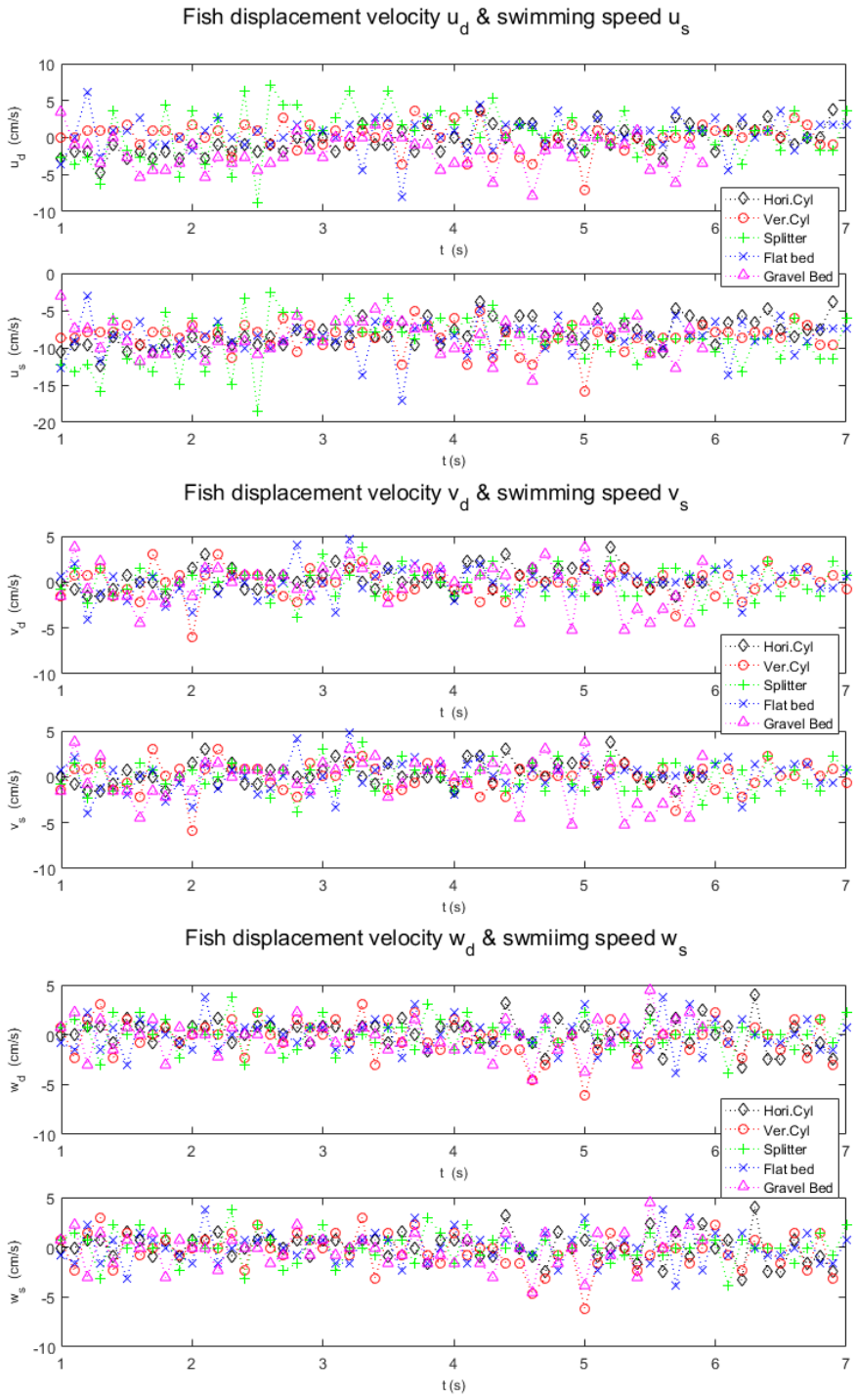

Figure 3.52: Fish displacement speed (u_d) and swimming speed (u_s)

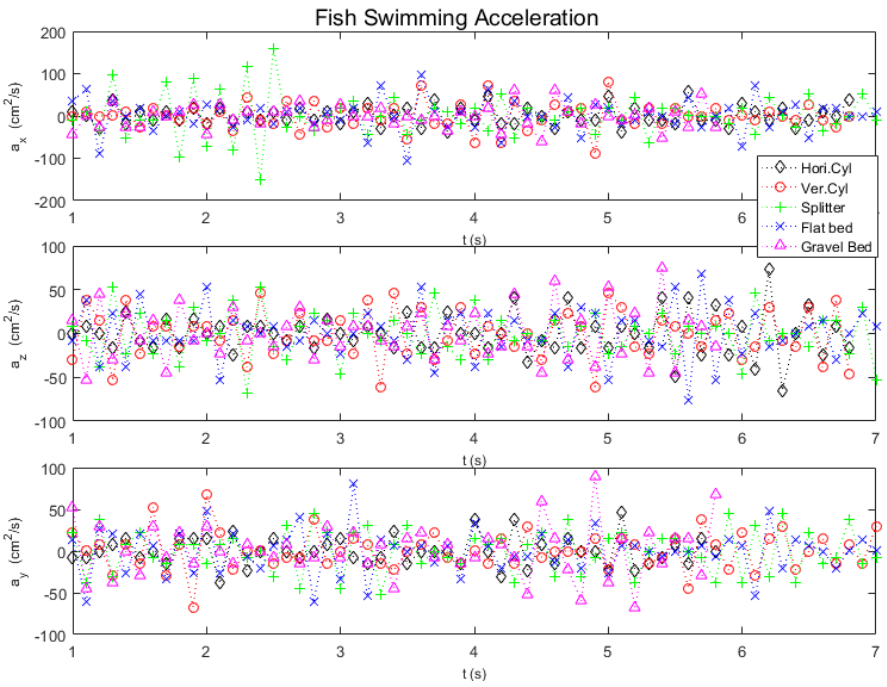

Figure 3.53: Fish swimming acceleration

3.2.3 Tail Beat Characterization

The tail beat frequency and amplitude were manually calculated based on the time series of Y-position of fish tail, with the x-y coordinates aligned to the fish body (i.e., the reference frame is rotated on each time step to correspond to the longitudinal axis of the fish body to remove the effects of changing orientation of the fish and isolate the motion of the tail). Each beat cycle was determined with graphic help for better identification. The y-direction distance between consecutive peak and bottom values in a cycle were determined as tail beat amplitude, while the time between peaks were calculated as the reversion of tail beat frequency (TBF). Results from all cases considered are presented in Table 3.1.

Table 3.1: Tail beat amplitude and frequency organized by fish number

Fish No.	Swim Condition	Tail Beat Frequency (Hz)	Tail Beat Amplitude (cm)	No-dimensional Tail Beat Amplitude ($\times 10^{-2}$)	Useful segments (s)
3	Splitter	1.856	1.812	9.889	58
4	Gravel Bed	2.024	2.053	11.241	102
5	Hori.Cyl	2.028	1.773	9.921	29
6	Vert.Cyl	1.864	1.929	9.876	15
7	Flat Bed	1.652	1.433	7.451	11
9	Hori.Cyl	1.819	1.921	10.439	21
10	Hori.Cyl	1.848	1.685	8.980	13
14	Vert.Cyl	1.917	1.550	7.786	21
16	Flat Bed	1.672	1.655	8.765	19

CHAPTER 4

DISCUSSION

In this section, the hydraulics data analysis and recorded fish swimming behavior are studied together in an effort to identify potential correlations between hydraulic and physiological data.

4.1 Tail Beat Behavior and Flow Characteristics

Tail beat frequency reveals the activity and cost of fish swimming behavior, which is proven to be linearly related to vortex shedding frequency of the flow by many studies. Figure 4.1 shows the relationship between tail beat frequency and vortex shedding frequency under each case, which has a basic linear relationship. This result is consistent with past findings, validating fish data-sets in the five tested cases.

Tail beat frequency and tail beat amplitude were plotted against maximum bulk velocity (Figure 4.2) and turbulent characteristics, including Reynolds stress (Figure 4.3), turbulent intensity (Figure 4.4), turbulent kinetic energy (Figure 4.5) and vorticity (Figure 4.6), to investigate how different flow parameters influence fish swimming response. The compared value of hydraulic parameters (using absolute values to account for negative and positive extremes) is calculated over a volume contained within x=0 - 50 mm, across all y- and z-values to pick the maximum value. It is noted that there is no particular change or identifiable tendency of neither frequency nor amplitude due to bulk velocities (see Figure 4.2). In Figure 4.3, Figure 4.4, and Figure 4.6, the non-dimensional tail beat amplitude had a rough linear relationship with Reynolds stress ($u'v'$), turbulent intensity (v_{rms}) and vorticity, respectively.

Therefore, bulk velocity does not seem to drive fish response, and thus more attention should be paid to turbulent characteristics with the help of

advanced measurement techniques such as the 3D velocimetry system used in the present study, for better understanding of fish swimming mechanism and better prediction of fish position in rivers altered with in-stream structures.

Figure 4.7 illustrates the mean swimming speed of fish with standard error and the intensity of its fluctuation (u_{srms}, v_{srms}, w_{srms}) for all 5 scenarios. The intensity of swimming speed fluctuations were calculated in the same way of turbulent intensity. In this figure, swimming against the mean flow direction is identified as negative.

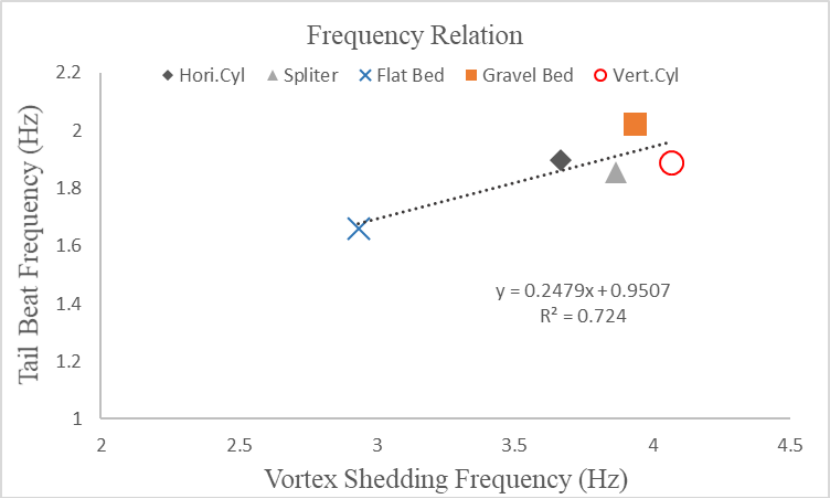

Figure 4.1: Correlation between vortex shedding frequency and tail beat frequency

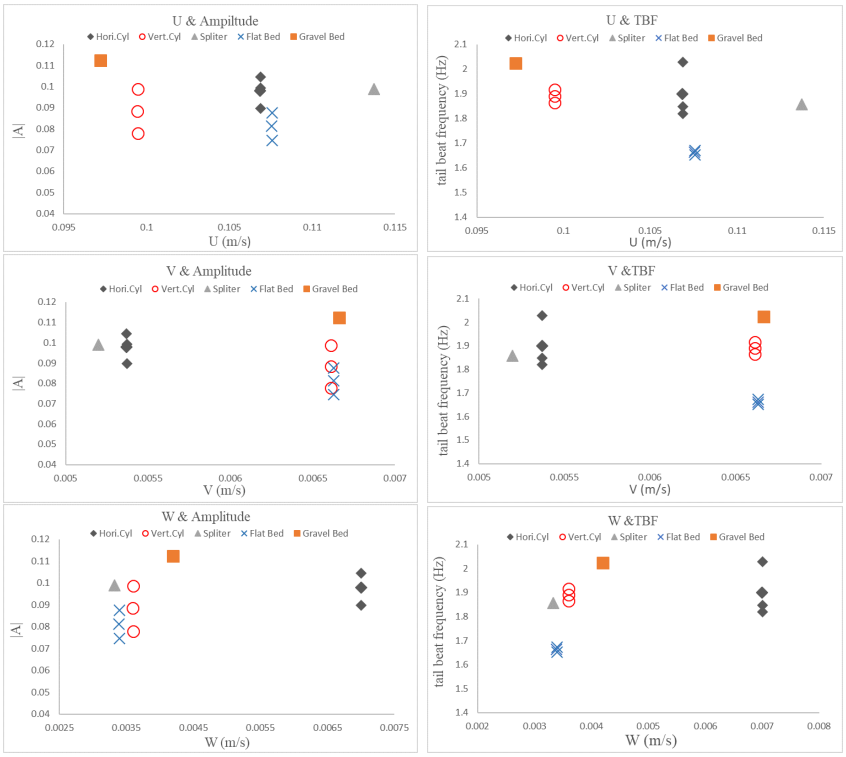

Figure 4.2: Correlation between tail beat behavior and mean bulk velocity

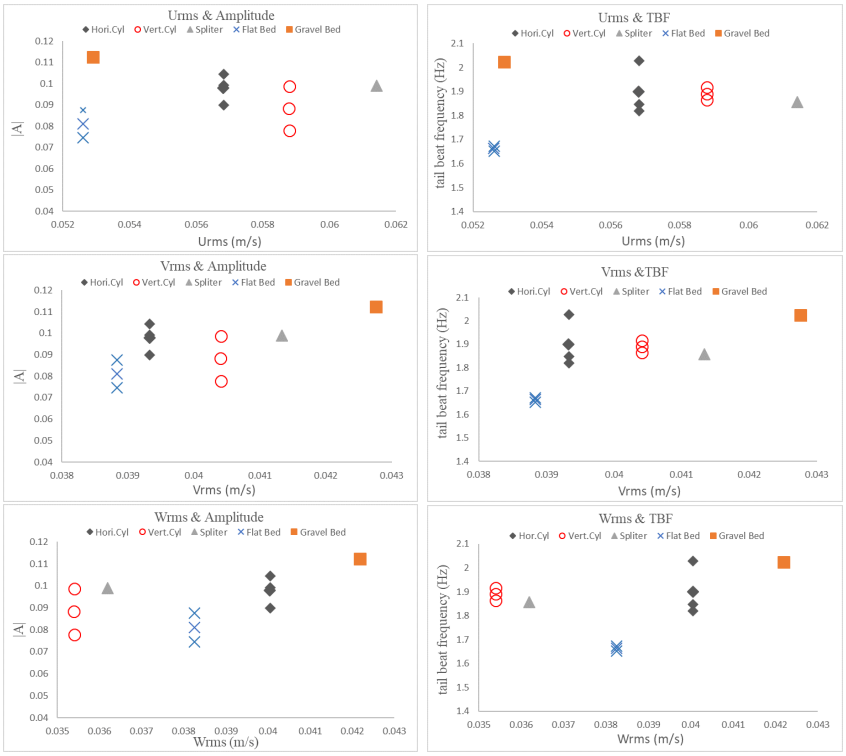

Figure 4.3: Correlation between tail beat behavior and turbulent intensity

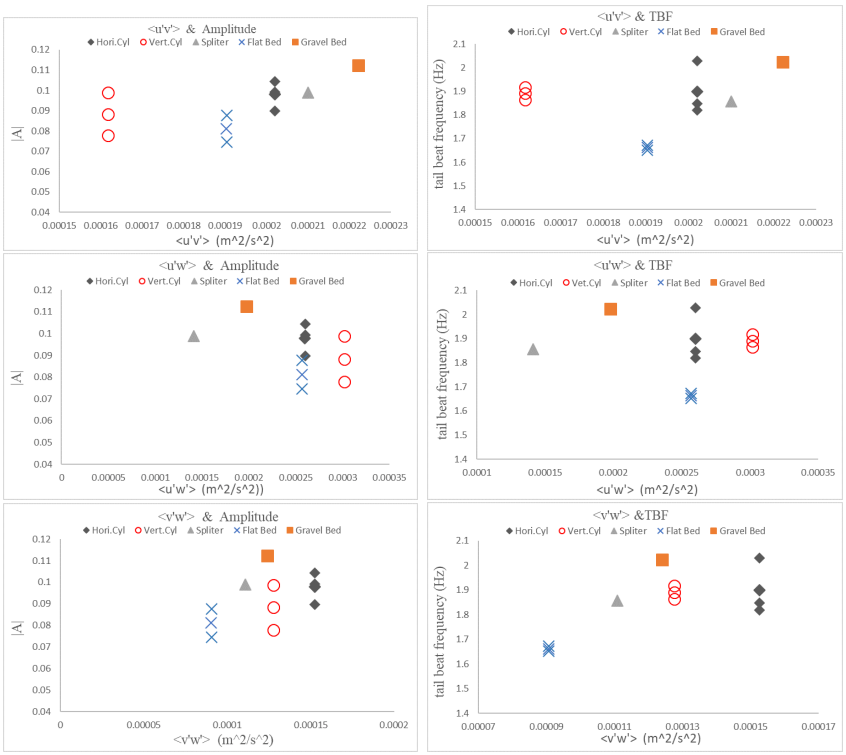

Figure 4.4: Correlation between tail beat behavior and Reynolds stress

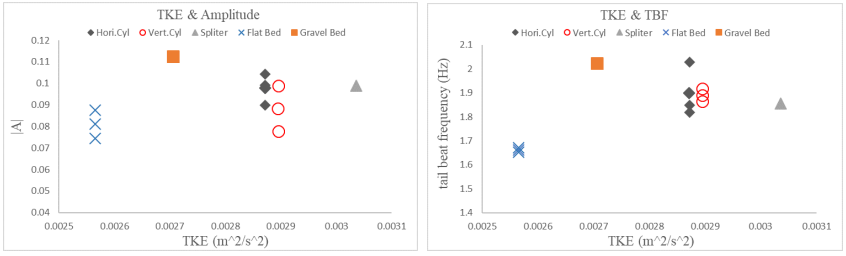

Figure 4.5: Correlation between tail beat behavior and turbulent kinetic energy

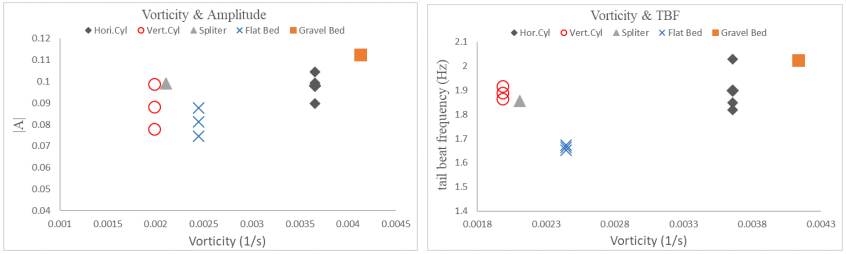

Figure 4.6: Correlation between tail beat behavior and vorticity

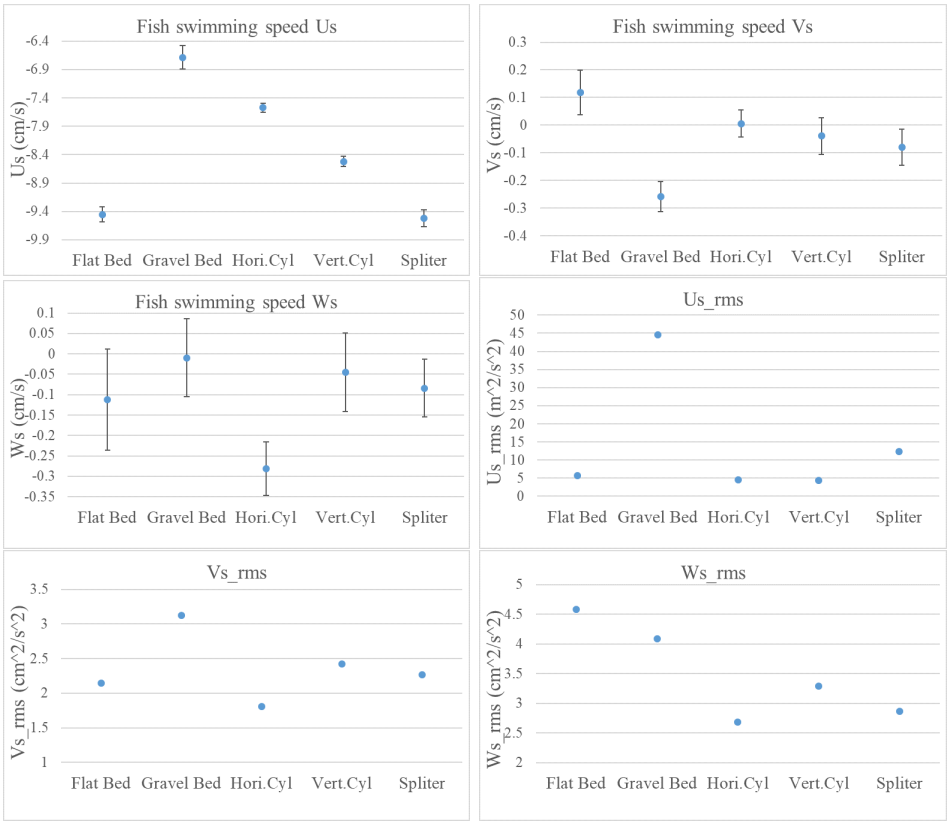

Figure 4.7: Mean fish swimming velocity and fluctuation intensity

4.2 Fish Locomotion and Flow Characteristics

Fish position was plotted against flow parameters including mean velocities and turbulent characteristics (Figure 4.8–4.29). The chosen slides were determined by the frequency of fish appearance. For example, the chosen Z for XY plane was obtained by the Z position where fish appeared most frequently. The chosen Z value for XY plane of flat bed, gravel bed, horizontal cylinder, vertical cylinder and splitter case were 30, 70, 25, 29, 39 mm, respectively. And the chosen Y value for XZ plane of the above case were 81, 90, 13, 22, 29 mm respectively. Besides, since data-sets of fish position for several cases were obtained from more than one fish, different markers $(\times, \circ, \triangle)$ were used for tested fish. It is found that fish tend to swim towards the outer wall in most cases, which falls outside the field of view of the V3V system.

Under flat bed and gravel bed cases, fish appeared in regions of lower longitudinal velocity more frequently, while under the other cases, they appeared in regions of higher longitudinal velocity (Figure 4.8–4.9), resulting in no specific position preferences related to mean bulk velocity (Figure 4.8–4.13). In contrast, Figures 4.14–4.19 clearly indicate that fish preferred areas with low turbulent intensity. However, this is not observed for all cases. For example, in the two cylinder cases, fish were also observed in regions with high turbulent intensity (v_{rms} and w_{rms}). Figure 4.20–4.25 revealed that fish were more active in regions with high Reynolds stress. Lower turbulent kinetic energy areas seemed to be easier for fish to swim, while with the presence of horizontal cylinder, vertical cylinder and splitter plate, fish are also capable of swimming in higher TKE regions (Figure 4.26–4.27). Regions with low vorticity (absolute value of ω_{xy}, ω_{xz}) also seemed to attract fish, as seen in Figure 4.28–4.29 .

For the horizontal cylinder case, fish stayed in areas with high longitudinal velocity or at the edge between low and high u velocity, where the lateral velocity is negative or close to zero, and the vertical velocity is relatively high. The longitudinal and vertical turbulent intensity of preferred regions are seemingly lower, right behind high intensity areas, while some preferred regions also had high lateral turbulent intensity. Fish in horizontal cylinder cases are mainly attracted to high Reynolds stress. Low turbulent kinetic energy areas attracted fish the most, coinciding with relatively high vorticity levels.

For the vertical cylinder case, fish appeared in both high and low longitudinal velocity regions with no specific preference, where the lateral velocity are mainly positive. The vertical velocity showed no clear influence on fish locomotion in this case. Fish still appeared frequently in low turbulent intensity regions. However, the presence of the vertical cylinder may result in the more frequent trail in high turbulent intensity region. In this case, fish were still active in regions with high Reynolds stress, but appeared in transit regions more frequently compared with the horizontal cylinder case. Low turbulent kinetic energy regions were dominant as a fish choice, with fish also often observed in regions with high turbulent kinetic energy with relatively high vorticity.

For the splitter plate, fish were found basically in high longitudinal velocity regions, with large negative lateral velocity. This is unlike the above two

cases, where fish also appeared in transit regions. The higher vertical velocity areas seem attractive for fish swimming. High Reynolds stress $u'v'$ (positive) and $u'w'$ (negative) regions were preferred by fish, where the $v'w'$ values were near the edge of negative values. Similarly to vertical cylinder case, fish stayed mostly in low TKE regions with few appearing in high TKE regions.

For the gravel bed case, most locations of fish were outside the studied volume with hydrodynamic data available. Based on the limited information, it can be predicted that fish stayed in possible low longitudinal velocity region. Vertical velocity didn't show a clear influence on fish position choice. Low turbulent intensity regions were more popular for fish which was consistent with other cases. High Reynolds stress regions were attractive for fish, but more specimens were found in transit regions between high and low Reynolds stress than other cases. Fish stayed in low turbulent kinetic energy regions in this case, where the vorticity values were still low in absolute value.

For the flat bed case, fish preferred areas near the back wall and stayed in regions close to the bed. In this case, fish was not always in regions with high longitudinal velocity, while the lateral velocities were also large (negative), and vertical velocities were low. Fish stayed in low turbulent intensity regions (u_{rms}, v_{rms}, w_{rms}) like other cases, where the Reynolds stress were high and the turbulent kinetic energy were low. The vorticity along y-direction (ω_{xz}) in regions where fish frequently appeared were relatively low, while the vorticity ω_{xy} was relatively high at those preferred areas.

From the horizontal view, fish positions spread uniformly along the y-direction in all 5 cases. In the vertical cylinder case, fish appeared on both sides of the vertical cylinder, which means that its existence probably disturbed the stability of fish, forcing the fish to explore different regions. The splitter plate had a similar influence on fish, which can be seen from their hydraulic environment patterns and the fish location distribution.

From the vertical view it is found that, for the horizontal cylinder, fish position are along a consistent line in regions below the cylinder, while for other cases the spread is more uniform, especially in the gravel bed case. Fish seemingly avoid the near-bed region in gravel beds, plagued by high turbulence levels, and move towards the top pf the tunnel, in contrast to the flat bed case, where fish are able to swim closer to the bottom. This is probably because of the higher turbulent fluctuation (w_rms) and TKE in the bottom region making harder for fish to maintain position and stability.

To further investigate fish swimming response, the oxygen consumption under each case was considered (Data provided by Prof. Cory Suski, a collaborator at UIUC). Figure 4.30 reflected the swimming costs under each scenario, among which fish swimming behind a horizontal cylinder had the lowest energy cost. One reasonable explanation is the fish utilizing the vertical vortices generated by the horizontal cylinder. However, the energy cost of fish swimming with gravel bed was highest, likely due to the abundance of small eddies generated in the near bed region increasing swimming difficulty. This finding is consistent with the increased tail beat amplitude and frequency identified in the gravel bed case.

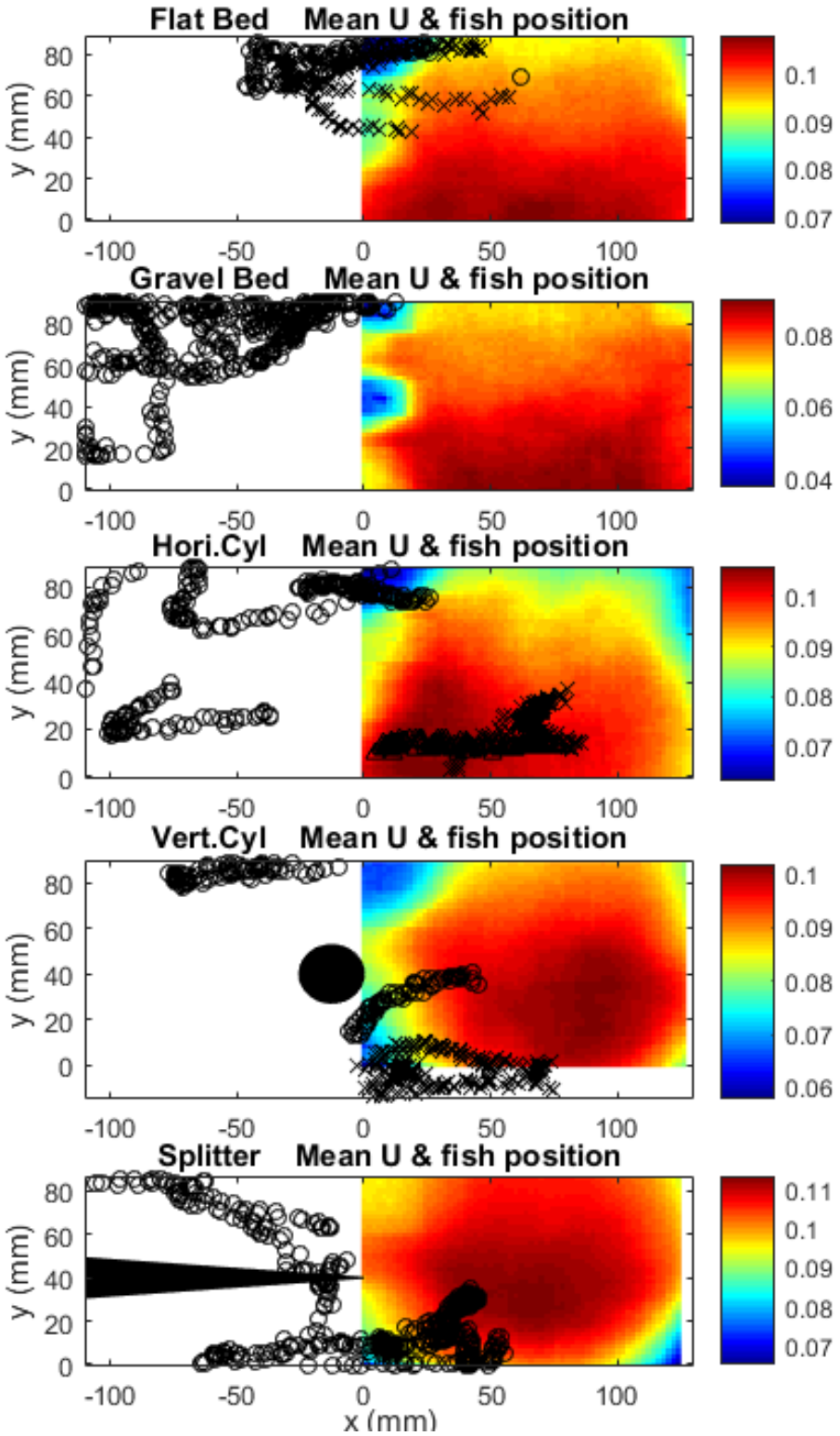

Figure 4.8: Correlation between fish position choice on XY plane and mean longitudinal velocity (m/s)

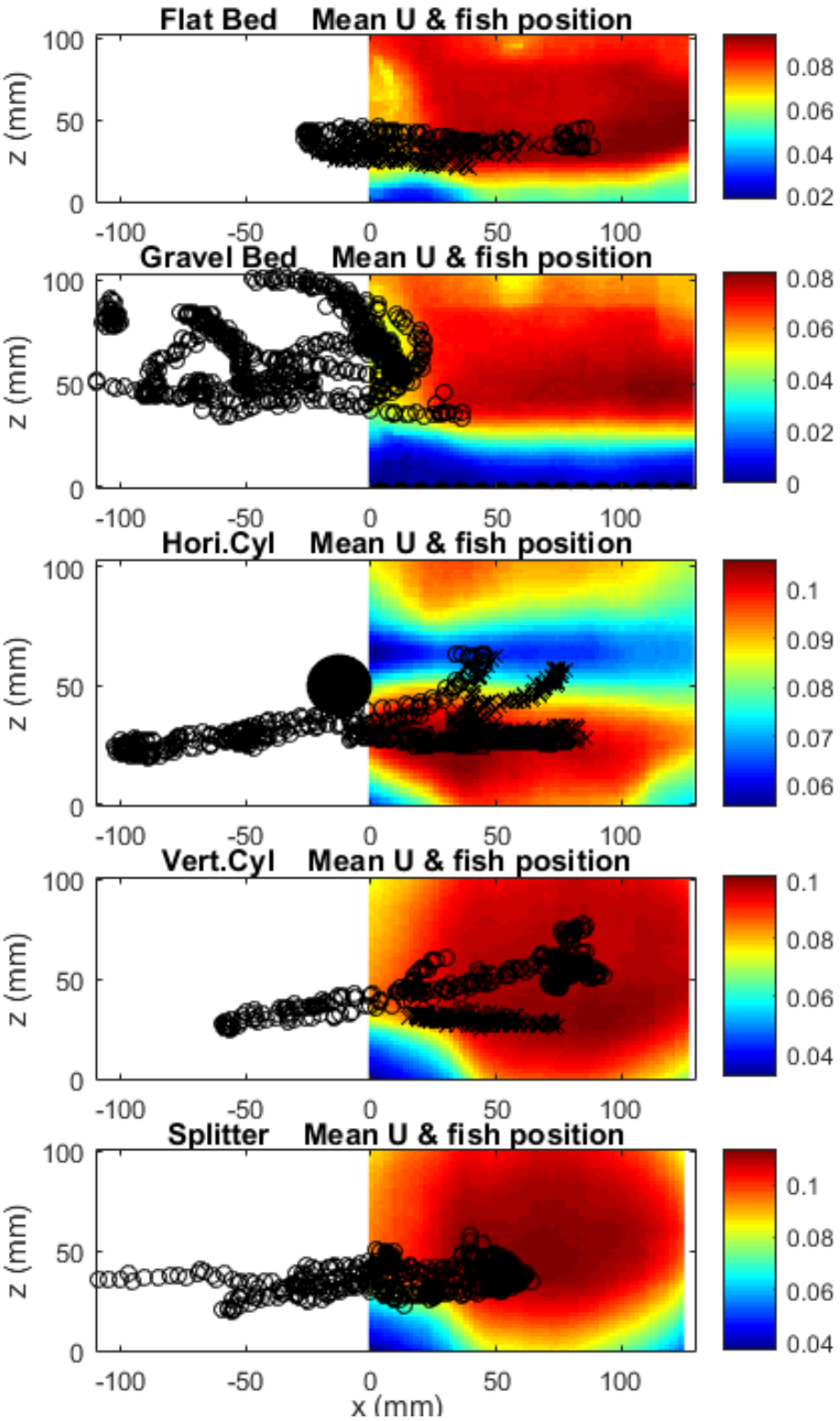

Figure 4.9: Correlation between fish position choice on XZ plane and mean longitudinal velocity (m/s)

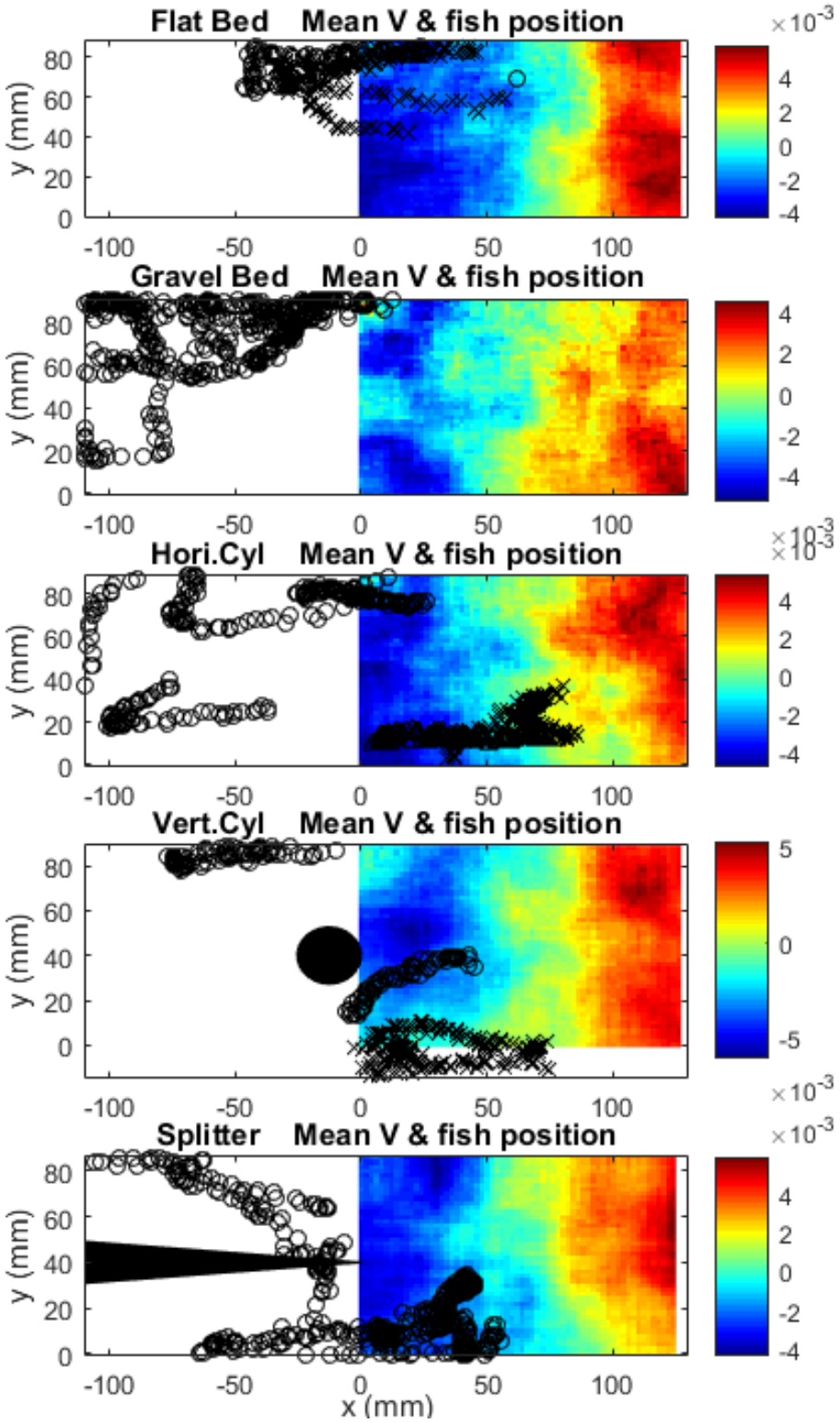

Figure 4.10: Correlation between fish position choice on XY plane and mean lateral velocity (m/s)

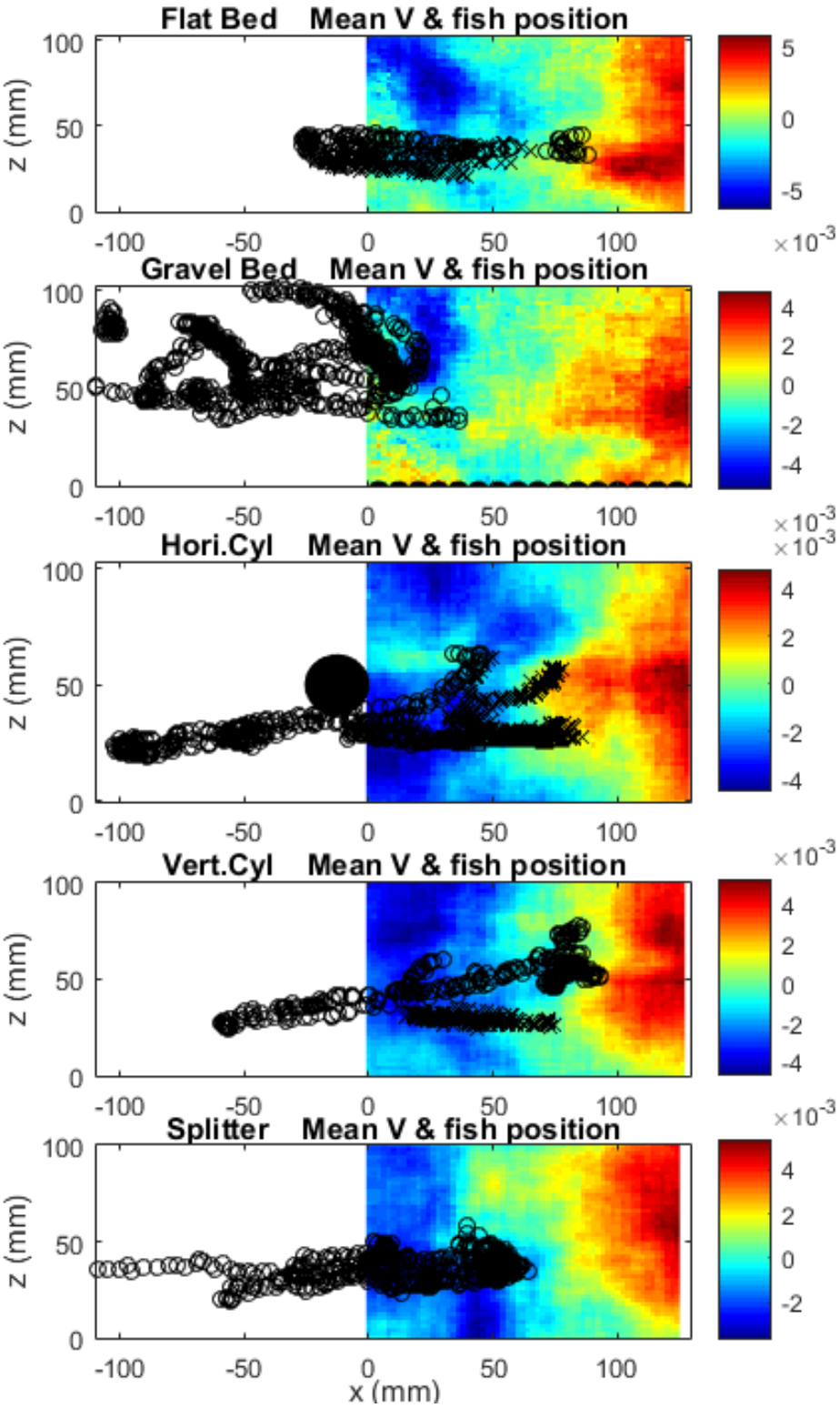

Figure 4.11: Correlation between fish position choice on XZ plane and mean lateral velocity (m/s)

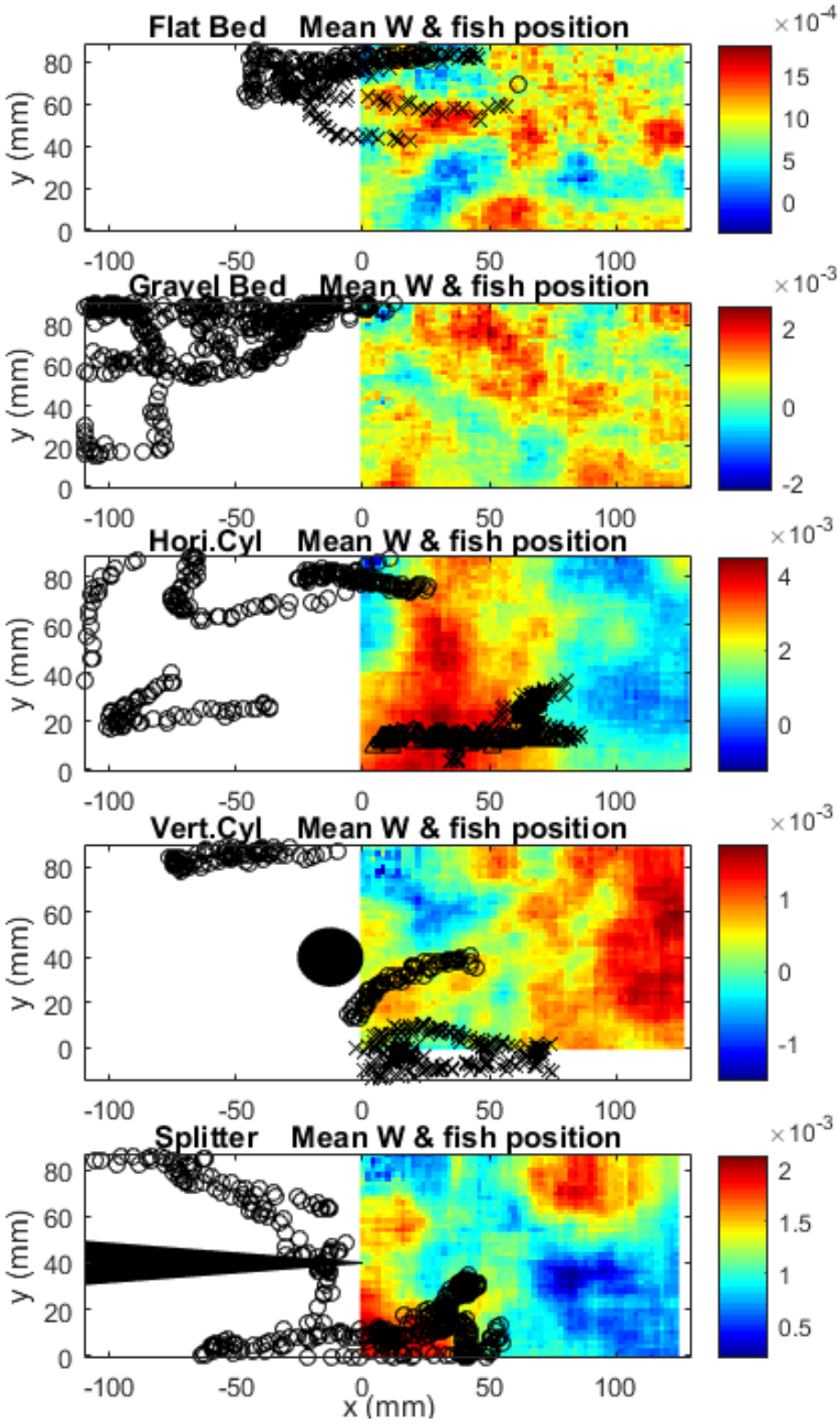

Figure 4.12: Correlation between fish position choice on XY plane and mean vertical velocity (m/s)

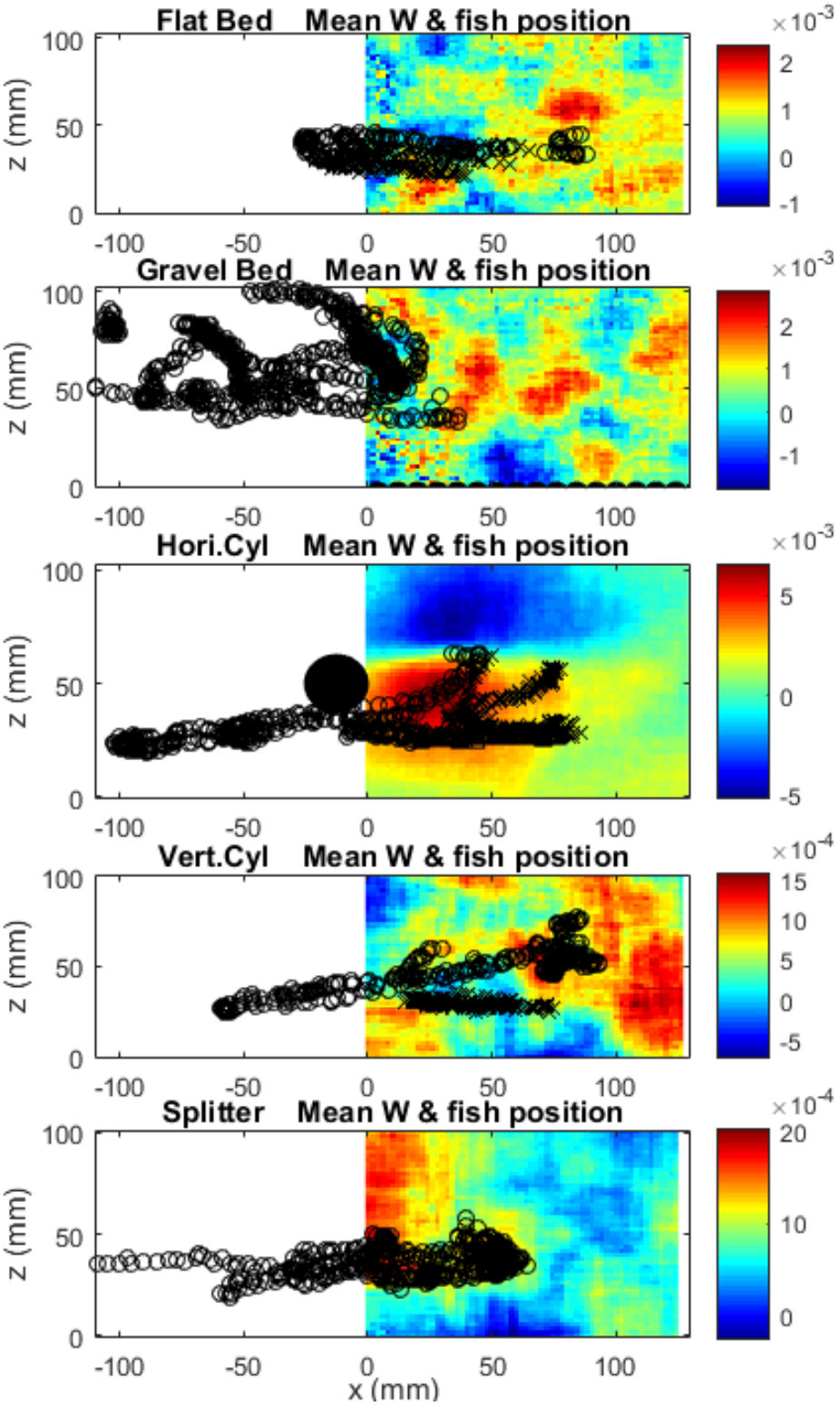

Figure 4.13: Correlation between fish position choice on XZ plane and mean vertical velocity (m/s)

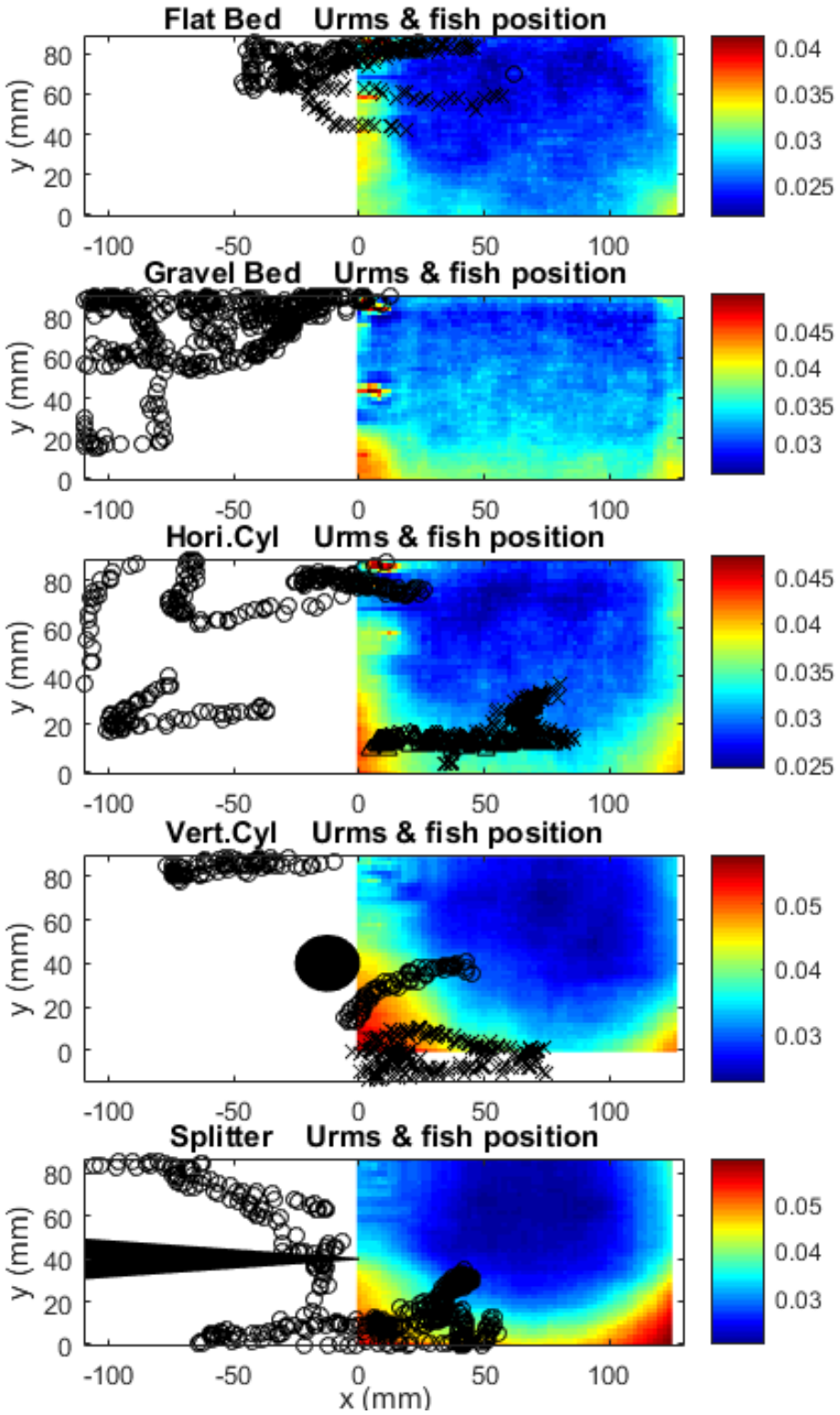

Figure 4.14: Correlation between fish position choice on XY plane and turbulent intensity, u_rms (m/s)

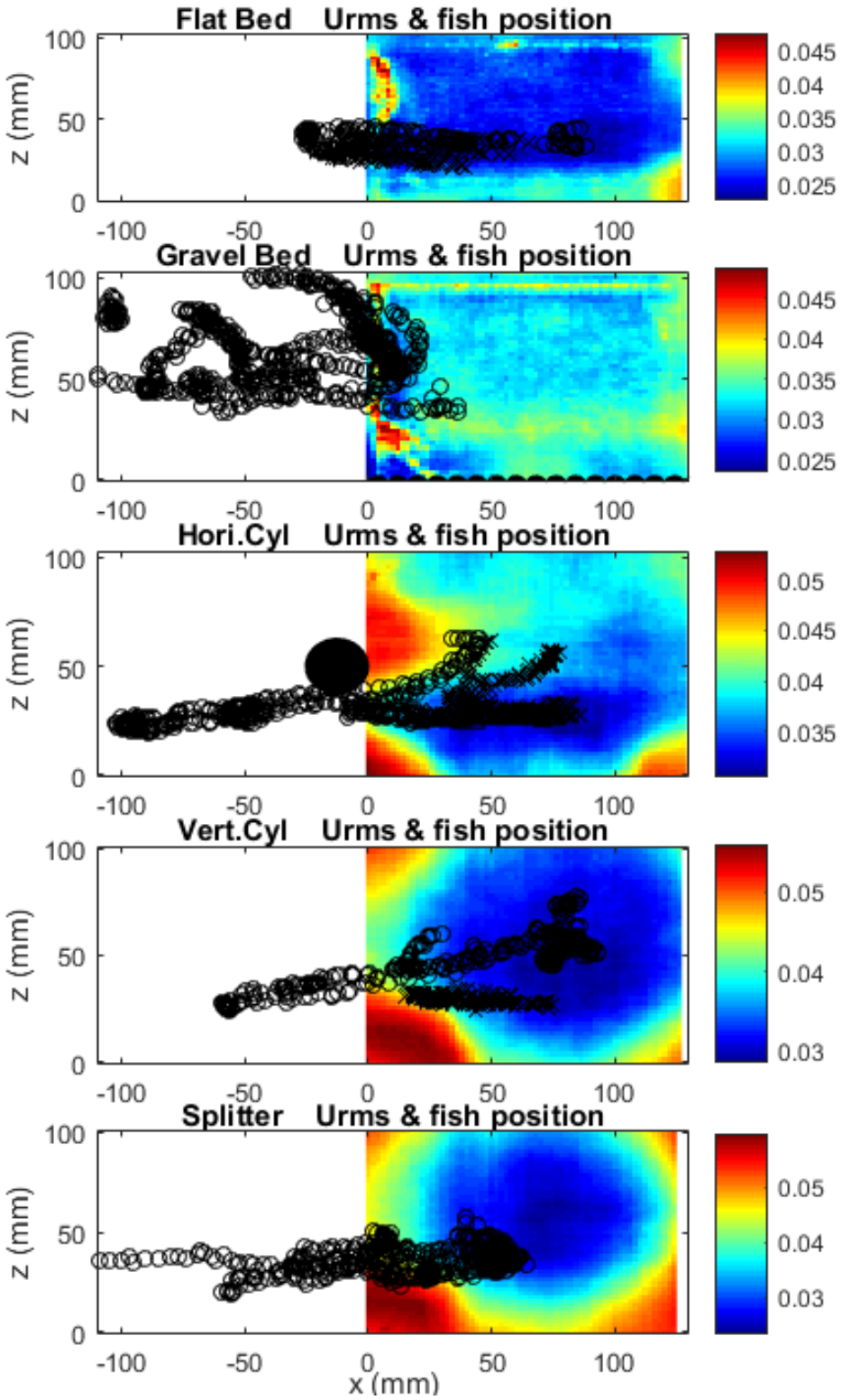

Figure 4.15: Correlation between fish position choice on XZ plane and turbulent intensity, u_rms (m/s)

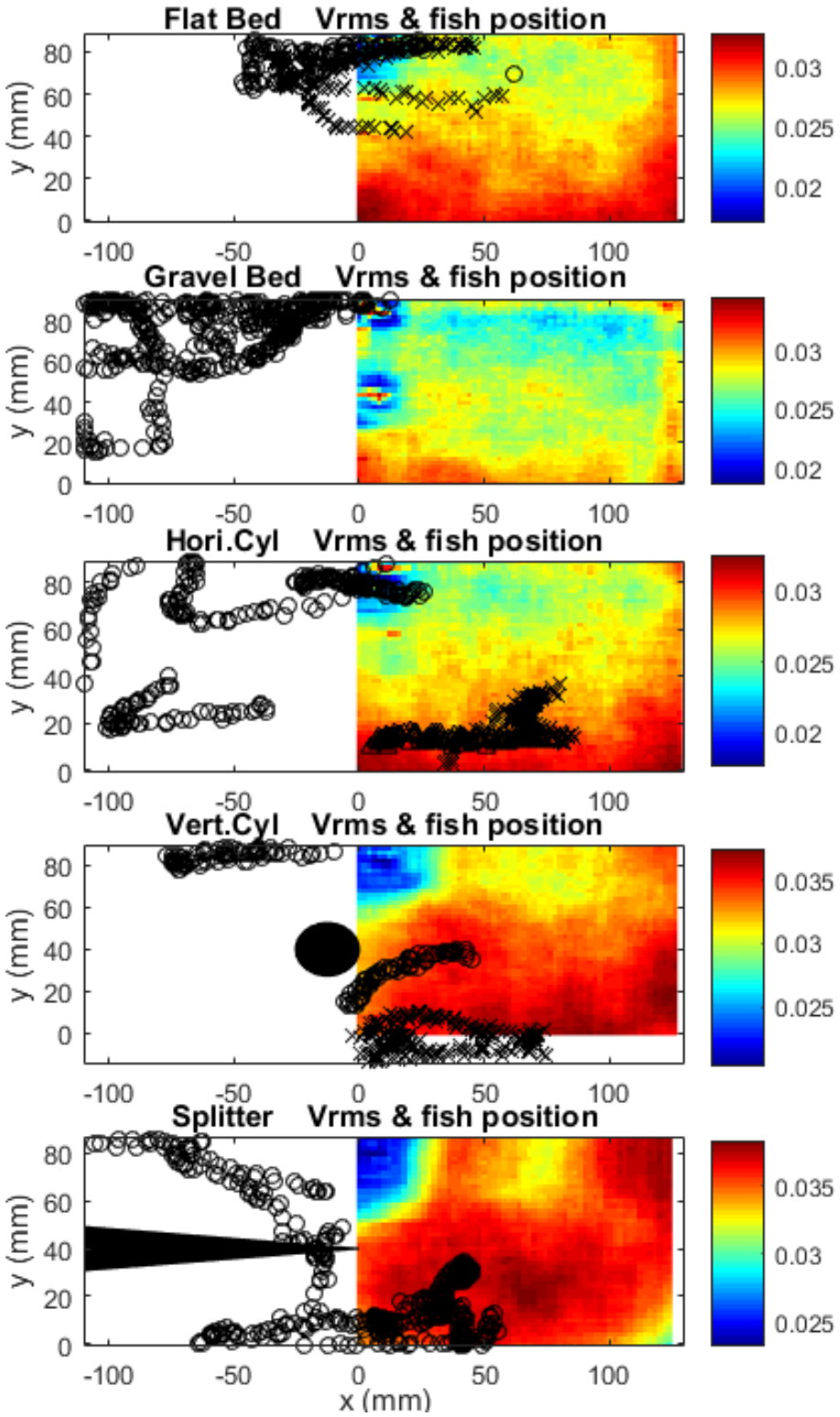

Figure 4.16: Correlation between fish position choice on XY plane and turbulent intensity, v_rms (m/s)

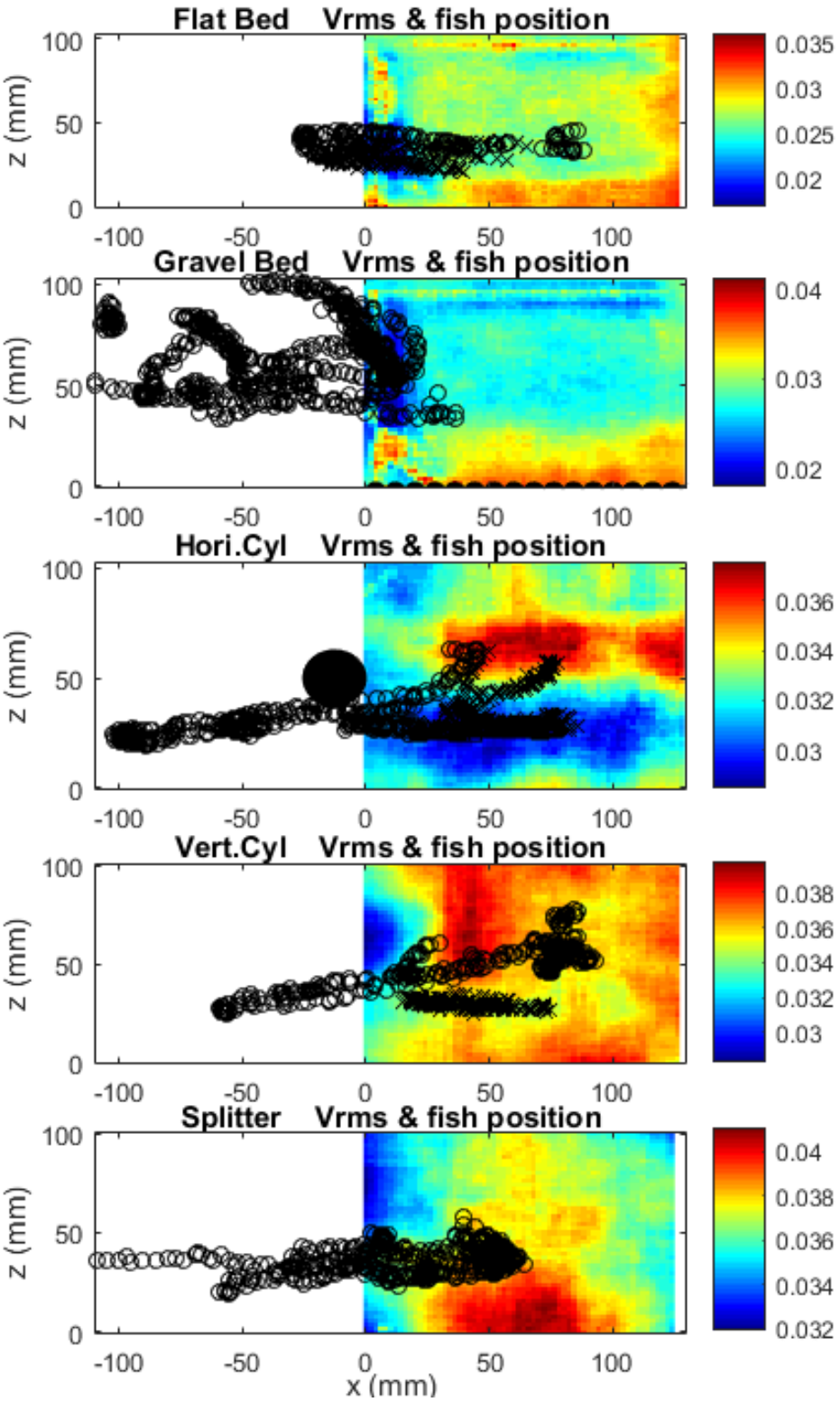

Figure 4.17: Correlation between fish position choice on XZ plane and turbulent intensity, v_rms (m/s)

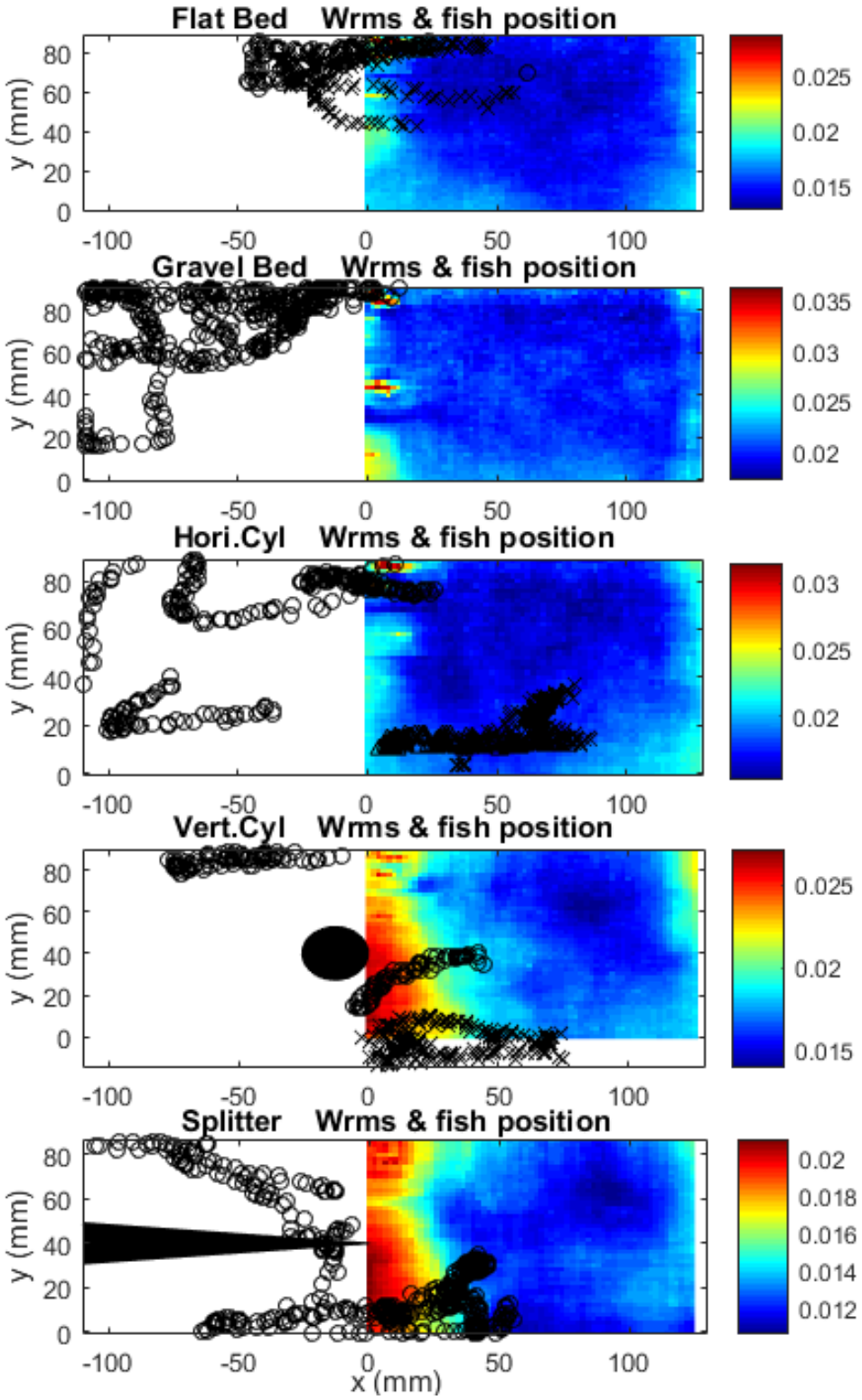

Figure 4.18: Correlation between fish position choice on XY plane and turbulent intensity, W_rms (m/s)

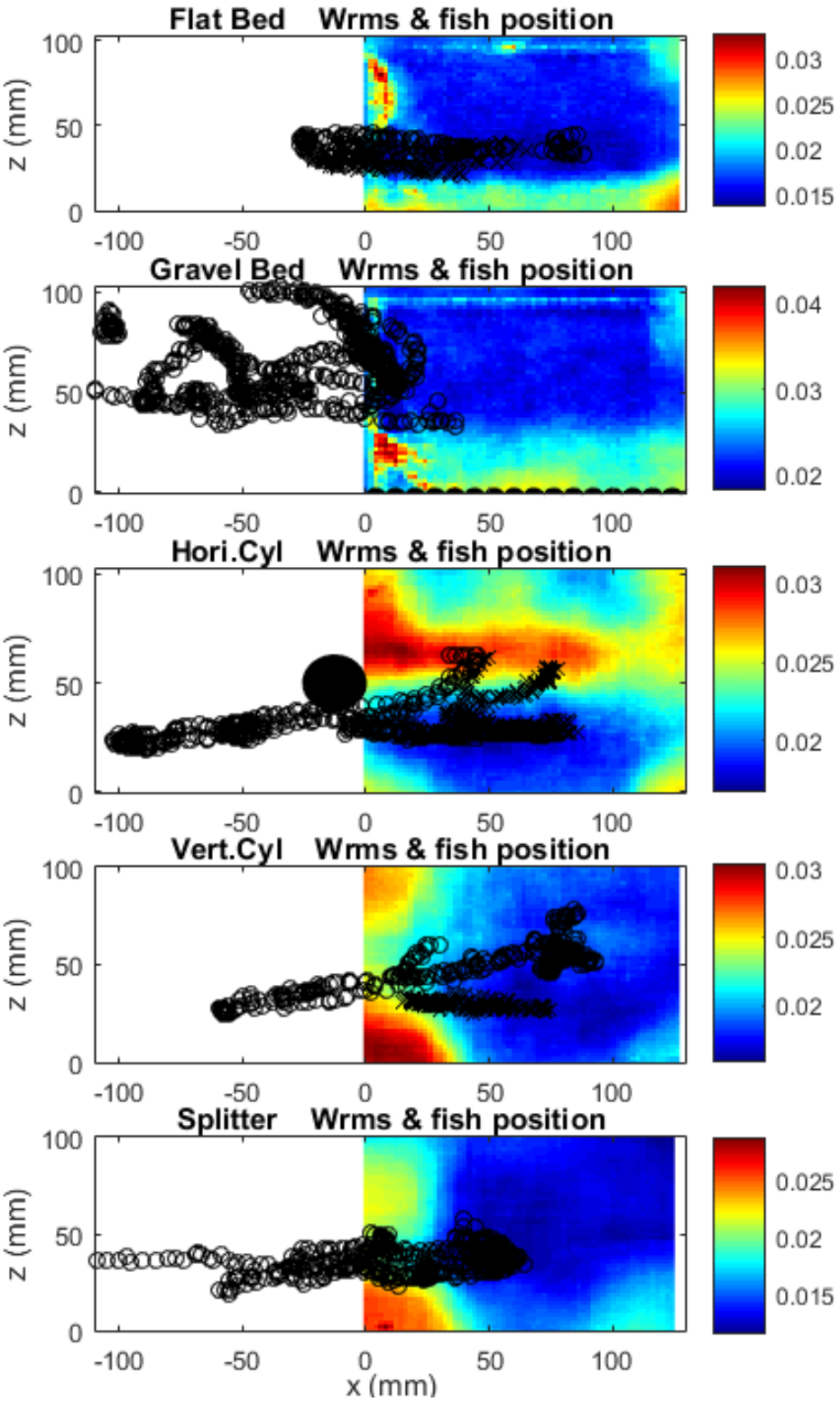

Figure 4.19: Correlation between fish position choice on XZ plane and turbulent intensity, W_rms (m/s)

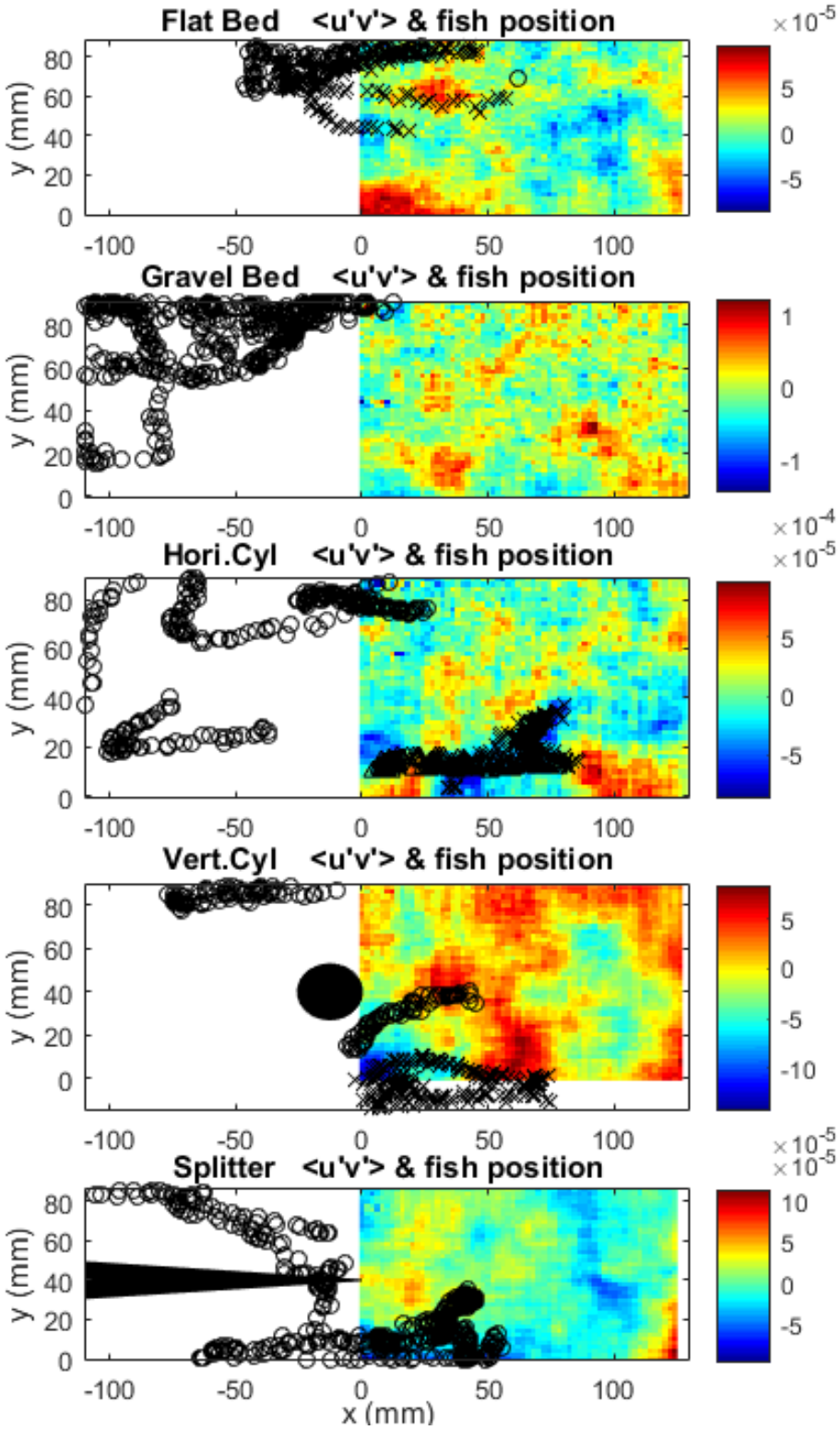

Figure 4.20: Correlation between fish position choice on XY plane and Reynolds stress, $u'v'$ (m^2/s^2)

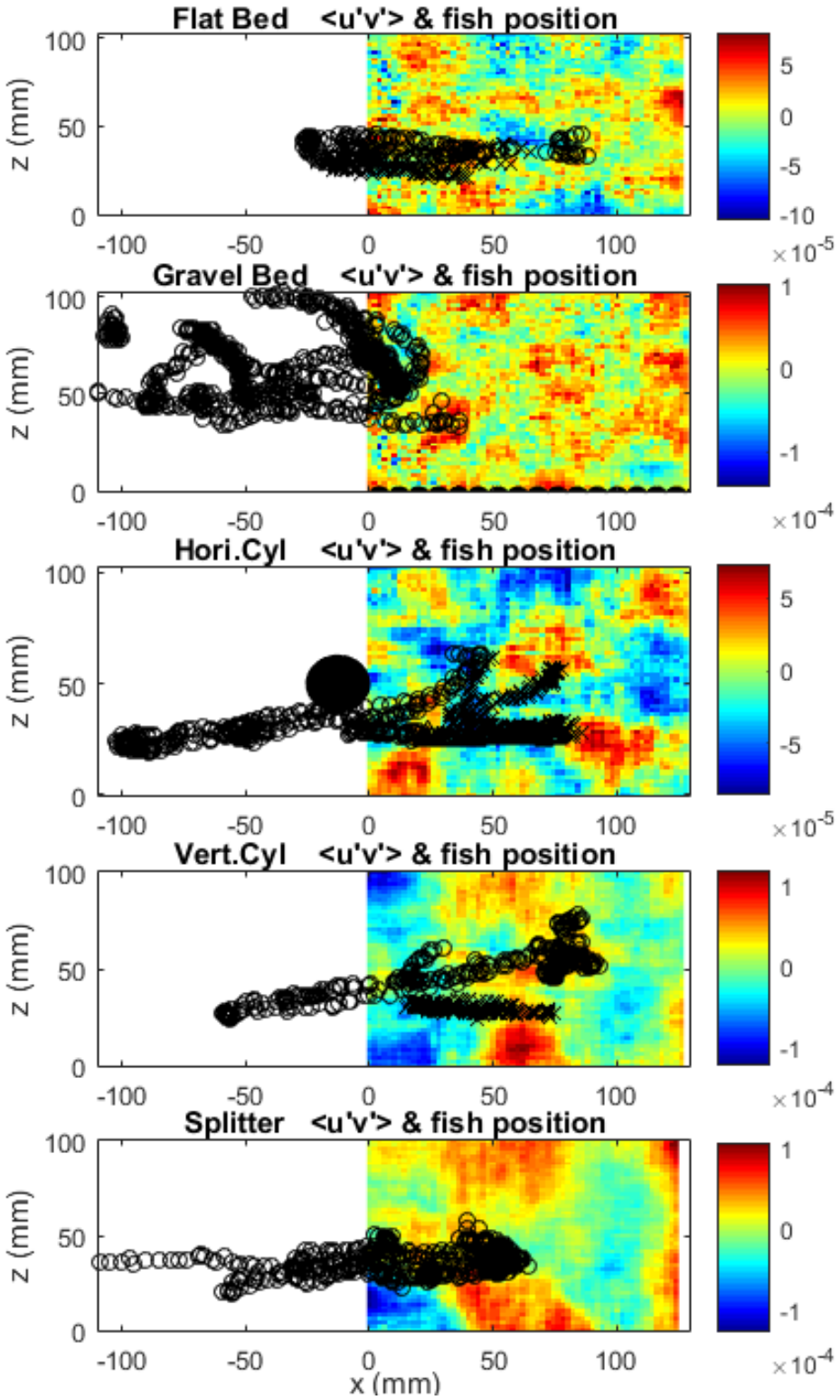

Figure 4.21: Correlation between fish position choice on XZ plane and Reynolds stress, $u'v'$ (m^2/s^2)

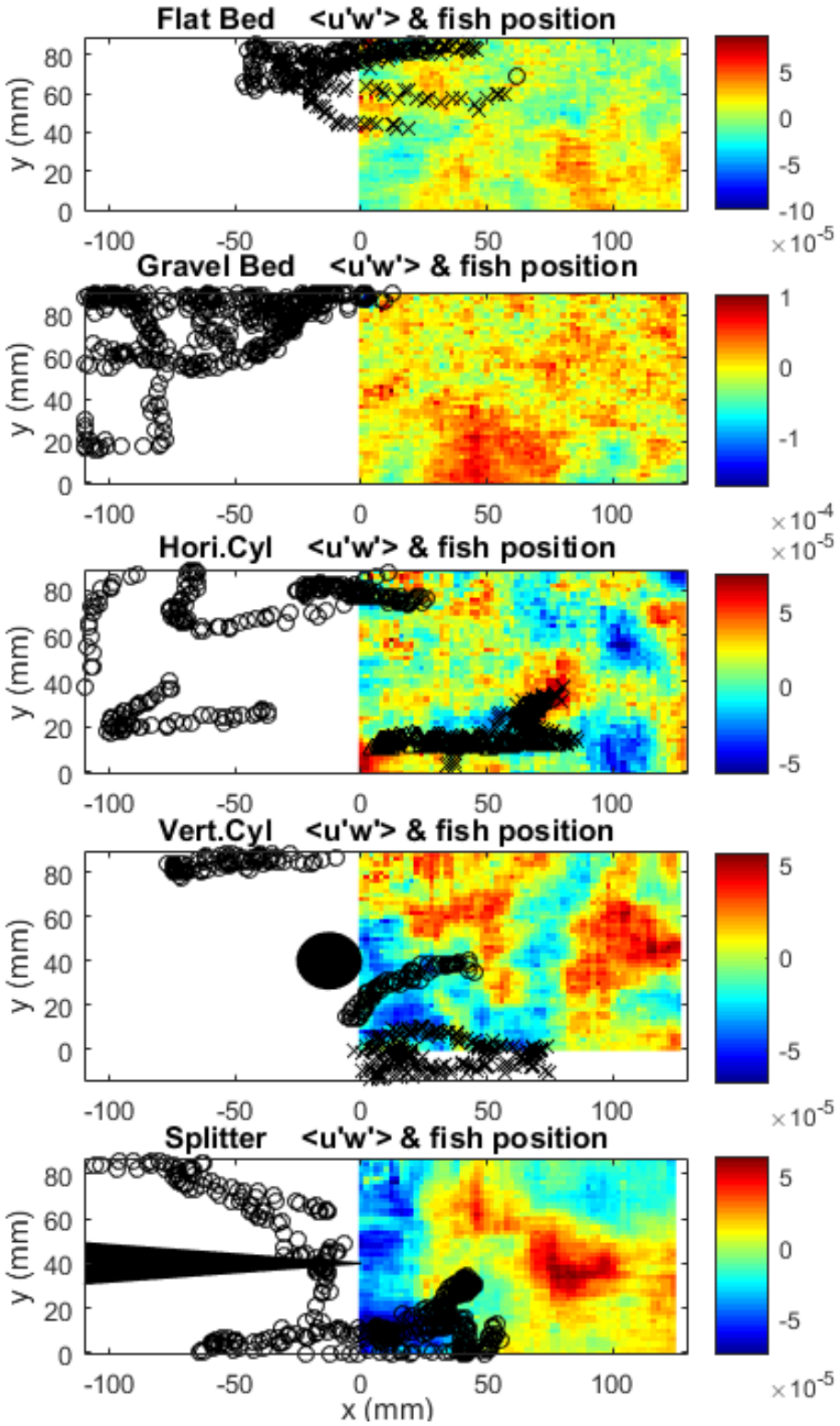

Figure 4.22: Correlation between fish position choice on XY plane and Reynolds stress, $u'w'$ (m^2/s^2)

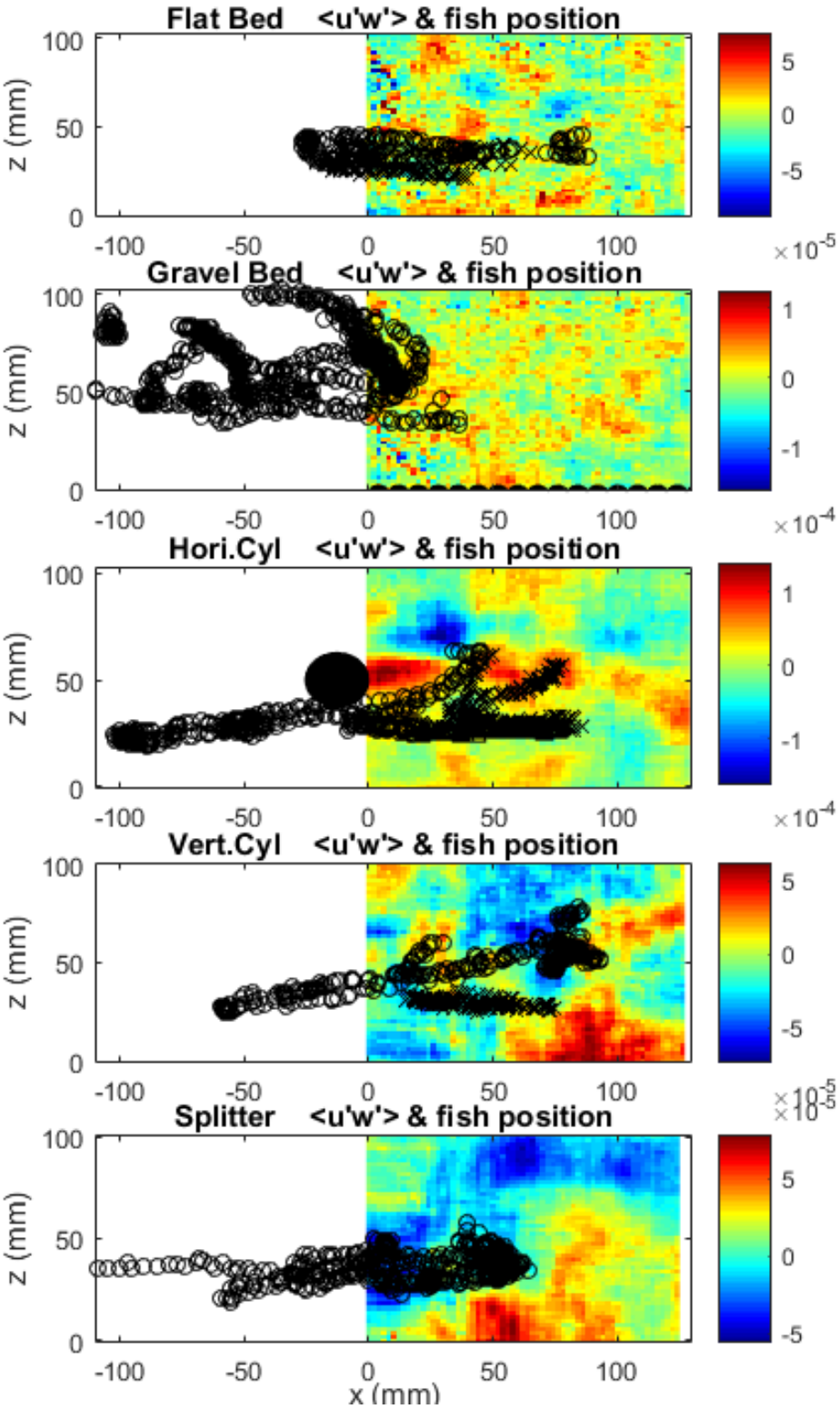

Figure 4.23: Correlation between fish position choice on XZ plane and Reynolds stress, $u'w'$ (m^2/s^2)

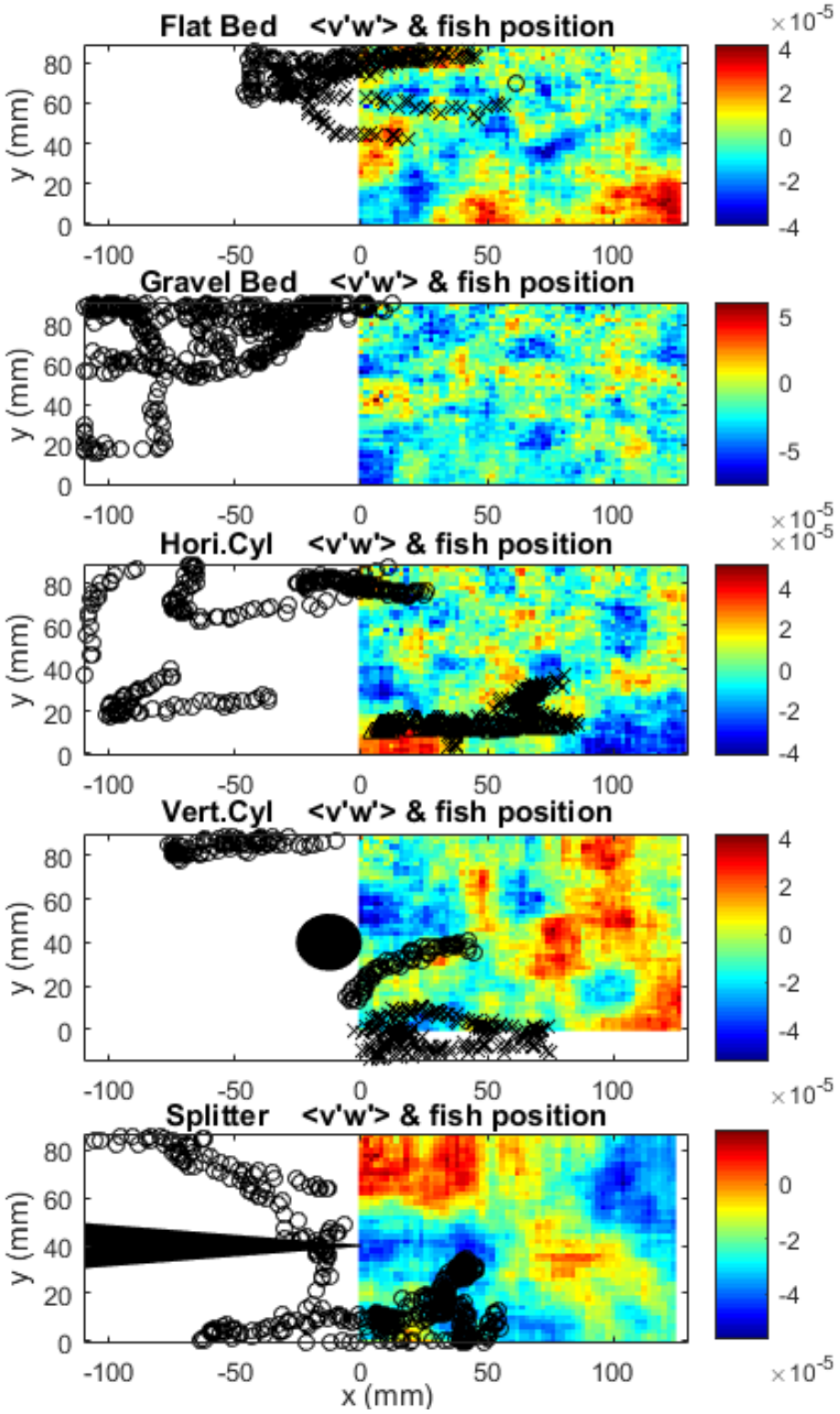

Figure 4.24: Correlation between fish position choice on XY plane and Reynolds stress, $v'w'$ (m^2/s^2)

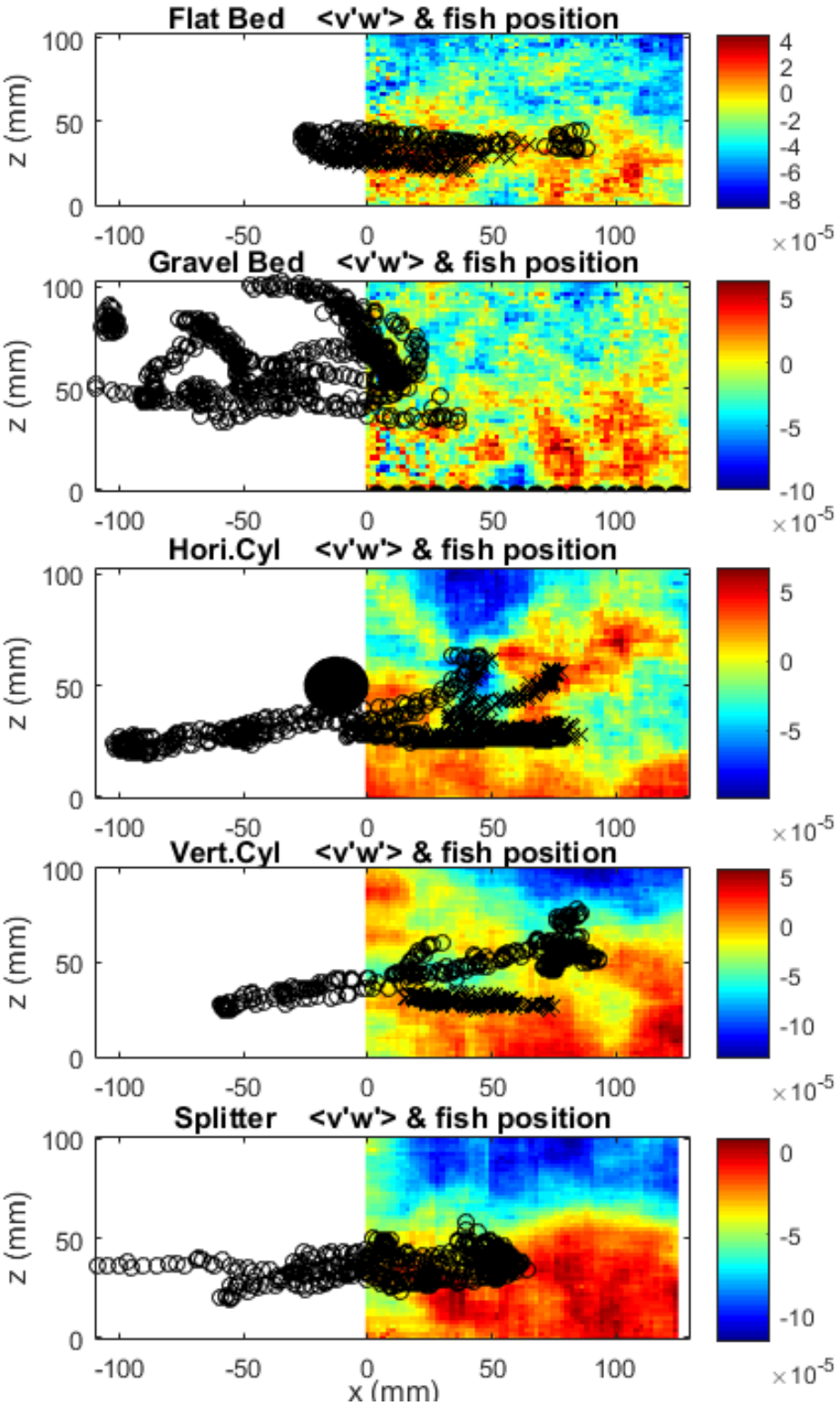

Figure 4.25: Correlation between fish position choice on XZ plane and Reynolds stress, $v'w'$ (m^2/s^2)

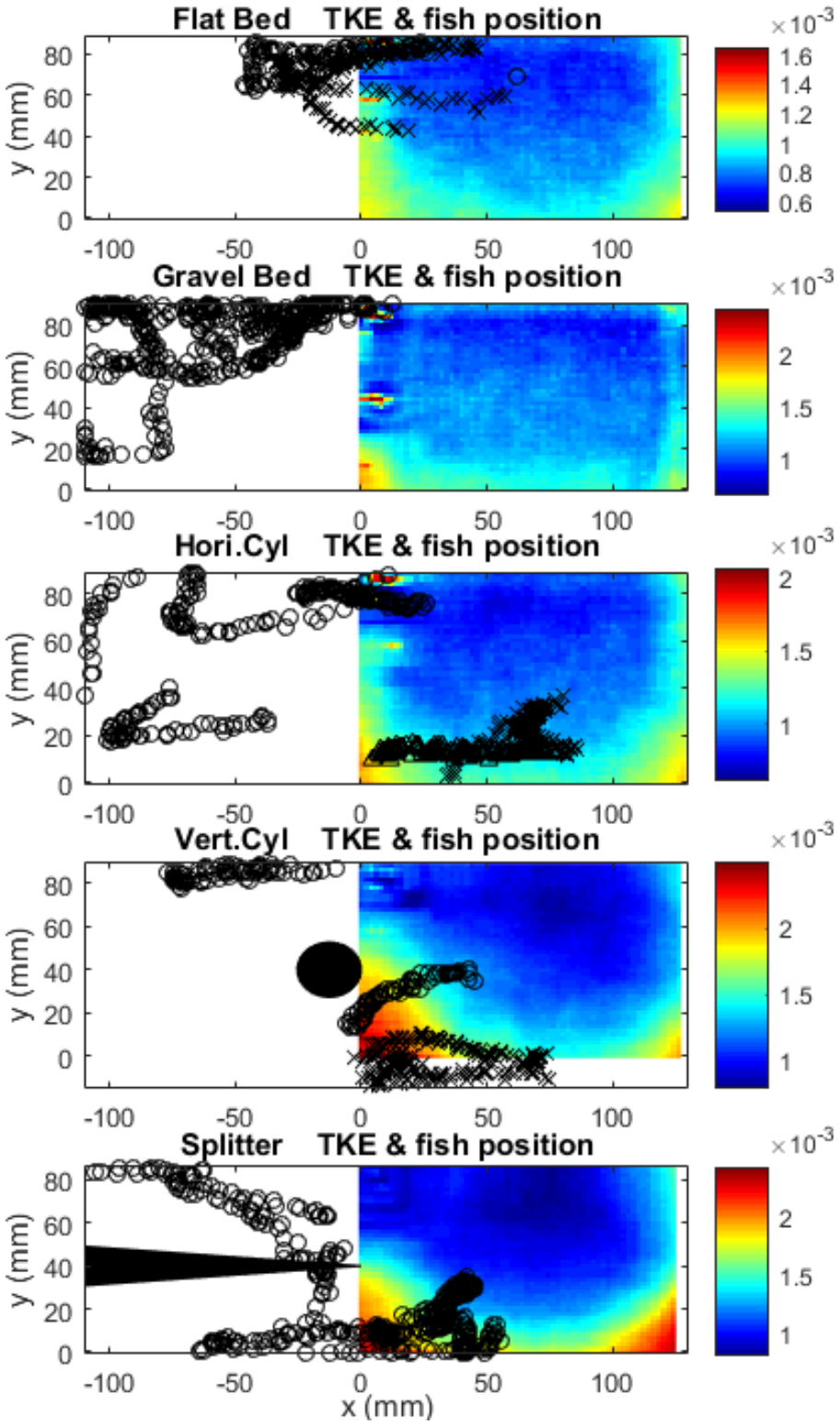

Figure 4.26: Correlation between fish position choice on XY plane and turbulent kinetic energy (m^2/s^2)

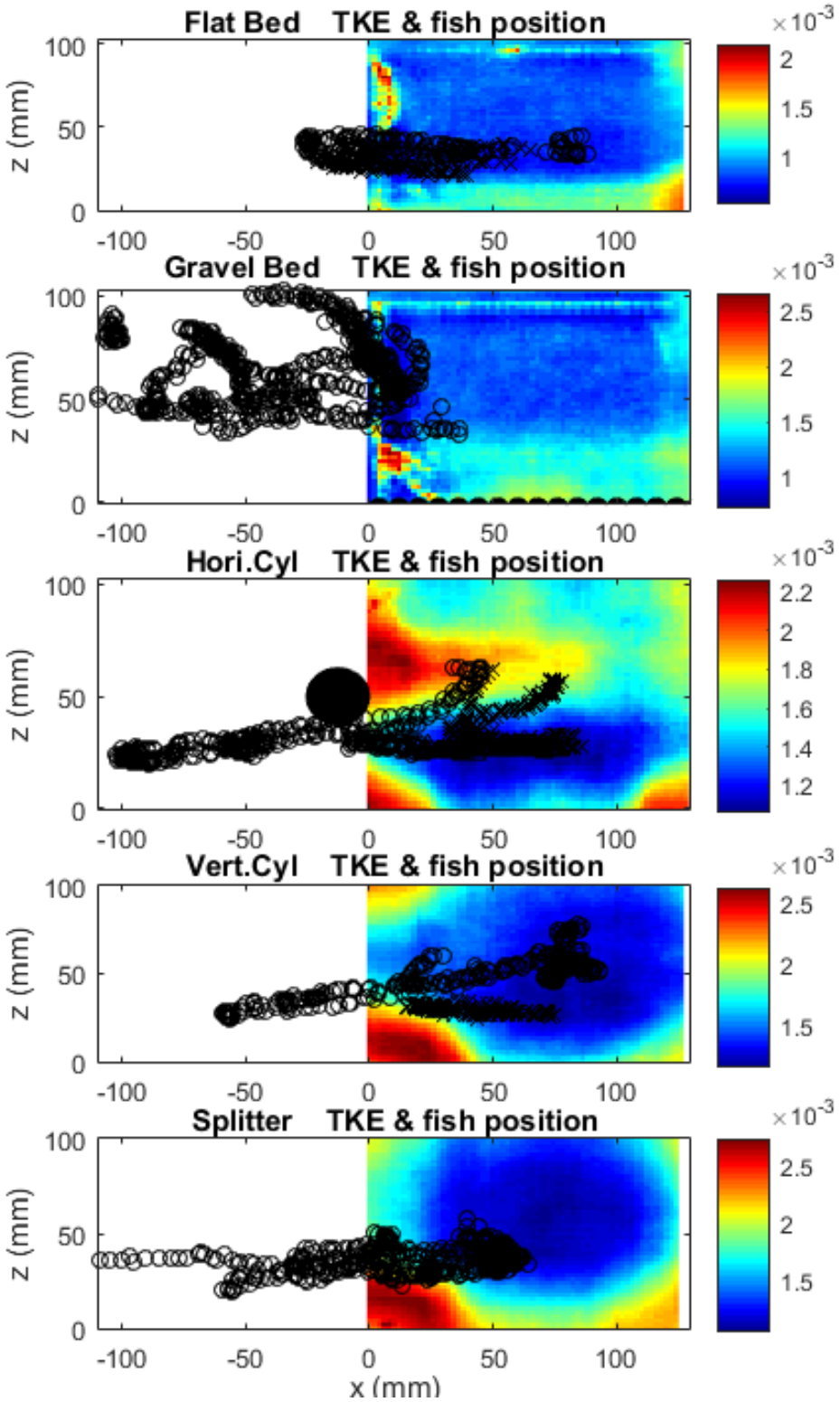

Figure 4.27: Correlation between fish position choice on XZ plane and turbulent kinetic energy (m^2/s^2)

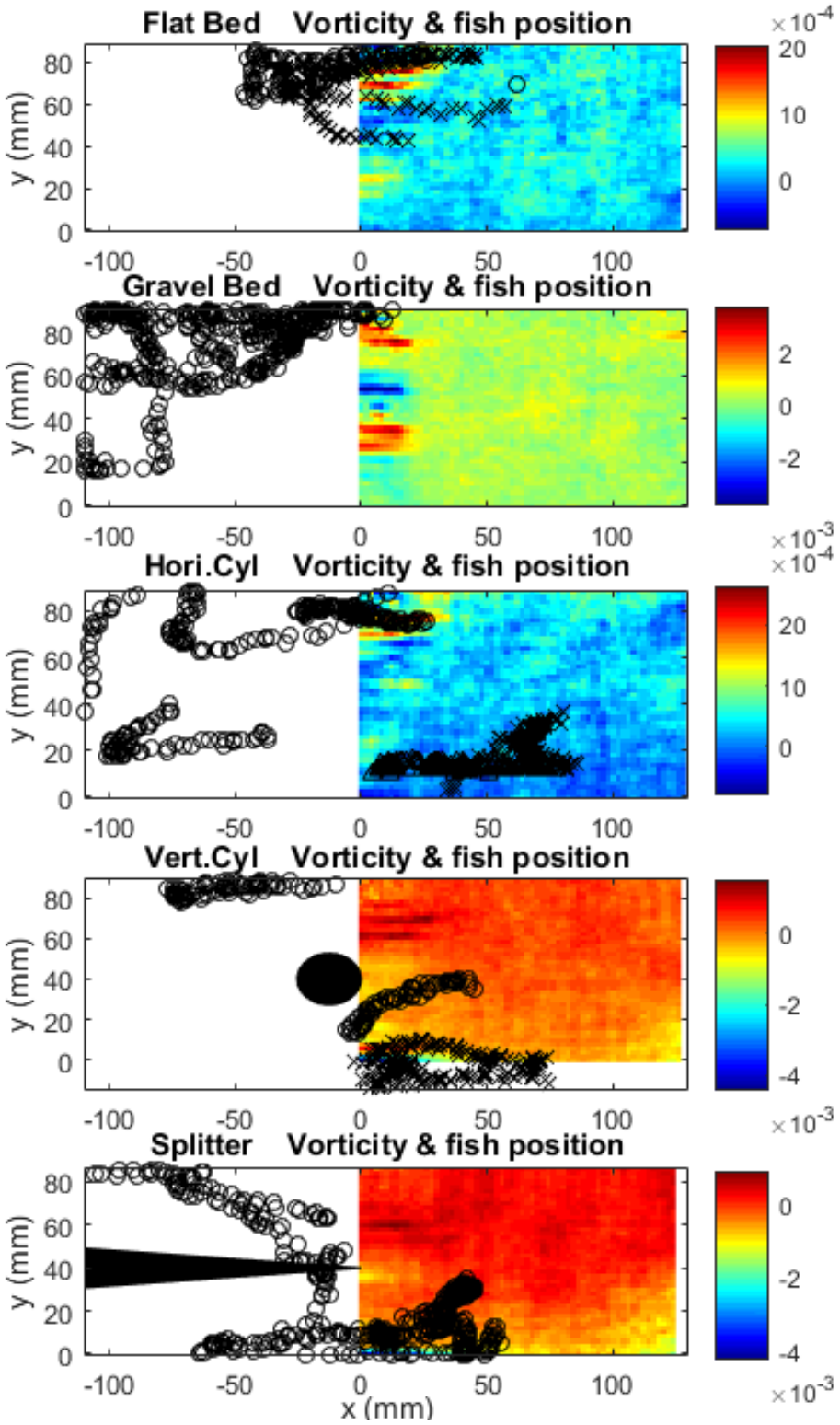

Figure 4.28: Correlation between fish position choice on XY plane and vorticity (1/s)

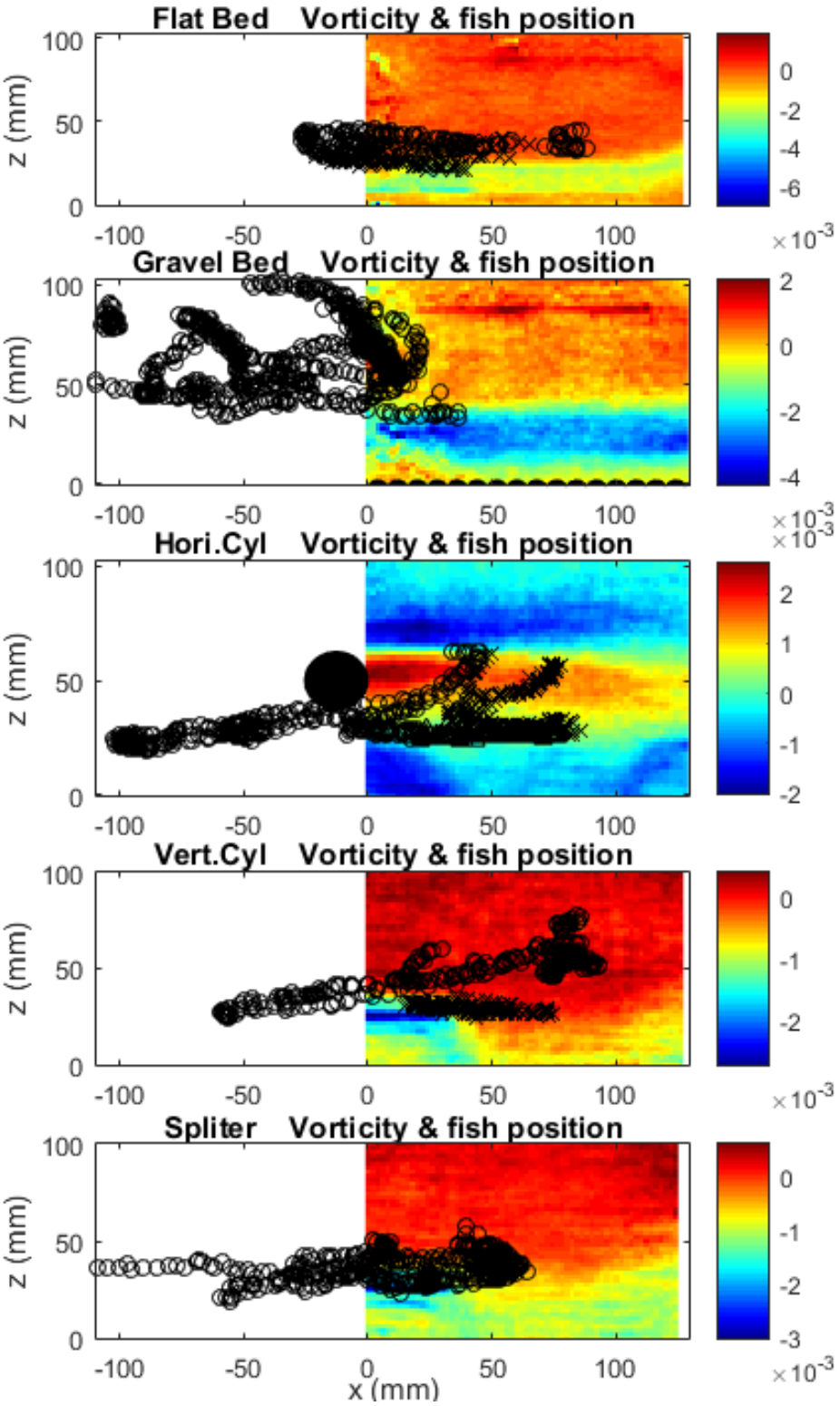

Figure 4.29: Correlation between fish position choice on XZ plane and vorticity (1/s)

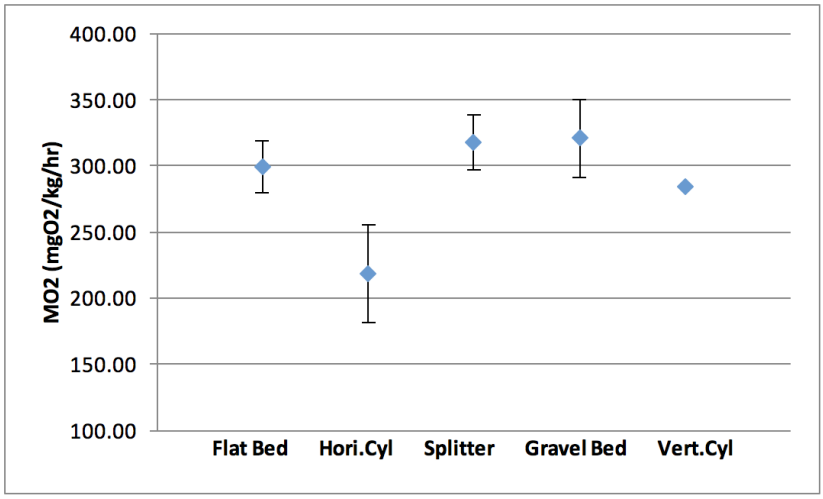

Figure 4.30: Oxygen consumption of fish under 5 cases, and fish were tested with a target when swimming

Overall, the following conclusions can be drawn. First, bulk velocities are not main factors that drive fish swimming behaviors, and more attention must be paid to turbulent characteristics. Second, regions with low turbulent intensity, turbulent kinetic energy and vorticity seem to attract Micropterus salmoides more effectively. Third, fish are capable of utilizing eddy energy, but the direction and scale of eddy matters. For example, large eddies in vertical direction generated by horizontal cylinder were employed to reduce swimming cost in this project, while that in lateral direction generated by vertical cylinder didn't show obvious function. However, the smaller vertical eddies generated by gravels increased the swimming cost, which means the scale of eddies that are useful were also important. Besides, the larger lateral eddies did increase the swimming difficulty more than the relative smaller one by vertical cylinder.

CHAPTER 5

CONCLUSIONS

This project employed a V3V system for detailed velocity profiles within a $14 \times 14 \times 10 cm^3$ region, based on which, mean velocities, turbulent intensity, Reynolds stress, turbulent kinetic energy and vorticity patterns were obtained and analyzed. The 3D, volumetric data, allowed us to examine all mean and turbulent statistics at various horizontal (XY) and vertical (XZ, YZ) planes to explore both intensity and orientation of the generated coherent flow structures due to various obstructions representing in-stream obstructions in rivers. Among the in-stream obstructions, horizontal cylinder and gravel bed were found to generate the strongest vertical coherent flow structures, altering the distribution of corresponding hydraulic parameters like w_{rms} and ω_{xz}, while vertical cylinder and splitter plate mainly strengthened the lateral coherent flow structures. Wakes behind the horizontal cylinder caused large scale rotation in the vertical plane, increasing turbulent intensity and kinetic energy past the cylinder. The gravel bed increased roughness, resulting in higher turbulence levels near the bed and propagating towards the top of the tunnel. Unlike the patterns created by the horizontal cylinder, effects by the gravel bed were more uniformly distributed along the bed and with eddies of multiple length scales, rather than localized behind the obstruction at the wake-scale. Vertical cylinder and the splitter plate shared similar hydraulic characteristics. For the mean velocity parameters, they didn't significantly alter their distribution, especially in vertical components. However, changes were more evident for the turbulent characteristics, with clear increases of v_{rms} and TKE.

Fish swimming mechanics was studied for all five scenarios through frame by frame analysis of videos using custom routines in MATLAB to identify fish position and orientation, providing data for the calculation of fish swimming speed, tail beat amplitude and tail beat frequency. For the swimming speed, fish in the presence of the splitter plate varied their speed more dras-

tically than in other cases. It is also found that fish tail beat frequency and amplitudes were the largest for the gravel bed scenario, where bed-generated turbulence seemingly created the most complicated environment for the fish to swim.

Analyzing together the hydraulic environment and fish swimming response led us to several observations: Mean hydrodynamic statistics were not driving factors for fish locomotion. Instead, turbulent characteristics showed a consistent influence on fish: regions with low turbulent intensity, turbulent kinetic energy and vorticity attract fish. Fish were able to swim efficiently within wake regions behind horizontal cylinders, while vertical cylinder or splitter plate could increase the difficulty for fish to keep stable. Fish also tend to swim actively to escape from rough bed.

Though the flow conditions and obstructions geometries were selected to recreate simplified versions of real stream environments, the small scale of the laboratory experiment may lead to draw different conclusions compared to large-scale experiments due to space constraints for fish motion. The findings of this study reveal the importance of turbulent hydrodynamics statistics, rather than mean bulk values, as the drivers of fish swimming responses. They can contribute to better predictions of fish habitat choice as well as enhance the design of in-stream structures for fish migration. For example, branches or fallen trees set in the stream horizontally seem to be better at assisting fish passing areas with high turbulent intensity or kinetic energy. Combining this flow analysis with habitat information and historical migration patterns, a model could be established for predicting the location of specific fish species throughout various seasons.

There are several limitations of this study that prevent further generalizations. First, the size of fish chosen was seemingly too large for the flume size, reducing the fish ability to maneuver around the obstructions. Second, the amount of collected data-sets for fish swimming kinematics are limited, and many potential errors may arise due to the accuracy of manually selecting fish position when analyzing video frames in MATLAB. Third, the coverage areas of hydraulic environment are smaller than required, since some fish swam outside of the measured volume. Therefore, in future studies smaller fish should be selected to better fit the flume size, or larger scale facilities could be utilized with larger fish. Field experiments can be considered to investigate behavior in natural environment if possible. Besides, more data

of fish swimming response should be collected by videos, using existing software to identify fish position and tail beat behavior automatically to reduce errors, and allow for more correlated data to provide useful models for fish energetics that account for the turbulence characteristics of the flow.

REFERENCES

[1] M. A. Wilkes, I. Maddock, F. Visser, and M. C. Acreman, "Incorporating hydrodynamics into ecohydraulics: The role of turbulence in the swimming performance and habitat selection of stream-dwelling fish," *Ecohydraulics: an integrated approach*, pp. 7–30, 2013.

[2] G. M. Kondolf, E. W. Larsen, and J. G. Williams, "Measuring and modeling the hydraulic environment for assessing instream flows," *North American Journal of Fisheries Management*, vol. 20, no. 4, pp. 1016–1028, 2000.

[3] D. Weihs, "Energetic advantages of burst swimming of fish," *Journal of Theoretical Biology*, vol. 48, no. 1, pp. 215–229, 1974.

[4] P. W. WEBB, "steadyswimming kinematics of tiger musky, an esociform accelerator, and rainbow trout, a generalist cruiser," *Journal of Experimental Biology*, vol. 138, no. 1, pp. 51–69, 1988.

[5] J. C. Liao, "A review of fish swimming mechanics and behaviour in altered flows," *Philosophical Transactions of the Royal Society B: Biological Sciences*, vol. 362, no. 1487, pp. 1973–1993, 2007.

[6] J. C. Liao, D. N. Beal, G. V. Lauder, and M. S. Triantafyllou, "Fish exploiting vortices decrease muscle activity," *Science*, vol. 302, no. 5650, pp. 1566–1569, 2003.

[7] D. G. Roche, M. K. Taylor, S. A. Binning, J. L. Johansen, P. Domenici, and J. F. Steffensen, "Unsteady flow affects swimming energetics in a labriform fish (cymatogaster aggregata)," *Journal of Experimental Biology*, vol. 217, no. 3, pp. 414–422, 2014.

[8] P. Webb and A. Cotel, "Turbulence: does vorticity affect the structure and shape of body and fin propulsors?" *Integrative and comparative biology*, vol. 50, no. 6, pp. 1155–1166, 2010.

[9] R. Kawabe, T. Kawano, N. Nakano, N. Yamashita, T. Hiraishi, and Y. Naito, "Simultaneous measurement of swimming speed and tail beat activity of free-swimming rainbow trout oncorhynchus mykiss using an acceleration data-logger," *Fisheries science*, vol. 69, no. 5, pp. 959–965, 2003.

[10] R. Bainbridge, "The speed of swimming of fish as related to size and to the frequency and amplitude of the tail beat," *Journal of experimental biology*, vol. 35, no. 1, pp. 109–133, 1958.

[11] O. Akanyeti and J. C. Liao, "The effect of flow speed and body size on kármán gait kinematics in rainbow trout," *Journal of Experimental Biology*, vol. 216, no. 18, pp. 3442–3449, 2013.

[12] A. Silva, C. Katopodis, M. Tachie, J. Santos, and M. Ferreira, "Downstream swimming behaviour of catadromous and potamodromous fish over spillways," *River Research and Applications*, vol. 32, no. 5, pp. 935–945, 2016.

[13] J. C. Liao, D. N. Beal, G. V. Lauder, and M. S. Triantafyllou, "The kármán gait: novel body kinematics of rainbow trout swimming in a vortex street," *Journal of experimental biology*, vol. 206, no. 6, pp. 1059–1073, 2003.

[14] W. J. Stewart, F.-b. Tian, O. Akanyeti, C. J. Walker, and J. C. Liao, "Refuging rainbow trout selectively exploit flows behind tandem cylinders," *Journal of Experimental Biology*, vol. 219, no. 14, pp. 2182–2191, 2016.

[15] I. Ahlbeck Bergendahl, S. Miller, C. Depasquale, L. Giralico, and V. Braithwaite, "Becoming a better swimmer: structural complexity enhances agility in a captive-reared fish," *Journal of fish biology*, vol. 90, no. 3, pp. 1112–1117, 2017.

[16] A. Sutterlin and S. Waddy, "Possible role of the posterior lateral line in obstacle entrainment by brook trout (salvelinus fontinalis)," *Journal of the Fisheries Board of Canada*, vol. 32, no. 12, pp. 2441–2446, 1975.

[17] M. W. ROSEN, "Water flow about a swimming fish," NAVAL ORDNANCE TEST STATION CHINA LAKE CA, Tech. Rep., 1959.

[18] J. O. Dabiri, "Biomechanics: How fish feel the flow," *Nature*, vol. 547, no. 7664, p. 406, 2017.

[19] O. Akanyeti, P. Thornycroft, G. Lauder, Y. Yanagitsuru, A. Peterson, and J. Liao, "Fish optimize sensing and respiration during undulatory swimming," *Nature communications*, vol. 7, p. 11044, 2016.

[20] R. Lacey, V. S. Neary, J. C. Liao, E. C. Enders, and H. M. Tritico, "The ipos framework: linking fish swimming performance in altered flows from laboratory experiments to rivers," *River Research and Applications*, vol. 28, no. 4, pp. 429–443, 2012.

[21] A. Lupandin, "Effect of flow turbulence on swimming speed of fish," *Biology Bulletin*, vol. 32, no. 5, pp. 461–466, 2005.

[22] G. V. Lauder and E. G. Drucker, "Morphology and experimental hydrodynamics of fish fin control surfaces," *IEEE journal of oceanic engineering*, vol. 29, no. 3, pp. 556–571, 2004.

[23] E. D. Tytell and G. V. Lauder, "Hydrodynamics of the escape response in bluegill sunfish, lepomis macrochirus," *Journal of Experimental Biology*, vol. 211, no. 21, pp. 3359–3369, 2008.

[24] D. L. Smith, E. L. Brannon, and M. Odeh, "Response of juvenile rainbow trout to turbulence produced by prismatoidal shapes," *Transactions of the American Fisheries Society*, vol. 134, no. 3, pp. 741–753, 2005.

[25] I. Nezu, "Open-channel flow turbulence and its research prospect in the 21st century," *Journal of Hydraulic Engineering*, vol. 131, no. 4, pp. 229–246, 2005.

[26] T. Utami and T. Ueno, "Experimental study on the coherent structure of turbulent open-channel flow using visualization and picture processing," *Journal of Fluid Mechanics*, vol. 174, pp. 399–440, 1987.

[27] F. Alavyoon, D. S. Henningson, and P. H. Alfredsson, "Turbulent spots in plane poiseuille flow–flow visualization," *The Physics of fluids*, vol. 29, no. 4, pp. 1328–1331, 1986.

[28] S. K. Robinson, "Coherent motions in the turbulent boundary layer," *Annual Review of Fluid Mechanics*, vol. 23, no. 1, pp. 601–639, 1991.

[29] D. Coles, "The law of the wake in the turbulent boundary layer," *Journal of Fluid Mechanics*, vol. 1, no. 2, pp. 191–226, 1956.

[30] H. Fiedler, "Coherent structures in turbulent flows," *Progress in Aerospace Sciences*, vol. 25, no. 3, pp. 231–269, 1988.

[31] A. F. Hussain, "Coherent structures and turbulence," *Journal of Fluid Mechanics*, vol. 173, pp. 303–356, 1986.

[32] C. H. Williamson and A. Roshko, "Vortex formation in the wake of an oscillating cylinder," *Journal of fluids and structures*, vol. 2, no. 4, pp. 355–381, 1988.

[33] R. Wille, "Karman vortex streets," in *Advances in Applied Mechanics*. Elsevier, 1960, vol. 6, pp. 273–287.

[34] R. D. Blevins, "Flow-induced vibration," 1990.

[35] D. Cacchione and D. Drake, "A new instrument system to investigate sediment dynamics on continental shelves," *Marine Geology*, vol. 30, no. 3-4, pp. 299–312, 1979.

[36] G. R. T. and E. B. Thornton, "Local and shoaled comparisons of sea surface elevations, pressures and velocities," *Journal of Geophysical Research*, pp. 1524–1530, 1980.

[37] J. Trowbridge and A. Williams, "Measurement of turbulent fluxes and dissipation rates in the coastal bottom boundary layer," WOODS HOLE OCEANOGRAPHIC INSTITUTION MA DEPT OF APPLIED OCEAN PHYSICS AND ENGINEERING, Tech. Rep., 1998.

[38] Y. A. Yusoff, F. Mohamad, M. S. Sunar, and A. Selamat, "Flow visualization techniques: A review," in *International Conference on Industrial, Engineering and Other Applications of Applied Intelligent Systems*. Springer, 2016, pp. 527–538.

[39] F. Pereira and M. Gharib, "Defocusing digital particle image velocimetry and the three-dimensional characterization of two-phase flows," *Measurement Science and Technology*, vol. 13, no. 5, p. 683, 2002.

[40] D. G. Goring and V. I. Nikora, "Despiking acoustic doppler velocimeter data," *Journal of Hydraulic Engineering*, vol. 128, no. 1, pp. 117–126, 2002.